THE DETERMINATION OF STRUCTURE FACTORS FROM KINEMATIC AND DYNAMIC EFFECTS IN X-RAY DIFFRACTION

V. C. Sharma

A Thesis Submitted for the Degree of PhD
at the
University of St Andrews

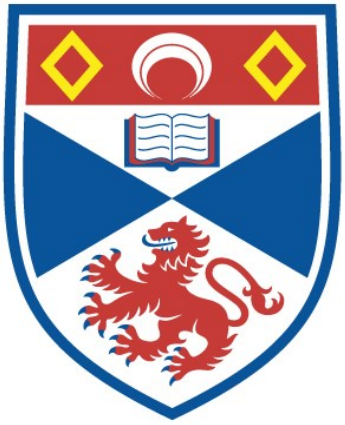

1973

THE DETERMINATION OF STRUCTURE FACTORS FROM KINEMATIC AND DYNAMIC EFFECTS IN X-RAY DIFFRACTION

A thesis

presented by

V. C. Sharma, M.Sc.,

to the

University of St. Andrews

in application for the Degree

of Doctor of Philosophy

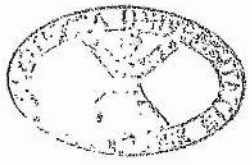

Th

7010

DECLARATION

I hereby certify that this thesis has been composed by me, and is a record of work done by me, and has not previously been presented for a higher Degree.

This research was carried out in the Physical Science Laboratory of St. Salvator's College, in the University of St. Andrews, under the supervision of Dr. R. C. G. Killean.

Vinod Chander Sharma

CAREER

In July 1964, I graduated with first class M.Sc. in Physics from the University of Jabalpur (M.P.), India. After my graduation in 1964, I was appointed as a Lecturer in Physics at a Postgraduate College of Science Jabalpur and held this post for a period of five years.

In October 1969, I was enrolled under Ordinance 16 as a research student in the School of Physical Sciences, University of St. Andrews, under the supervision of Dr. R. C. G. Killean.

CERTIFICATE

I certify that Vinod Chander Sharma, M.Sc., has spent nine terms at research work in the Physical Science Laboratory of St. Salvator's College, in the University of St. Andrews, under my direction, that he has fulfilled the conditions of Ordinance No. 16 (St. Andrews) and that he is qualified to submit the accompanying thesis in application for the Degree of Doctor of Philosophy.

R. C. G. Killean

Research Supervisor

ACKNOWLEDGEMENTS

The author wishes to express his gratitude to Dr. R. C. G. Killean, Dr. J. L. Lawrence and Dr. D. F. Grant for their guidance, advice, discussion and constructive criticism. His thanks are also due to Professor J. F. Allen, F.R.S., for the encouragement and research facilities made available in the Department of Physics, University of St. Andrews, where this work was carried out. The author also wishes to thank Mrs. S. Weaver for typing the thesis and Mr. D. Speight for the photographic work and the preparation of the tables and diagrams. Finally, he expresses his sincere thanks to the University of St. Andrews for the award of a scholarship which made this work possible.

CONTENTS

CHAPTER 1

INTRODUCTION

X-rays are electromagnetic radiations of short wavelength. Since an electric field exerts a force on a charged particle such as an electron, the oscillating electric field of an X-ray beam will set any electron in its path into forced oscillations with the frequency of the incident wave. Now an accelerating or decelerating electron emits an electromagnetic wave. In this way an electron is said to scatter X-rays, the scattered wave being simply the wave radiated by the electron under the action of the incident wave. The scattered wave has the same wavelength and frequency as the incident wave and is said to be coherent with it, since there is a constant phase difference, π , between the once scattered and the incident wave.

The X-rays are scattered in all directions by an electron but the intensity of the scattered wave is dependent upon the angle of scattering. For an unpolarized X-ray beam the intensity I_e scattered by a single electron of charge e and mass m at a distance r from the electron is given by

$$I_e = \frac{I_o e^4}{r^2 m^2 c^4} \cdot \frac{(1 + \cos^2 2\theta)}{2} \qquad (1.0)$$

where $\frac{(1 + \cos^2 2\theta)}{2}$ is a polarization factor.

θ is the scattering angle

and c is the velocity of light.

This is called the Thomson formula.

The wave scattered by a stationary atom is simply the sum of the waves scattered by its component electrons. If the scattering is in the forward direction ($2\theta = 0$) then the waves scattered by all the electrons of the atom are in phase and therefore the amplitudes of all the waves are added directly. The fact that electrons are situated at different positions in space around the atom introduces differences in phase between the waves scattered and so the resultant amplitude decreases as $\sin\theta$ increases. According to wave mechanics, the point electrons of classical theory are replaced by a smoothly varying function of electron cloud $\psi(\underline{r})$, surrounding the atom. If now $\rho(\underline{r})$ is defined as the electron density (i.e., number of electrons per unit volume) at a vector distance $\underline{r}$ from the centre of the atom then

$$\rho(\underline{r}) = |\psi(\underline{r})|^2 \qquad (1.1)$$

where $\psi(\underline{r})$ is the solution of the Schroedinger equation for the electron system.

For coherent scattering, the amplitudes of the waves scattered by n electrons are added and the intensity of the total wave scattered by an atom is given by

$$I_A = I_e\left(\sum_{j=1}^{j=n} f_j\right)^2 = I_e.f^2 \qquad (1.2)$$

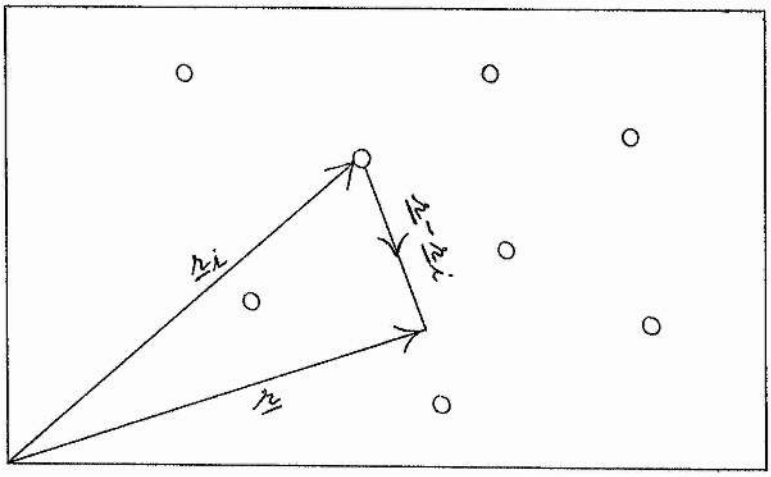

FIG. 1

where f is called the atomic scattering factor of the atom and f_j is the scattering factor for the jth electron given by

$$f_j = \int \rho_j(\underline{r}) \exp (2\pi i \, \underline{S}\cdot\underline{r}) \, d v \qquad (1.3)$$

where $|\underline{S}| = \frac{2 \sin\theta}{\lambda}$ is the scattering vector and $\underline{r}$ represents a vector from an origin to the jth electron.

The atomic scattering factor 'f' can also be described as the 'efficiency' of scattering for a given atom in a given direction. It may be defined as the ratio of amplitude of the wave scattered by an atom to the amplitude of the wave scattered by one electron placed at the origin.

The atomic form factors for various atoms have been calculated theoretically using various approximations in the electronic wave functions (International Tables, Volume III, 1962); (Freeman 1959); Berghuis et al 1955); (Cromer and Waber 1965) and these authors assume that the atom is at rest and has a perfectly spherical charge distribution.

The pattern unit of the arrangement of atoms in a crystal from which the whole crystal is built up is called the unit cell. If $\rho(\underline{r})$ is the electron density at a point $\underline{r}$ in the unit cell, then the amount of scattering matter in the volume dv is $\rho(\underline{r})dv$. The total amplitude of the wave scattered from such a unit cell is given by

$$F(\underline{S}) = \int_v \rho(\underline{r}) \exp (2\pi i \, \underline{r}\cdot\underline{S}) \, d v \qquad (1.4)$$

In Fig. 1 the vector between the ith atom at position $\underline{r}_i$ and the point of observation situated at $\underline{r}$ is $(\underline{r} - \underline{r}_i)$.

Now assuming no overlap of the electron density

$$\rho(\underline{r}) = \sum_{i=1}^{N} \rho_i(\underline{r} - \underline{r}_i)$$

Equation 1.4 can then be written as

$$F(\underline{S}) = \int_v \sum_{i=1}^{N} \rho_i(\underline{r} - \underline{r}_i) \exp 2\pi i(\underline{r} - \underline{r}_i).\underline{S} \exp 2\pi i \underline{r}_i \cdot \underline{S} \, d v$$

$$= \sum_{i=1}^{N} \left[\int_v \rho_i(\underline{r} - \underline{r}_i) \exp 2\pi i(\underline{r} - \underline{r}_i).S \, d v \right] \exp 2\pi i \underline{r}_i.\underline{S}$$

$$\text{or } F(\underline{S}) = \sum_{i=1}^{N} f_i \exp 2\pi i \underline{r}_i.\underline{S} \qquad (1.5)$$

where f_i is the scattering factor for the ith atom at the position $\underline{r}_i$.

The function $F(\underline{S})$ is the Fourier transform of the set of atoms in the unit cell and is continuous. The vector $\underline{r}_i$ represents the position of the ith atom in the unit cell.

Now if another unit cell at a vector distance $(\underline{r}_i + \underline{a})$ from the origin is considered then the scattering from this new unit cell is given by

$$F_2(\underline{S}) = \sum_{i=1}^{N} f_i \exp \left[2\pi i(\underline{r}_i + \underline{a}).\underline{S} \right]$$

$$\text{or } F_2(\underline{S}) = \left[\exp 2\pi i \, \underline{a}.\underline{S}\right] .F(\underline{S}) \qquad (1.6)$$

which shows that a change of phase does occur with a change of position of the unit cell. Therefore the total Fourier transform assuming a one dimensional lattice having U unit cells is given by

$$F_T(\underline{S}) = F(\underline{S}) \Big[1 + \exp 2\pi i \, \underline{a}.\underline{S} + \exp 2\pi i \, 2 \, \underline{a}.\underline{S} + \exp 2\pi i \, 3 \, \underline{a}.\underline{S} + \text{----+} \exp 2\pi i (U - 1)\underline{a}.\underline{S} \Big]$$

$$\text{or } F_T(\underline{S}) = F(\underline{S}) \left[\exp i \, (U - 1) \, 2\pi \, \underline{a}.\underline{S} \; \frac{\sin U \pi \underline{a}.\underline{S}}{\sin \pi \underline{a}.\underline{S}} \right] \qquad (1.7)$$

The exponential term since it has a unit modulus does not affect the intensity of scattering and the expression $\frac{\sin U\pi \underline{a}.\underline{S}}{\sin \pi \underline{a}.\underline{S}}$ is of importance. By a similar argument it can be shown that for a three dimensional lattice the amplitude of the wave scattered is the product of three similar terms given by

$$\frac{\sin U\pi \underline{a}.\underline{S}}{\sin \pi \underline{a}.\underline{S}} \qquad \frac{\sin V\pi \underline{b}.\underline{S}}{\sin \pi \underline{b}.\underline{S}} \qquad \frac{\sin W\pi \underline{c}.\underline{S}}{\sin \pi \underline{c}.\underline{S}}$$

U, V, W are the number of unit cells composing the lattice in three dimensions and $\underline{a}$, $\underline{b}$, $\underline{c}$ are the unit cell translations. The amplitude of the diffracted beam is maximum when

$$\begin{aligned} \underline{a}.\underline{S} &= h \\ \underline{b}.\underline{S} &= k \\ \underline{c}.\underline{S} &= \ell \end{aligned} \qquad (1.8)$$

where h, k, ℓ are integers and can have +ve, -ve or zero values. These equations are called the Laue equations and Bragg's law can be deduced from these equations. Each of the three equations represents a set of parallel equidistant planes perpendicular to the axes a, b, c respectively. The values of $\underline{S}$ that correspond to diffracted beams are those whose ends lie upon the intersections of the three sets of planes. These equations imply that the transform of the crystal contents has non-zero value only at specific points represented by the integers h, k, ℓ in the reciprocal space. At these sample points the Fourier transform has values called the structure factors.

Now expressing $\underline{r}_i$ in terms of x_i, y_i, z_i, where x_i, y_i, z_i are the fractional coordinates for the ith atom

$$\underline{r}_i = x_i \cdot \underline{a} + y_i \cdot \underline{b} + z_i \cdot \underline{c}$$

and denoting $F(h\ k\ \ell)$ as the value of $F(\underline{S})$ at which Laue equations hold then

$$F(h\ k\ \ell) = \sum_{i=1}^{N} f_i \exp 2\pi i(x_i\ \underline{a}.\underline{S} + y_i\ \underline{b}.\underline{S} + z_i\ \underline{c}.\underline{S})$$

$$\text{or } F(\underline{h}) = \sum_{i=1}^{N} f_i \exp 2\pi i(x_i\ h + y_i\ k + z_i\ \ell) \qquad (1.9)$$

It can thus be seen that the structure factors arise as special values of the transform. The structure factor $F(\underline{h})$ is in general a complex number and it expresses both the amplitude and phase of the resultant wave.

The total wave scattered by a unit cell has been described under the assumption that the atoms are stationary. However, at all temperatures the atoms are oscillating about their mean position with a finite amplitude. Since the frequency of their oscillation is much smaller than the frequency of X-rays, the atoms may be considered to be displaced from their mean positions. Thermal motion has the effect of smearing out the electron cloud of the atoms over a larger volume resulting in out of phase scattering of the X-ray waves. It can thus be assumed that X-ray diffraction pattern is produced by atoms which are fixed in position, the observed intensity being the average of the diffracted intensities for all the possible positions of the atoms from their true mean position.

Now consider a crystal with a simple lattice containing a single atom per unit cell. If $\Delta\ \underline{r}_i$ is the displacement of the atom in an ith unit cell from its mean position, then the average values of $\Delta\ \underline{r}_i$ for all the atoms at a given time are identical to the average value of $\Delta\ \underline{r}_i$ in time for a given atom. The modified scattering

factor can thus be written as

$$f_m = f_i \overline{\exp\ (-\ 2\pi i\ \underline{S}\cdot \Delta\underline{r}_i)}$$

$$\approx f_i\ (1 - 2\ \pi^2\ \overline{(\underline{S}.\ \Delta\underline{r}_i)^2}$$

which after substituting $|\underline{S}| = \frac{2\ \sin\theta}{\lambda}$ and a little simplification becomes

$$f_m = f_i\ \exp\ (-\ \frac{8\pi^2\ \sin^2\theta}{\lambda^2}\ .\ \overline{U^2}) \qquad (1.10)$$

where $\overline{U^2} = \frac{1}{3}\ \overline{\Delta\underline{r}_i^2}$ for isotropic motion and $\overline{\Delta\underline{r}_i^2}$ is called the root mean square displacement.

It is clear from the above expression that the effect of thermal motion is to decrease the amplitude of the scattered wave from an atom.

However, if the thermal motion of the atoms is not isotropic then in this case the electron cloud is assumed to be an ellipsoid and the modified scattering factor for such a motion is given by (Cruickshank, 1956).

$$f_m = f\ \exp\ -\ (B_{11}h^2 + B_{22}k^2 + B_{33}\ell^2 + B_{12}hk + B_{23}k\ell + B_{13}h\ell)$$

where the B_{ij} are constants for a given atom at a given temperature and are measures of the anisotropic motion.

The quantity actually measured in X-ray diffraction experiments is the integrated intensity $I(\underline{h})$ of the diffracted beam for each reflection. The observed structure factors are derived from $I(\underline{h})$ using the following expression, which is a modification of the Thomson formula by Bragg, James and Bosanquet (1921a)

$$\frac{E(\underline{h}).\omega}{I_o} = I(\underline{h}) = \frac{N^2 \lambda^3 e^4}{m^2 c^4} L\, p.\, |F_o(\underline{h})|^2\, dv. \qquad (1.11)$$

where E(L) is the total diffracted energy at $\underline{h}$

$I(\underline{h})$ is the diffracted intensity at $\underline{h}$

I_o is the intensity of the incident X-ray beam

dv is the volume of the crystal bathed in the X-ray beam

ω is the angular velocity of the rotation of the crystal

N is the number of unit cells per unit volume

$P = \frac{1 + \cos^2 2\theta}{2}$ is the polarization factor

and L is the Lorentz factor, which arises as a scale factor due to different times taken by the reciprocal lattice points to roll through the Ewald sphere. For a normal beam geometry such as used in the present experiments $L = \frac{1}{\sin 2\theta}$

$$\therefore\ |F_o(\underline{h})|^2 = \text{constant} \cdot (Lp)^{-1} \cdot I(\underline{h}) \qquad (1.12)$$

This gives a set of relative observed structure factors. The temperature factor B for isotropic motion of the atoms or B_{11}, B_{22}, B_{33} ... etc. for anisotropic motion are usually adjusted along with other parameters by comparing $F_o(\underline{h})$ and $F_c(\underline{h})$ for successive refinements of a crystal structure. This process of refinement has been adopted for α-rhamnose monohydrate (chapter III).

1.1 The Kinematic Theory of X-Ray Diffraction

Darwin (1922) proposed a very simple model to explain the diffraction of X-rays from real crystals. He assumed that most of the crystals are composed of a very large number of small domains which he called 'mosaic blocks'. These blocks are considered to have random orientations and are optically independent.

Thus to obtain integrated intensities, the crystal has to be oscillated through a small angular range so that a group of blocks or each block diffracts in turn when at exact Bragg angle. No phase relation is maintained between the beams diffracted from various blocks, whereas each block is sufficiently perfect to diffract the beam coherently. Darwin called such crystals mosaic crystals and made the following assumptions to derive the intensity formula from such crystals.

(a) The X-ray beam travels through the crystal with the velocity of light in free space.

(b) The X-ray beam once scattered is not rescattered.

(c) No account is taken of the exchange of energy between the incident and diffracted beams.

The observed integrated intensity from a mosaic crystal is then given by

$$I(\underline{h}) = \frac{E(\underline{h}).\omega}{I_o} = \left(\frac{Ne^2}{mc^2}\right)^2 . \lambda^3 . \frac{(1 + \cos^2 2\theta)}{2 \sin 2\theta} . |F_o(\underline{h})|^2 . dv \qquad (1.13)$$

where the symbols have the meaning already explained.

However, this intensity formula did not explain satisfactorily the intensities obtained for strong reflections in some simple structures like Nacℓ (Bragg, James and Bosanquet, 1921*b*). The experimental integrated intensities were lower than the expected ones, even after normal photoelectric absoprtion corrections. This was first explained theoretically by Darwin, who pointed out that due to small angular misorientations of the adjacent mosaic blocks the X-ray beam penetrates deeply into a mosaic crystal before reaching the mosaic blocks which are identical in orientation to those near to the X-ray source and which will reflect the same

part of the beam again. Attenuation of the X-ray beam by Bragg scattering from identically oriented mosaic blocks is known as 'secondary' extinction for which there is no coherence between the beams diffracted from various blocks and therefore intensities are added up and not the amplitudes. In fact, the idea of mosaic blocks is purely hypothetical and has been adopted for mathematical convenience. A more realistic model would be the one based on dislocations and other defects in the crystals but this makes the problem very complex to solve.

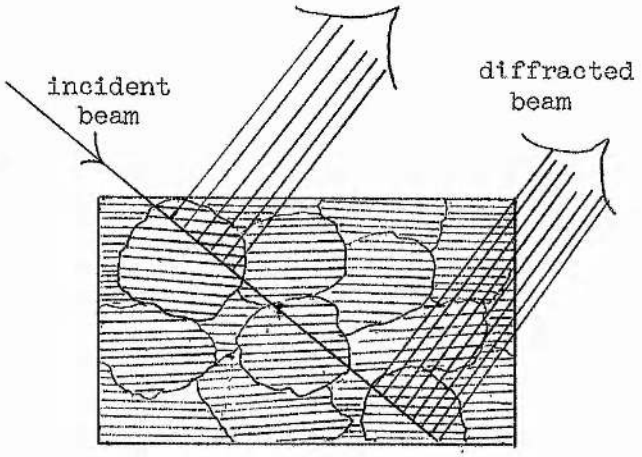

Randomly oriented mosaic blocks.

In the case of a single mosaic block the atomic planes are aligned and each atom scatters a fraction of the incident energy into the diffracted beam. Thus the atoms further away from the X-ray source receive less energy by the amount diffracted by the preceding atoms. Also the beams which are twice, four times, six times scattered differ in phase from the primary beam by multiples of π . A similar situation arises for once, three times and five times scattered beams. These effects result in the attenuation of the primary beam and Darwin who first studied the effect theoretically called it 'primary extinction'.

In perfect crystals, the waves scattered are strictly coherent and hence their amplitudes are added to obtain the scattering from the whole crystal. The integrated reflection from a semi-infinite non-absorbing perfect crystal in symmetrical Bragg case is given by

$$\frac{E(\underline{h}).\omega}{I_o} = I(\underline{h}) = \frac{8\, N\, e^2 \lambda^2}{3\ \pi mc^2} \quad \frac{(1 + |\cos 2\theta|)}{2 \sin 2\theta} \cdot |F_o(\underline{h})| \qquad (1.14)$$

It can be seen from equations 1.13 and 1.14 that for mosaic crystals the integrated intensity is proportional to $|F_o(\underline{h})|^2$, whereas, for perfect crystals the integrated intensity is proportional to $|F_o(h)|$.

For a more satisfactory explanation of the integrated intensities from a finite size crystal, Zachariasen (1967) has developed a general theory of X-ray diffraction. He has assumed Darwin's model of a mosaic crystal and taken into account the exchange of energy between the incident and the diffracted beams within each perfect block composing the real crystal.

According to Zachariasen the intensity formula for a sphere with small absorption is

$$P = P_k\, y$$

where P is the observed integrated intensity

P_k the kinematic intensity

y the extinction factor

and further

$$P_k = P_o\, v.\, Q_o.A(\mu).p_1$$

$$\text{and } y = \left(1 + 2\,\frac{p_2}{p_1}\,\bar{x}_o\right)^{-\frac{1}{2}}$$

$$\text{where } Q_o = \left|\frac{e^2\, F_k(\underline{h})}{mc^2\, V}\right|^2 \frac{\lambda^3}{\sin 2\theta}$$

$$\frac{p_2}{p_1} = \frac{1 + \cos^4 2\theta}{1 + \cos^2 2\theta}$$

$$p_1 = \frac{1 + \cos^2 2\theta}{2}$$

$$\bar{x}_o = \beta\, Q_o \left[\bar{t} + (\bar{T} - \bar{t}) \Big/ \sqrt{1 + \left(\frac{\beta}{g}\right)^2}\right] \qquad (1.15)$$

$\beta = \frac{r}{\lambda}$ for a spherical domain of radius r.

$\bar{t}$ is the mean path length through a single domain and is assumed to be $^3/_2$ r.

$\bar{T}$ is the mean path length through the crystal.

V is the volume of a unit cell.

r is the mean radius of a perfect crystal domain in the specimen.

g is a measure of the width of the mosaic spread distribution.

P_o is the incident intensity.

v is the irradiated crystal volume.

$A(\mu)$ is the transmission factor and can be written as

$$A(\mu) = \frac{\int \exp(-\mu T) dv}{v}$$

μ being the linear absorption coefficient and T the path through the crystal.

It is assumed that the observations are made in the plane of the incident and diffracted beams and that $r \ll \bar{T}$. Misalignment of the domains is assumed to obey an isotropic Gaussian distribution law, $W(\Delta) = \sqrt{2}.g \exp(-2\pi g^2 \Delta^2)$ where Δ is the angular deviation from the mean orientation and half width, $\Delta_{\frac{1}{2}}$, is given by

$$\Delta_{\frac{1}{2}} = g^{-1} (\text{Log}2/2\pi)^{\frac{1}{2}} = \frac{0.332}{g} \qquad (1.16)$$

The terms $\beta Q_o \bar{t}$ and $\beta Q_o(\bar{T}-\bar{t}) \Big/ \sqrt{(1 + (\frac{\beta}{g})^2}$ represent the corrections for primary and secondary extinctions. According to Zachariasen, primary extinction is assumed to be negligible in most mosaic crystals of small size, then equation 1.15 reduces to

$$\bar{x}_o = \frac{r Q_o \bar{T}}{\lambda} \left[1 + \left(\frac{r}{\lambda g}\right)^2\right]^{-\frac{1}{2}} \qquad (1.17)$$

or $$\bar{x}_o = \frac{r^* \bar{T} Q_o}{\lambda}$$

where $r^* = r \left[1 + (\frac{r}{\lambda g})^2\right]^{-\frac{1}{2}}$

Equation (1.17) represents the equation for secondary extinction.

Hence Zachariasen defines the real mosaic crystals to be of two types.

Type I

In such crystals the distribution function W is much wider that the diffraction pattern from a single domain, i.e.,

$$r/\lambda g \gg 1$$

$$\therefore \quad \bar{x}_o = g \, Q_o \, \bar{T}$$

$$\text{or } \bar{x}_o = g \left| \frac{e^2 F_K(\underline{h})}{mc^2 V} \right|^2 \frac{\lambda^3}{\sin 2\theta} \cdot \bar{T} \qquad (1.18)$$

This equation shows explicitly that extinction in type I crystals is λ^3 dependent.

Type II

In these crystals, the diffracted pattern from a single domain is much wider than the distribution function W

$$\text{i.e.,} \quad \frac{r}{\lambda g} \ll 1$$

$\therefore$ Equation (1.17) reduces to

$$\bar{x}_o = \frac{r}{\lambda} Q_o \bar{T}$$

$$\text{or } \bar{x}_o = r \left| \frac{e^2 F_K(\underline{h})}{m.c^2.V.} \right|^2 \frac{\lambda^2}{\sin 2\theta} . \bar{T} \qquad (1.19)$$

Thus the extinction in type II crystals is λ^2 dependent. Also it is clear that the integrated intensity for a type I crystal is dependent upon g whereas in type II crystals, it is dependent upon r.

The extinction parameters r and g can be determined by using two or more wavelengths. It can be seen that the greater the value of Q_o, the greater the extinction and so extinction effects are important for low order reflections. Extinction effects are more severe on diffracted intensities from larger crystals than those from the smaller ones because of the longer path lengths traversed.

The Zachariasen's theory for secondary extinction correction has been applied to the observed structure factors for a lithium fluoride crystal and in chapter IV it is shown that although the application of Zachariasen's theory to a small crystal improves the fit between the observed and calculated structure factors, the value of r^* so obtained is physically unreasonable. It is also deduced that the particular sample of lithium fluoride crystal used approximates closely to type II of the two crystal types. A different procedure has been adopted to make extinction corrections for α-glycine data. This consists in using four different wavelengths and thus varying the extinction parameters. This work has been described in chapter V.

In the above work, the integrated intensities are measured on a relative scale and the inherent difficulty of finding the absolute scale of the observed structure factors poses a problem. For solving this problem a new method called the Pendellösung method has been developed and used to find the absolute value of structure factors for silicon crystals. This work has been described in chapter VI.

CHAPTER II

EXPERIMENTAL

2.1 The Siemens Four-Circle Diffractometer

X-ray intensity measurements by photographic methods are both tiresome and time consuming and yield results of limited accuracy. Automatic four-circle diffractometers have gained increasing importance and make it possible to measure integrated intensities to a predetermined counting statistics accuracy. For this reason the on-line Siemens four-circle diffractometer, designed by W. Hoppe, was used to obtain accurate intensity measurements for α-rhamnose monohydrate (chapter III), lithium fluoride (chapter IV) and α-glycine (chapter V). Consequently, a detailed account of this instrument will be given in this chapter.

The Siemens four-circle diffractometer has a quarter χ-circle and is designed on the principle of normal beam equatorial geometry, in which both the primary and diffracted beams lie in the equatorial plane normal to the oscillation axis ω as shown in fig. 1. To bring any h k ℓ reflection into the diffracting position, the corresponding reciprocal lattice point P can be moved to a point R on the Ewald sphere by ω rotation and then turned through an angle to bring into diffracting position D on the equatorial plane. In a three circle diffractometer (Busing and Levy 1967) this can be done only in two ways but in a four-circle diffractometer this can be done in an infinite number of ways.

A perspective view of the four circle diffractometer is shown in fig. 2 for zero position of the circles. The 2θ-circle which controls the detector is mounted on the outside of the heavy base of the diffractometer and the ω circle is concentric with it.

Normally the ω and 2θ -circles are coupled together by a magnetic clutch but these can be uncoupled by demagnetising the clutch. The χ -circle can move through an arc of a vertical circle around the horizontal χ-axis. The ϕ circle is supported at segment S on a metal base with a height adjustable goniometer head. Three stepping motors drive the ϕ, χ and ω circles. One step corresponds to 0.01° on ω, ϕ and χ circles and 0.02 on 2θ-circle, the 2θ and ω circles being coupled in the gear ratio of 2:1. Digitizer drums on all three circles enable the fractional settings to be checked to $\frac{1^\circ}{100}$. The zeros of the ω, χ and ϕ digitizers correspond to the zero setting of the three circles when the circles are in null position. The zero positions of the circles are first sensed by micro-switches and then adjusted to zero by digitizers. The circumference of the digitizers corresponds to $\frac{1}{2}^\circ$. A correction to the nominal value is within $\pm$ 0.25° during a digitizer check. Any major setting errors must be detected during the zero checks.

Two discs which can revolve freely and independently about concentric axis are connected to the diffractometer in the path of the incident X-ray beam. One of these discs contains five aluminium attenuators of various thicknesses for progressively reducing the primary beam. In the second disc houses the K-β filter and a lead shield.

The diffracted intensity is received by a scintillation counter and is recorded by a counting rate-meter in the form of pulse counts.

For checking the crystal alignment, the front of the detector window is fitted with half-shutters dividing the aperture vertically and horizontally. The crystal is correctly adjusted when the

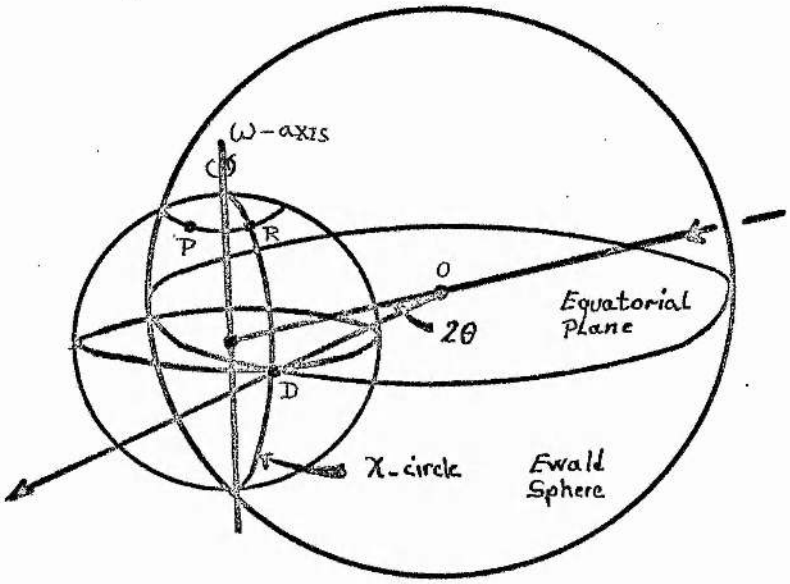

FIG 1.

Figure 2

The Siemens four-circle diffractometer

1. ϕ -circle
2. Quarter χ -circle
3. 2θ -ring
4. Scintillation counter
5. Adjusting screw for shifting the X-ray tube along its longitudinal direction
6. Goniometer head
7. Heavy goniometer base
8. Rigid top of the X-ray generator table
9. β-filter and attenuator discs unit
10. Extension at the base plate for mounting the adjusting microscope stand

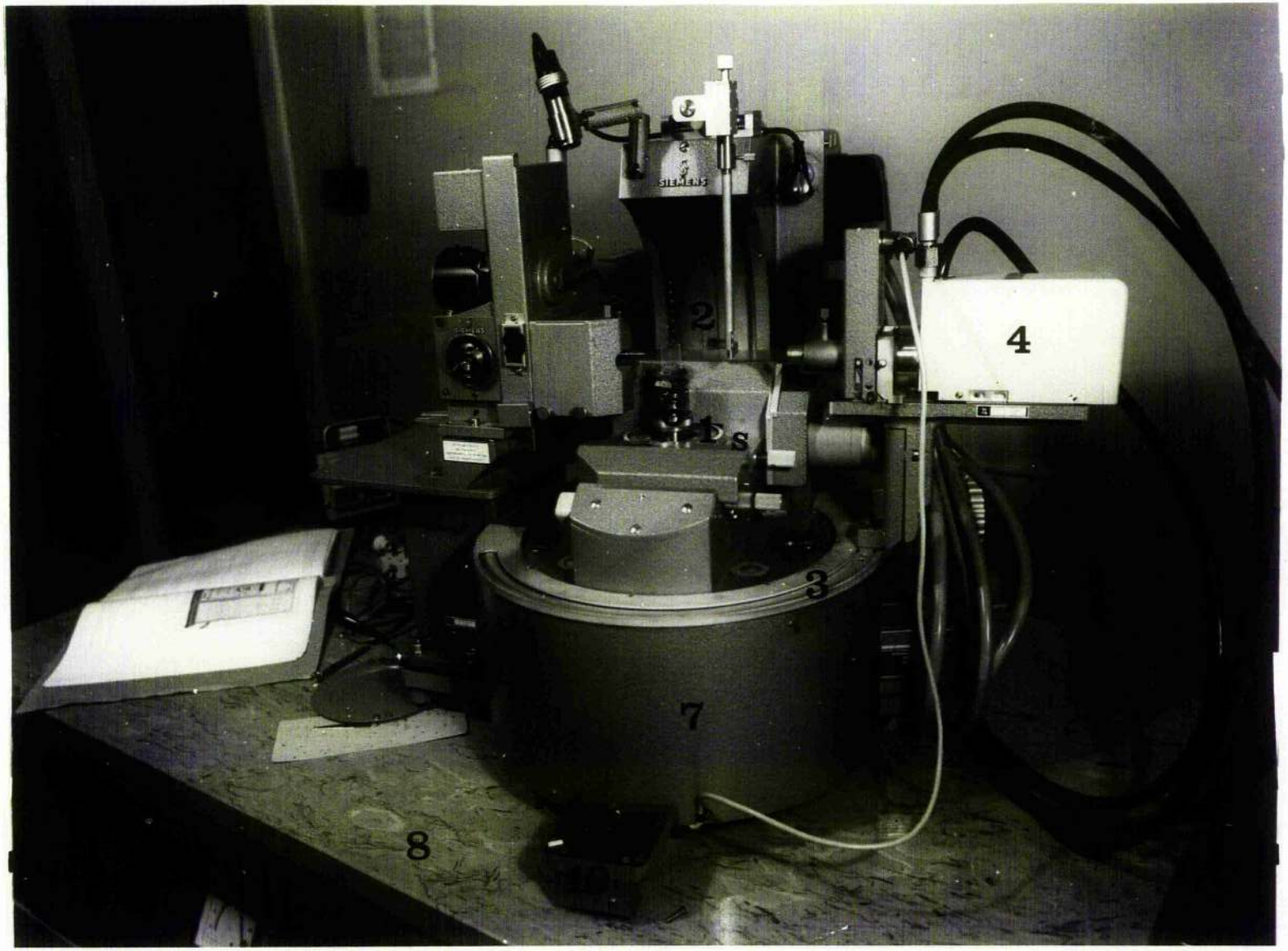
SIEMENS
2
4
3
7
8

crystal centre is at the position of intersection of ϕ, χ and ω-axes and the introduction of half shutters reduces the diffracted intensity exactly to half in all cases.

2.2 Crystal Alignment

Before starting the experiment for intensity measurements, it was ensured that the crystal was completely immersed in the X-ray beam. The crystal was centred by using the alignment microscope and adjusting the translational movements of the goniometer head. Then a reflection was put into the diffracting position and the X-ray focal spot adjusted by translatory motion of the X-ray tube for the maximum diffracted intensity. The crystal alignment was checked by comparing the integrated intensity of h k ℓ and its equivalent reflections. For the measurement of integrated intensities on a diffractometer, it is preferable to mount the crystal in an arbitrary setting. If the crystal was mounted along a principal axis (in cubic crystals) or a unique axis (in monoclinic crystals) then it was off-set by a few degrees to avoid multiple reflections.

2.3 Types of Scan

The integrated intensity of a reflection is proportional to the amount of energy diffracted by a crystal when moving with a uniform angular velocity through the Bragg reflecting position. The integrated intensity is proportional to the total number of X-ray quanta received by the detector as the crystal rotates through a small angular range about the Bragg position. During such movement of the crystal the detector can either be kept stationary or be coupled to the crystal motion. Accordingly there are two usual procedures which can be adopted to measure the diffracted intensity

(a) Moving crystal - moving detector.

(b) Moving crystal - stationary detector

In the present experiments moving crystal moving detector technique was used. This type of scan is called ω-2θ scan. The scintillation detector shaft is coupled to the crystal shaft by the gear ratio 2:1 so that when the crystal rotates through an angle (θ - $\delta\theta$) to (θ + $\delta\theta$), the detector moves through an angle (2θ - 2$\delta\theta$) to (2θ + 2$\delta\theta$), where 2$\delta\theta$ is the small angular range about the exact Bragg position.

However, Werner (1972) has pointed out that ω-2θ scan is essentially not the best procedure for the measurement of integrated intensities. He suggests an optimum scan in which the crystal and detector motions are coupled in a way such that the centroid of the diffracted beam always aligns with the centre line of the detector.

To be sure that the full diffracted beam entered the scintillation counter, preliminary experiments were carried out using different sizes of the receiving collimators at the detector window and that collimator selected which gave the best peak to background ratio. However, this condition is not independent of the angle of scan. If the angle of scan is too small it may not include the whole of the peak or if it is too large the background counts of one reflection may include a part of the neighbouring peak. Therefore, tests were made by using different angles of scan for various reflections widely spaced in the reciprocal space to ensure that λ_1, λ_2 components were included in the integration process. The best values chosen gave the best peak to background ratio and uniform background on either side of the peak.

2.4 On Line Operation of the Four-circle Diffractometer with the IBM 1130 Computer

The setting of the crystal and detector shafts of a diffractometer and the measurement of each Bragg reflection involves repetition of the same process and therefore computers are best suited for this purpose. The Siemens four-circle diffractometer can be operated on line for automatic data collection or from the keyboard of the IBM 1130 computer. The computer has a 16 bit word plus two check bits and consists of a memory of 16K immediate access store and a disc of half a million words capacity. It has been programmed by Dr. D.F. Grant of this department for automatic control of the diffractometer and this has made it possible to measure the integrated intensities from a single crystal to a very high degree of accuracy. All the diffractometer programmes are stored in core image on the computer disc. Calling of a programme DSET2 can perform the following operations in any sequence when operated from the keyboard of the computer, using coded switch settings.

(a) Zero Circles: This operation drives the three circles to zero position (null position). Their positions are checked and adjusted.

(b) Set Circles: Through this operation the circles move simultaneously through given angles but their positions are not checked.

(c) Set Attenuators: This operation sets one of the six attenuators in the path of X-ray beam and also inserts β-filter.

(d) Set Filters: This operation sets the filter or the lead shield in the path of X-ray beam.

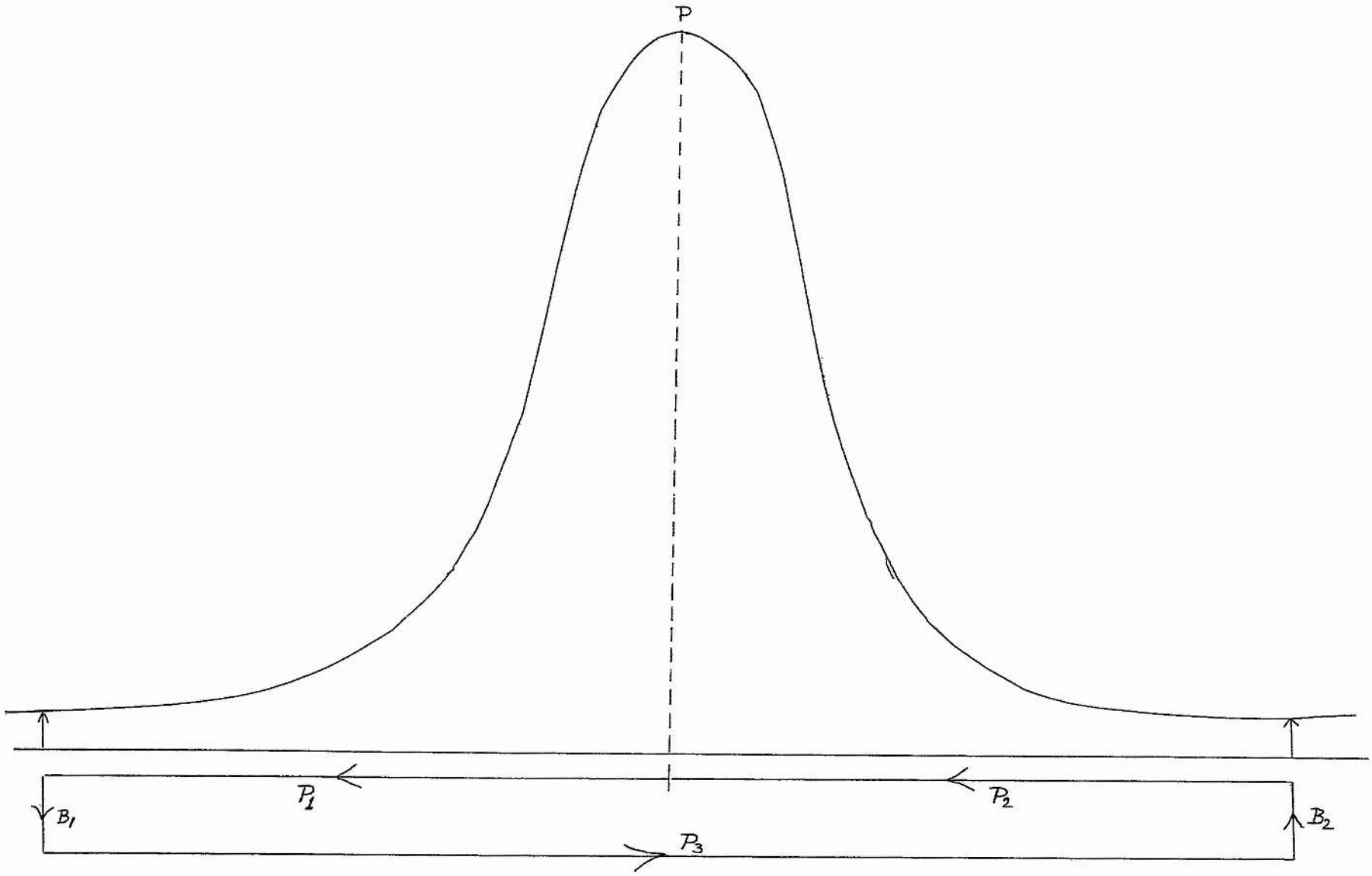

FIG 3.

(e) Orientation Matrix: Orientation matrix defines the original position of the crystal on the diffractometer. From the (h k ℓ) indices and the ϕ, χ, ω and 2θ values of any three non-coplanar reflections forming a right handed system, this operation determines the orientation matrix. From the matrix, it extracts the reciprocal and real cell parameters (Busing and Levy, 1967) and punches on to the cards the elements of the orientation matrix. This forms a part of the data cards to be used for automatic control of the diffractometer.

(f) Five Point Measurement: The five point measuring cycle is illustrated diagramatically in fig. 3. This operation opens the shutter at the peak of the reflection. The counter then scans through the half peak P_1, measures background B_1, goes through the peak P_3, measures background B_2 and finally measures the half peak P_2. The time spent for measuring the full peak is double the time for measuring the backgrounds so that the integrated counts for the peak are given by

$$P = (P_1 + P_2 + P_3) - 2(B_1 + B_2)$$

$$= (P_K - B)$$

The time spent for measuring a reflection can be chosen to keep the counting statistics at a desired level. In all the diffractometer experiments, for intensity data collection, the five point measuring cycle was employed. By counting for 0.5 millisecond at the peak of the reflection with maximum attenuation, the correct attenuator setting is made automatically to ensure that maximum counting rate does not exceed a limit where

counts will be lost in the counter. If using maximum attenuation the recorded counts are still exceeding the maximum count limit, then, this is indicated. Dead time corrections are required for such reflections. However, this situation never arose during the data collection of any of the crystals used. Facilities are also available to measure a given reflection using a particular attenuator.

The five point measuring cycle has the following advantages:

Any mis-setting of the crystal manifests itself in the two half peaks or two backgrounds being highly asymmetric. Thus it gives a good check on any movement of the crystal during the data collection period. Measurement of half peaks also gives information about the shape of the individual peaks.

(g) Line Profile: The ω-2θ scan as used in the four-circle diffractometer is a step scan of minimum step size 0.02°. By using this operation the counts can be accumulated at every step for a given time and for a given angle of scan. The angle of scan and time per step can be varied at will.

(h) Clutch in and Half-Shutters out: Calling of this operation restores the clutch and half shutters to their normal position.

(k) Clutch out: This operation disengages the ω-2θ clutch.

(m) Vertical Half-Shutters : This operation places the vertical half-shutters in front of the scintillation counter.

BLOCK DIAGRAM FOR DIFF 6 PROGRAMME

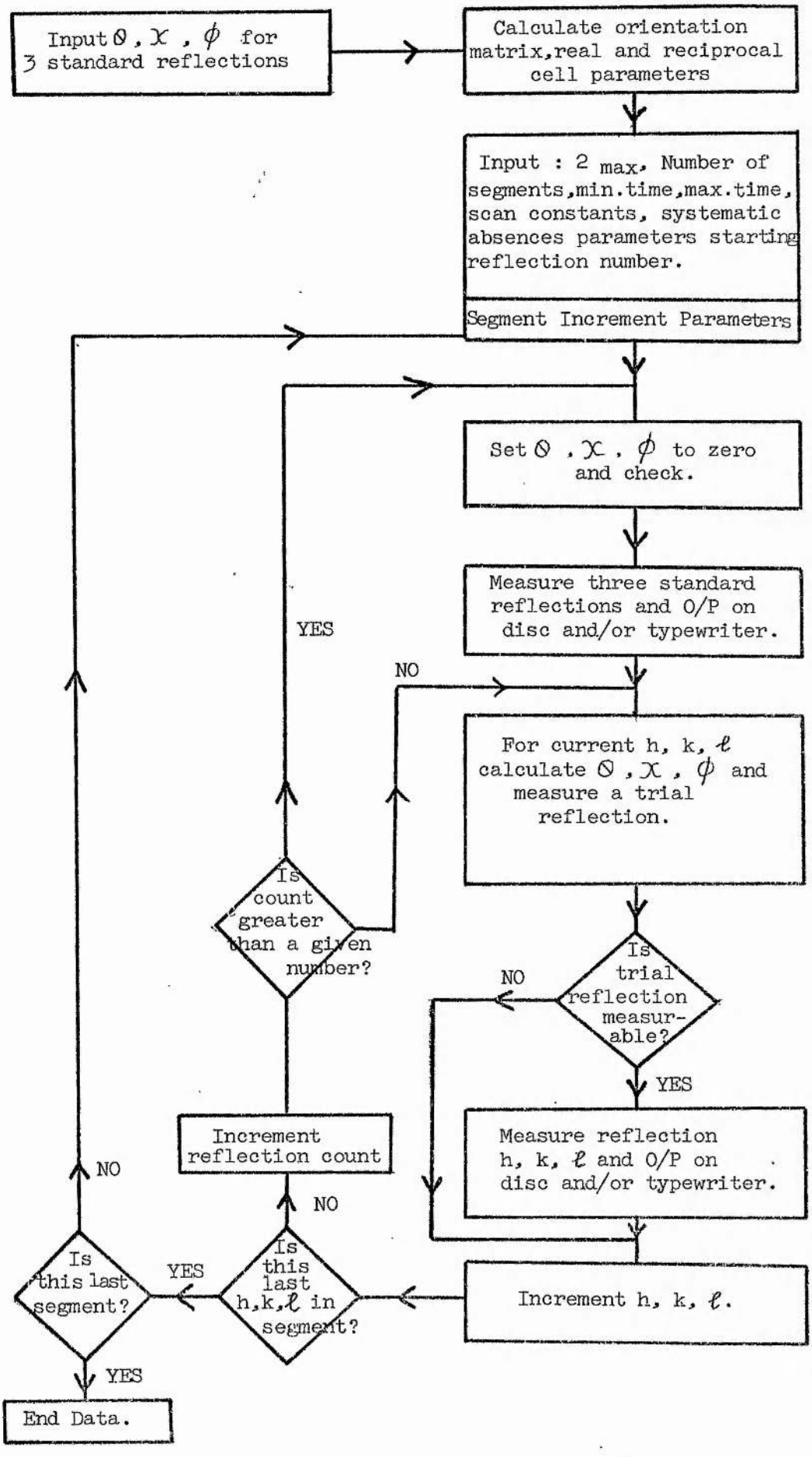

DIAGRAM 4.

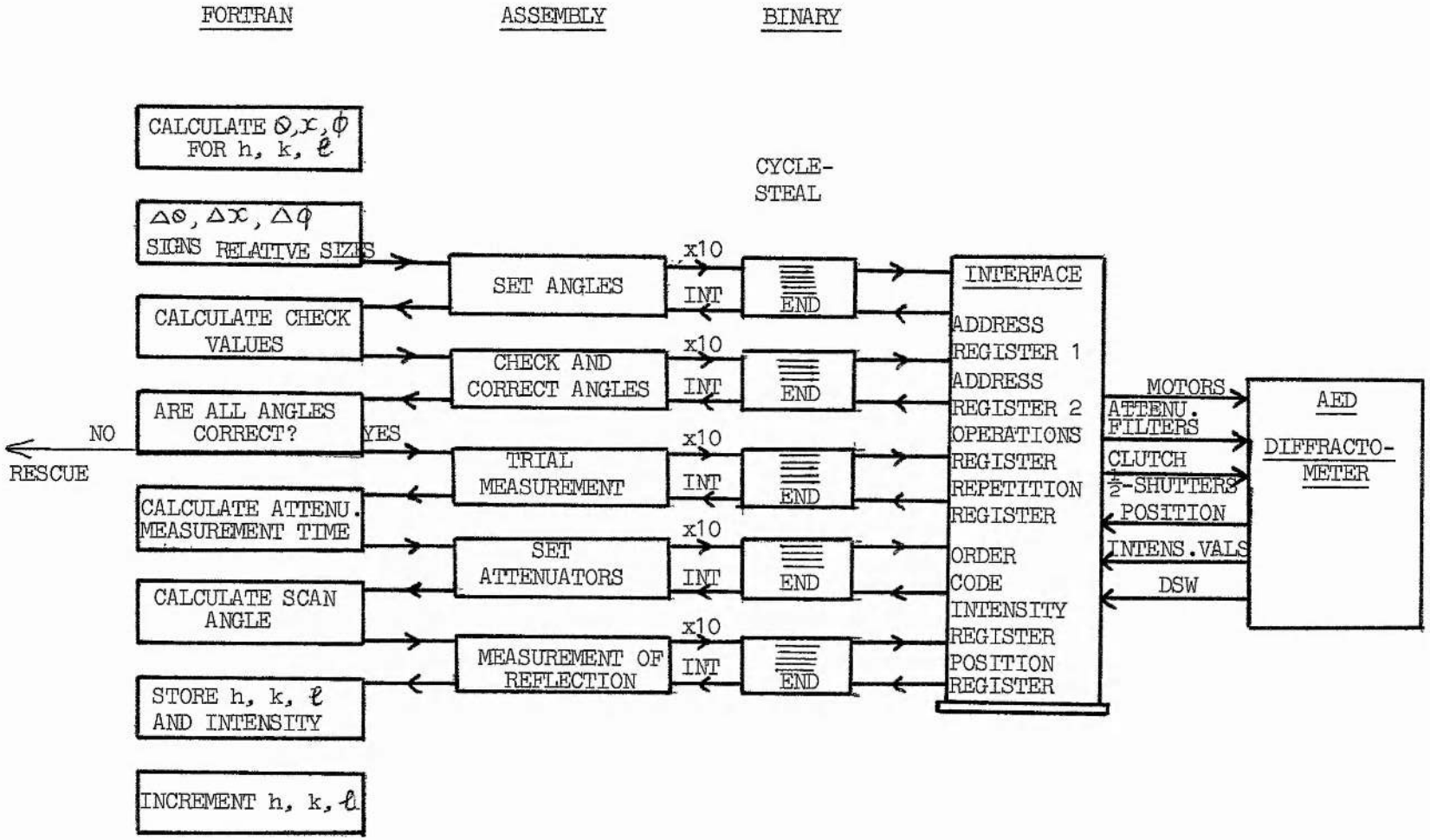
FORTRAN
ASSEMBLY
BINARY
CALCULATE Θ, χ, φ FOR h, k, ℓ
ΔΘ, Δχ, Δφ SIGNS RELATIVE SIZES
CALCULATE CHECK VALUES
ARE ALL ANGLES CORRECT?
NO
RESCUE
YES
CALCULATE ATTENU. MEASUREMENT TIME
CALCULATE SCAN ANGLE
STORE h, k, ℓ AND INTENSITY
INCREMENT h, k, ℓ
CYCLE-STEAL
SET ANGLES
CHECK AND CORRECT ANGLES
TRIAL MEASUREMENT
SET ATTENUATORS
MEASUREMENT OF REFLECTION
x10
INT
END
INTERFACE
ADDRESS REGISTER 1
ADDRESS REGISTER 2
OPERATIONS REGISTER
REPETITION REGISTER
ORDER CODE
INTENSITY REGISTER
POSITION REGISTER
MOTORS
ATTENU. FILTERS
CLUTCH
½-SHUTTERS
POSITION
INTENS.VALS
DSW
AED
DIFFRACTO-METER

Diagram 5

(n) Horizontal Half-Shutters: Calling of this operation places the horizontal half-shutters in position in front of the scintillation counter.

2.5 Automatic Control

For on-line operation the diffractometer is directly connected to the controlling computer, the computer being connected to the input and output channels of the diffractometer through an interface. Initially, three non-coplanar reflections forming a right handed system are chosen and the orientation matrix determined. The orientation matrix give sufficient and necessary information about the initial setting of the crystal on the diffractometer. This information combined with the information about the segments of the reciprocal space to be measured, minimum and maximum value of 2θ required, the order in which the reflection indices are to be taken and knowledge of the systematic absences, enables reciprocal space to be measured in a systematic way. The programme allows for a variable angle scan or a fixed angle scan (see appendix C).

The DIFF6 programme also offers the facility of using a test scan for a short time before the measurement of each reflection. The block diagram 4 shows how the reciprocal space is measured systematically on a closed loop operation. Diagram 5 shows the full control of the diffractometer. Facilities also exist for the measurement of a given number of reflections in any order. The program used for this purpose is DIFC1.

CHAPTER III

THE REFINEMENT OF THE CRYSTAL STRUCTURE OF α-RHAMNOSE MONOHYDRATE

3.1 Introduction

The crystal structure of α-rhamnose monodydrate ($C_6H_{12}O_5.H_2O$) was determined by McGeachin and Beevers (1957); $a = (7.910 \pm 0.005)$Å; $b = (7.914 \pm 0.004)$Å; $c = (6.674 \pm 0.004)$Å; $\beta = 95.52° \pm 0.10°$, space group $P2_1$. The least-squares refinement had been carried out on data on two projections with $R_{h\,o\,\ell} = 7.6\%$ and $R_{h\,k\,o} = 6.3\%$ and the isotropic thermal parameters were given no absolute significance. It was therefore felt in view of the current interest in pyranose ring geometry (Chu and Jeffrey, 1968) that a more accurate structure should be obtained using full three-dimensional data.

In the original work, the large structure factors were systematically lower than the calculated structure factors, indicating extinction in the observed data. The empirical formula used for extinction corrections was $I' = \frac{I}{(1-gI)}$ where I is the integrated intensity and g is an extinction parameter the value of which was assumed to be 8.1×10^{-5}. It was therefore decided to investigate extinction in the structure with a view to make more reliable corrections (Zachariasen, 1967). It was also thought desirable to make a statistical comparison of bond distances and angles with those of other pyranose structures recently reported (Rogers and Haugh, 1968, Chu and Jeffrey, 1968).

3.2 Experimental

A commercially available powder sample was used to grow single crystals of α-rhamnose monohydrate by slow evaporation of a

solution of 90% methyl alcohol and 10% water at 18°C. The crystal obtained were colourless and needleshaped. An approximately cylindrical crystal (dimensions 0.03 x 0.02 cm in diameter) was chosen. Small particles of the crystal powder sticking to its surface were dissolved in a small drop of methyl alcohol spread over a clean glass plate and the crystal quickly removed. It was then stuck at the end of a glass fibre with shellac and mounted on the goniometer head along the needle axis with Sira wax. Preliminary diffraction work on a Weissenberg camera indicated that the crystal was mounted along the c-axis. A zero layer Weissenberg photograph showed the crystal to be single and suitable for intensity data collection. The density, found by flotation method in a mixture of benzene and chloroform, was 1.457 ± 0.002 gm/cm^3.

The crystal was removed from the Weissenberg goniometer and transferred to the computer-controlled Siemens four-circle diffractometer for the collection of intensity data. A manual search was made for three non-coplanar reflections forming a right handed system, two of these being chosen close to the equatorial plane of the diffractometer ($\chi \approx 2°$) and the third was located in the a^*c^* plane. As explained in appendix B, from a knowledge of setting angles for the three non-coplanar reflections and the wavelength used, reciprocal cell parameters were determined and from these direct cell parameters obtained. The unit cell dimensions and other crystal data are as follows

$a = 7.906 \pm 0.002$Å

$b = 7.921 \pm 0.002$Å

$c = 6.673 \pm 0.002$Å

$\beta = 95.59° \pm 0.05°$

$V = 415.87$A^3

$D = 1.457 \pm 0.002$ gms/cm^3

It can be seen that values of these parameters do not differ significantly from those of Beevers and McGeachin (1957).

3.3 Measurement of Intensities

The experimental conditions chosen were as follows

CuK$\bar{\alpha}$ radiation ($\bar{\lambda}$ = 1.5418Å) with a nickel β-filter.

Siemens Generator: 30KV; 18 M.A.

Pulse Height Analysis: Base line = 7.5 volts in integral position.

Scintillation Counter (NaI window)

E.H.T. applied = 1207.5 volts.

Diameter of receiving Collimator = 4 mm.

Size of step scan used = 0.01°.

A choice of the optimum size of the collimator at the scintillation counter was made as explained in chapter II. A short trial run gave an a-priori estimate of the measuring time for the weak reflections to keep the counting statistics below 2% on the integrated intensities. The moving crystal moving detector technique was employed with a 2Θ scan range of ± 1.2° and each reflection was measured for a total period of 3 minutes including background on a five point measuring cycle. Three standard reflections were measured after every two hours and no statistically significant changes in the intensities of these reflections were recorded over the data collection period of seven days.

All reflections with $\theta < 70°$ were measured, four reflections being discarded since their peaks were indistinguishable from the background and thus the integrated intensities of total of 833 reflections were obtained.

3.4 Data Processing

Since the integrated intensities were measured on different attenuators, attenuator factors of the six attenuators were determined by a separate experiment and each reflection intensity multiplied by its appropriate attenuator factor. The intensities were also corrected for Lorentz and polarization factors as explained in chapter I. Thus a set of relative observed structure factors $|F_o(\underline{h})|$ was obtained. No absorption corrections were applied. $\mu(CuK\bar{\alpha}) = 3.54\ cm^{-1}$.

3.5 Refinement and Accuracy

The refinement was carried out by a full-matrix least-squares programme on an IBM 360 computer. The initial positional parameters of the carbon and oxygen atoms were those given by McGeachin and Beevers (1957) and all atoms were given an initial temperature factor of $1.5A^2$. The atomic scattering factors used for computing the calculated structure factors were those given in the International Tables for X-ray Crystallography (1962), and all structure factors were initially given unit weight. After five cycles of refining positional parameters and isotropic temperature factors the R index was 0.089 and four further cycles with anisotropic temperature factors reduced the R index to 0.054. All fourteen hydrogen atoms were clearly visible from a difference Fourier synthesis and in all further refinements these atoms were included with their temperature factors of $1.5A^2$ but their parameters were not refined.

Individual weights $w(\underline{h})$ were assigned to each structure factor $F_o(\underline{h})$ as described by Killean and Lawrence (1969)

$$\left[w(\underline{h})\right]^{-1} = \sigma^2(\underline{h}) = \sigma_1^2(\underline{h}) + c^2 \left|F_o(\underline{h})\right|^2 + k^2 \left\langle \left| Fo(\underline{h}) \right|^2 \right\rangle$$

where $\sigma_1^2(\underline{h})$ is the variance of $F_o(\underline{h})$ due to counting statistics and as applied to four circle diffractometer with five point measuring cycle is given by

$$\sigma_1^2(\underline{h}) = \frac{K}{4(Lp)} \cdot \frac{(P_K + 2B)}{(P_K - B)}$$

C and k are constants for a given crystal, C being the assumed random instrument setting error and k being the fractional error in form factors due to bonding.

In this case $\sigma_1^2(\underline{h})$ was negligible for most reflections owing to a large number of counts accumulated during intensity measurements. A relationship between C^2 and k^2 was obtained by using a factor (Kitaigorodskii, 1957) as a measure of goodness-of-fit for random errors only.

$$G^2 = \frac{\sum_{\underline{h}} |\Delta(\underline{h})|^2}{\sum_{\underline{h}} |F_o(\underline{h})|^2}$$

By taking the estimate of $\sigma(\underline{h})$ as $\Delta(\underline{h})$

$$G^2 = \frac{\sum_{\underline{h}} \sigma^2(\underline{h})}{\sum_{\underline{h}} |F_o(\underline{h})|^2}$$

$$\text{or} \quad G^2 = \frac{\sum_{\underline{h}} \sigma_1^2(\underline{h})}{\sum_{\underline{h}} |F_o(h)|^2} + C^2 + k^2$$

$$\therefore G^2 = S^2 + C^2 + k^2$$

$$\text{or } G^2 - S^2 = C^2 + k^2$$

At this point of refinement $G^2 = 0.0033$; $S^2 = 0.0000$

$$\therefore C^2 + k^2 = 0.0033$$

subject to the condition that individual value of C and k were taken to be those for which

$$M = \frac{\sum_{\underline{h}} \omega(\underline{h}) . \left|\Delta(\underline{h})\right|^2}{(m - n)} \quad \text{was a minimum}$$

where m = number of reflections

n = number of parameters refined

The minimum value of M was 1.21 when

$$C^2 = 0.0000 \quad ; \quad k^2 = 0.0033$$

Using these values of C^2 and k^2 individual weights were then calculated for all reflections and three more cycles of refinement carried out. This reduced R to 0.047 and gave a value of M of 0.83- lower than the expected unity. It was clear that $\sigma^2(\underline{h})$ was overestimated. Therefore $C^2 + k^2$ was recalculated as before and the values obtained were

$$C^2 = 0.0000 \quad ; \quad k^2 = 0.0019$$

Further refinement then gave a final R index of 0.039 and a final M value of 1.01. The value obtained for C^2, which has been considered to be a measure of the accuracy of the intensity measurements suggests that observed structure factors have been determinined very accurately. The value obtained for $k^2 = 0.0019$ suggests about a 4% error in the scattering factor curves due to bonding (Killean and Lawrence, 1969).

A check on the validity of the weighting scheme was made towards the end of refinement. If the weights assigned to the structure factors were correct then distribution of $|\Delta(\underline{h})| / \sigma(\underline{h})$ should obey a Gaussian distribution law.

The computed value of distribution of $|\Delta(\underline{h})| / \sigma(\underline{h})$ was found to have approximately Gaussian form

$$N = 70.0 \exp \left\{ -(0.46) \left(\frac{|\Delta(\underline{h})|}{\sigma(\underline{h})} \right)^2 \right\}$$

65.9% of the reflections have a value of $\frac{|\Delta(\underline{h})|}{\sigma(\underline{h})}$ less than 1.0 and for 96.9% this value is less than 2.0. For one reflection 110, $|\Delta(\underline{h})|/\sigma(\underline{h})$ is 5.1 showing that it has been affected by systematic error. The observed and calculated structure factors have been shown in the Table 1, the final positional parameters in Table 2 and the thermal parameters in Table 3.

3.6 Conclusions

A close inspection of the large observed and calculated structure factors shows that the calculated values are not systematically larger than the observed values and hence for a particular sample of the crystal used no extinction corrections were necessary. A comparison between the observed structure for this work and those of McGeachin and Beevers shows that in the latter work some of the larger structure factors had been underestimated, which probably accounts for the very small temperature factors they obtained. However, it was thought justified to make a statistical comparison of bond lengths and bond angles with those of other sugar structures (Rogers and Haugh 1968, Chu and Jeffrey 1968).

A schematic diagram of the structure showing the identification of atoms is shown in fig. 1 and the bond lengths and bond angles with their standard deviations are listed in Table 4. The average C-C bond length is 1.524 $\pm$ 0.005Å with a standard deviation for each bond of 0.012Å as compared with a standard deviation of each bond from the least-squares refinement of about 0.004Å. The equivalent result for β-D glucose (Chu and Jeffrey, 1968) was 1.520 $\pm$ 0.003 Å and for α-D glucose monohydrate (Rogers and Haugh, 1968) 1.524 $\pm$ 0.003 Å which are not significantly different from that in the present experiment.

On the basis of t-test (Fisher and Yates, 1953) it can be seen that the C(4)-C(5) and C(5)-C(6) bond lengths are significantly different from each other and from all the other C-C bond lengths. In α-D-glucose monohydrate and β-D glucose, the C(5)-C(6) bond length is probably significantly smaller than the other C-C bond lengths but C(4)-C(5) is not.

The average C-O bond length, excluding the carbon atoms bonded to the oxygen atom in the ring and C(1)-O(1) is 1.424-0.003Å compared with 1.425 ± 0.003Å for both β-D-glucose and α-D-glucose monohydrate. As with these two sugars, the C(1)-O(1) bond length in α-rhamnose monohydrate, 1.401 ± 0.003Å was significantly different from the other bond lengths.

The C(5)-O(5) bond length differs significantly from all other C-O bond lengths while C(1)-O(5) does not. It has been noted by Snyder, Rosenstein, Kim and Jeffrey (1970) that in sugars where an oxygen atom is bonded to the C(6) atom in a direction parallel to the C(4)-C(5) bond as in α-D-glucose (Brown and Levy, 1965) no significant differences exist between bond lengths C(5)-O(5) and C(1)-O(5) but when the oxygen atom is bonded in a direction antiparallel to the C(5)-H(5) bond as in α-D-glucose monohydrate, a significant difference does exist. This difference can now be seen to exist when only hydrogen atoms are bonded to C(6). The bond lengths and angles differ significantly from those quoted by McGeachin and Beevers, the largest discrepancy being 0.049Å in the C(2)-O(2) bond which cannot now be considered significantly different from C(3)-O(3) and C(4)-O(4). The positions of hydrogen atoms are close to those given by McGeachin and Beevers with the exception of H(6) in the methyl group. The average C-H bond length for the earlier atoms in the ring was 0.96Å and for the methyl group was 1.06Å. The hydrogen bond distances are listed in Table 5 along with the O-H-O bond angles.

FIG 1

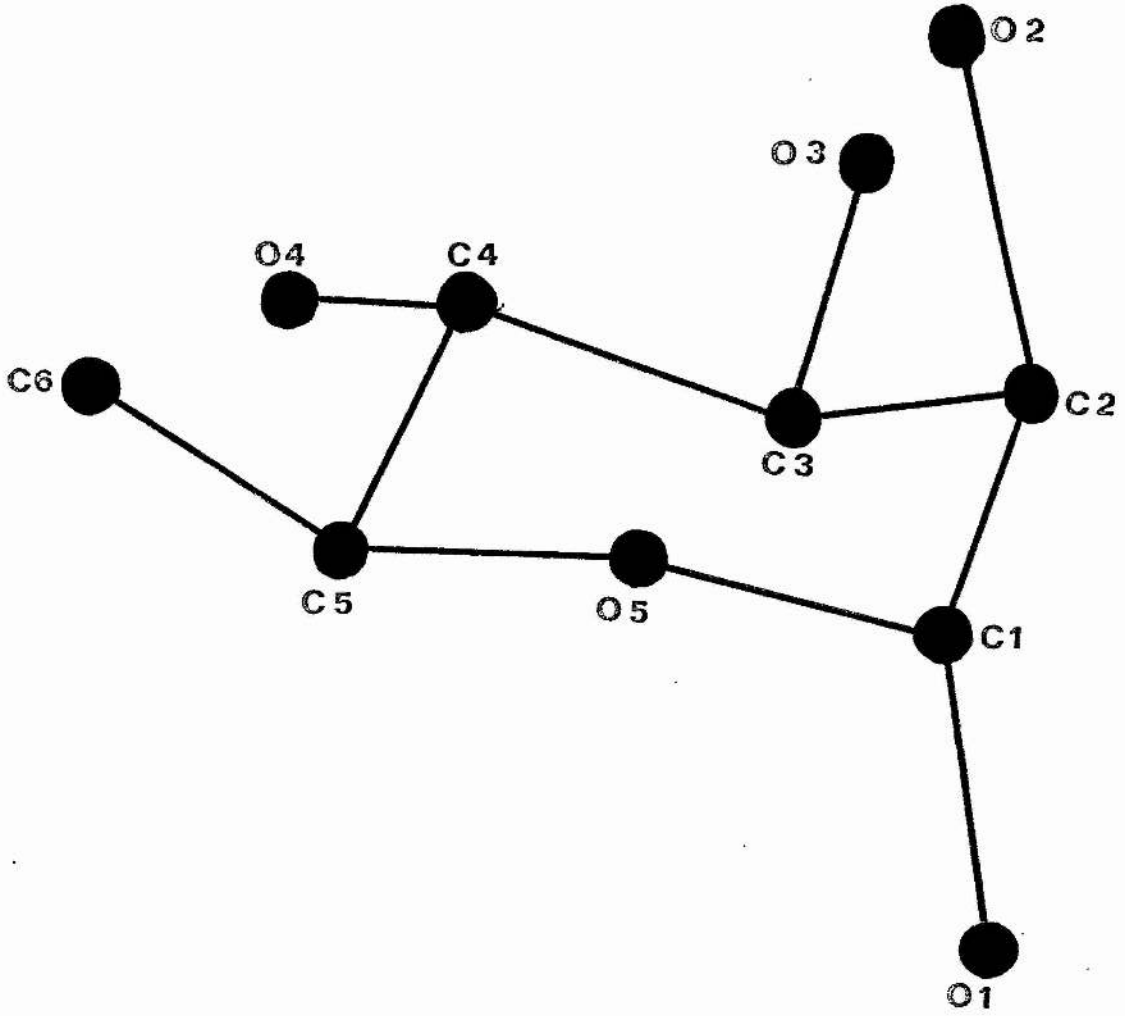

TABLE 1

A COMPARISON OF F_o AND F_c FOR α-RHAMNOSE MONOHYDRATE

TABLE 2

Final coordinates and standard deviation

	x/a	y/b	z/c
C(1)	0.0883 (3)	-0.1330	0.0789 (3)
C(2)	0.0083 (3)	-0.0909 (3)	0.2716 (3)
C(3)	0.1425 (3)	-0.0285 (3)	0.4330 (3)
C(4)	0.2333 (3)	0.1221 (3)	0.3511 (3)
C(5)	0.3145 (4)	0.0678 (3)	0.1601 (3)
C(6)	0.4023 (4)	0.2111 (5)	0.0609 (5)
O(1)	0.1898 (2)	-0.2771 (2)	0.1120 (2)
O(2)	-0.1187 (2)	0.0346 (3)	0.2244 (2)
O(3)	0.0576 (2)	0.0104 (2)	0.6052 (2)
O(4)	0.3602 (2)	0.1811 (3)	0.5012 (3)
O(5)	0.1820 (2)	0.0065 (2)	0.0139 (2)
O(6)	0.3266 (2)	0.5297 (3)	0.4624 (3)
H(1)	0.000	-0.140	-0.040
H(2)	-0.050	-0.185	0.320
H(3)	0.220	-0.113	0.460
H(9)	0.140	0.213	0.330
H(5)	0.380	-0.013	0.200
H(6)	0.460	0.135	-0.040
H(7)	0.320	0.313	0.010
H(8)	0.500	0.250	0.170
H(9)	0.140	0.035	0.705
H(10)	0.350	0.288	0.510
H(11)	0.405	0.585	0.455
H(12)	0.180	-0.325	0.020
H(13)	0.260	0.585	0.375
H(14)	-0.190	0.038	0.320

TABLE 3

Final anisotropic temperature factors x 10^5 defined as

$$-(h^2B_{11}+k^2B_{22}+l^2B_{33}+2hkB_{12}+2hlB_{13}+2klB_{23})$$

	B_{11}	B_{22}	B_{33}	B_{12}	B_{13}	B_{23}
C(1)	981 (33)	1054 (41)	810 (39)	-70 (30)	36 (29)	-132 (32)
C(2)	889 (31)	793 (38)	878 (41)	-95 (29)	135 (28)	23 (31)
C(3)	1078 (35)	696 (38)	747 (39)	121 (28)	45 (32)	14 (30)
C(4)	814 (32)	805 (40)	933 (41)	-12 (27)	-17 (30)	-78 (32)
C(5)	861 (30)	1164 (44)	1093 (43)	-45 (27)	104 (30)	-21 (34)
C(6)	1334 (44)	1804 (64)	1792 (60)	-506 (44)	386 (41)	164 (51)
O(1)	1353 (28)	1011 (29)	1194 (32)	76 (23)	49 (24)	-305 (25)
O(2)	933 (23)	1228 (33)	1077 (31)	137 (25)	125 (21)	245 (28)
O(3)	1255 (29)	1280 (36)	793 (31)	21 (29)	218 (23)	-108 (28)
O(4)	1053 (26)	1025 (33)	1399 (36)	-43 (25)	-266 (25)	-267 (27)
O(5)	1040 (25)	1279 (37)	748 (29)	-200 (26)	81 (21)	46 (28)
O(6)	1042 (25)	1086 (31)	1664 (38)	-105 (25)	71 (24)	-31 (30)

TABLE 4

Bond lengths and angles with standard deviations

i	j	D(ij)
C(1)	C(2)	1.526 (3) Å
C(2)	C(3)	1.522 (3)
C(3)	C(4)	1.521 (3)
C(4)	C(5)	1.543 (3)
C(5)	C(6)	1.509 (4)
C(1)	O(1)	1.401 (3)
C(2)	O(2)	1.429 (3)
C(3)	O(3)	1.419 (3)
C(4)	O(4)	1.424 (3)
C(5)	O(5)	1.444 (3)
C(1)	O(5)	1.422 (3)

i	j	k	ijk
C(1)	C(2)	C(3)	110.5 (3)°
C(2)	C(3)	C(4)	108.9 (3)
C(3)	C(4)	C(5)	109.1 (3)
C(4)	C(5)	O(5)	108.5 (3)
C(5)	O(5)	C(1)	115.0 (3)
O(5)	C(1)	C(2)	110.0 (3)
C(1)	C(2)	O(2)	107.7 (3)
O(2)	C(2)	C(3)	110.9 (3)
C(2)	C(3)	O(3)	106.7 (3)
O(3)	C(3)	C(4)	113.6 (3)
C(3)	C(4)	O(4)	108.9 (3)
O(4)	C(4)	C(5)	110.7 (3)
C(4)	C(5)	C(6)	113.4 (3)
C(6)	C(5)	O(5)	106.8 (3)
O(5)	C(1)	O(1)	111.9 (3)
O(1)	C(1)	C(2)	108.6 (3)

TABLE 5

Hydrogen bond lengths and angles

Symmetry code

a	x,	y,	z+1
b	1-x,	$\frac{1}{2}$+y,	1-z
c	-x,	-$\frac{1}{2}$+y,	-z
d	x,	1+y,	z
e	-x,	-$\frac{1}{2}$+y,	-z+1

i	j	k	D(ij)	D(jk)	ik	ijk
O(3)	H(9)	O(5a)	0.91 Å	2.07 Å	2.81 Å	138
O(4)	H(10)	O(6)	0.85	1.94	2.78	167
O(6)	H(11)	O(4b)	0.83	1.93	2.74	168
O(1)	H(12)	O(2c)	0.89	1.84	2.71	163
O(6)	H(13)	O(1d)	0.87	2.10	2.91	157
O(2)	H(14)	O(6e)	0.89	1.89	2.78	174

CHAPTER IV

EXTINCTION IN LITHIUM FLUORIDE - A COMMENT ON ZACHARIASEN'S THEORY OF EXTINCTION

4.1 Introduction

Darwin's theory (1922) for extinction corrections was criticized by Weiss (1952) for the studies of extinction in powders and by Vand (1955) for other crystalline materials. Darwin's theory was based on an infinite parallel plate with reflecting planes parallel to its surface. Neither condition is satisfied for powder samples and in single crystals one is mostly concerned with a finite size real crystal completely immersed in the X-ray beam. It was later shown by Zachariasen (1963) that Darwin's theory for secondary extinction was not correct and that the polarization factor was incorrectly treated in Darwin's paper.

Recently, Zachariasen (1967) has derived a general formula for integrated intensity of a real crystal and this formula is widely used for correcting the observed diffraction data for extinction. He claims that his intensity formula is valid over the entire range from ideally imperfect to perfect crystals, although, he points out that the application of his theory to small crystals involves mathematical approximations. Werner (1969) has commented that Zachariasen's theory does not take into account the phases of once and multiple diffracted beams. It is therefore likely to have serious shortcomings when primary extinction is present, although, Zachariasen states that primary extinction should on the basis of his theory and experiments be negligible even for the strongest reflections of most crystal specimens.

Zachariasen (1968) has supported the application of his theory to small crystals by examining extinction effects in a small lithium

fluoride sphere. He refined the extinction parameters, thermal parameters and scale factor using a least-squares method for the data obtained with CuKα and MoKα radiations. The atomic form factors used were those of Cromer and Waber (1965). His refinement for the Cu data set contained only four reflections and all the four reflections were highly extinguished. From his experiments and refinements he concluded that the sample of lithium fluoride he used was a type I mosaic crystal and that the mean domain radius was (1.14×10^{-5}) cm, an order of magnitude smaller than that required for the presence of primary extinction.

In view of the process adopted by Zachariasen to refine the extinction parameter, thermal parameters and scale factor to obtain r^*, for Cu data set, it was decided to reinvestigate the results obtained by Zachariasen (1968) using a lithium fluoride sphere from a block of the material. The extinction corrections to the observed structure factors are made using Zachariasen's formula (1967). These results are also compared with the results obtained by Lawrence (1972) for a large parallel sided crystal from the same batch of material. He has deduced from his experiments the mean radius of a mosaic domain by showing that the diffracted intensity per unit length of the crystal is constant and hence only primary extinction is predominant.

It is shown in the present experiments that Zachariasen's theory when applied to small crystals does not successfully account for extinction and gives a value of r^* which is physically unreasonable. It is also deduced that the sample is a type II crystal. The values of r^* are also obtained by using three more sets of atomic form factors for F^- ion, Freeman (1959), Berghuis et al (1955) and those published in the International Tables for

X-Ray Crystallography (1962). Table III shows that for selected values of $\sin\theta/\lambda$, differences of up to 10% exist between the atomic form factors of F^- ion. No such discrepancies exist for these sets for Li^+ ion. No significant changes in r^* values are obtained using the different form factors and the crystal type for all form factors approximated more closely to type II than type I. As is expected, the thermal parameters and scale factors differed significantly for the four sets of refinements.

4.2 Experimental

Large plates of lithium fluoride single crystal were supplied by Rank Precision Industries Ltd. Small cubes of approximate dimensions $(2 \times 2)mm^2$ were cut from a big sample of the material. Eight of these cubes were ground into small spheres by the method of Bond (1951). A spherical crystal has the advantage that the absorption corrections are the same for symmetry related reflections. The crystal fragments were ground in a disc shaped chamber lined with fine emery paper at an air pressure of 2 lbs/cm^2 for about 12 hours. The crystal spheres so obtained were finally polished by using a finer emery paper and a reduced air pressure of $\frac{1}{2}$ lb/cm^2. A sphere of diameter $(0.42 \pm 0.01)mm$ was chosen and preliminary X-ray diffraction work showed that the crystal was mounted in an arbitrary setting and suitable for intensity data collection.

The lattice parameters extracted from orientation matrix were

$a = (4.028 \pm 0.002)\text{Å}$; $\alpha = 90.00° \pm 0.05°$

$b = (4.028 \pm 0.002)\text{Å}$; $\beta = 90.00° \pm 0.04°$

$c = (4.028 \pm 0.002)\text{Å}$; $\gamma = 90.03° \pm 0.04°$

space group $Fm\bar{3}m$.

The values of cell parameters as given by Thewlis (1955) are $a = b = c = (4.0263 \pm 0.0001)\text{Å}$.

4.3 Measurement of Intensities

The experimental conditions chosen for CuKα radiation ($\lambda = 1.5418\text{Å}$) were the same as in the case of α-rhamnose monohydrate. For MoKα radiation ($\lambda = 0.7107\text{Å}$) the conditions were as follows

Mo radiation with zirconium β-filter.

Siemens Generator : 40 KV: 16 MA

Pulse Height Analysis : Base line = 15 volts

(in integral position).

Scintillation Counter (NaI window)

E.H.T. applied = 1137.5 volts.

Diameter of counter collimator = 4.0 mm.

Size of step scan used = 0.01°

A choice of the optimum size of the collimator at the scintillation counter and the angle of scan was made as explained in chapter II. This also gave an a-priori estimate of measuring time for the reflections to keep the counting statistics below 0.1% on integrated intensities of weak reflections. A five point measuring cycle was employed using a ω-2θ scan. Fixed scan method was used for all the reflections. The selection of an attenuator in the main beam was automatic as explained earlier. Three standard reflections were measured before every 30 reflections and no statistically significant changes in the intensities of these were noticed over the data collection period of 4 days. The time between the measurement of groups of standards was approximately 3 hours.

All the reflections having $\theta < 70°$ in a hemisphere of reciprocal space were measured so that the standard deviation for all integrated intensities due to counting statistics was less than 0.1% of the intensity. Background counts were measured at $\pm$ 1.2°

from the peak maxima. The observed structure factor for each reflection was taken to be the mean of all equivalent reflections and the corresponding standard deviation, $\sigma(\underline{h})$, was defined as the standard error in the mean. For all structure factors this error was never greater than 0.6% of the structure factor, this error occurring for the (1,1,1) reflection. The average error was 0.25% which compares with an average error due to counting statistics alone of less than 0.1%. It is clear that other residual errors exist in the data.

Two data sets were obtained, one using MoKα radiation ($\lambda K\bar{\alpha} = 0.7107$Å), the (Mo) data set and the other using CuKα radiation ($\lambda K\bar{\alpha} = 1.5418$Å), the (Cu) data set. In both cases β-filters were used with appropriate pulse height analysis.

4.4 Data Processing

Since the integrated intensities were measured at different attenuators, appropriate attenuator factors were applied to both sets of intensity data. The intensities were also corrected for Lorentz and polarization factors.

Thus a set of relative observed structure factors was obtained. There were fifty two independent reflections in the (Mo) data set and nine in the (Cu) data set. No corrections for anomalous dispersion were necessary for (Mo) data set as $\Delta f' = 0.0$ and $\Delta f'' = 0.0$ for fluorine ion for Mo radiation. Thermal diffuse scattering corrections were calculated for Mo radiation using the formula, Cooper and Rouse (1968)

$$I = I_o\ (1 + \alpha)$$

where $$\alpha = \frac{4\pi^2 h_B T}{\lambda^3}\ \bar{K}.\Delta\ .\ \sin 2\theta\ .\ \sin^2\theta$$

I_o = True Bragg intensity

$I_o\alpha$ = Correction to the observed intensity for thermal diffuse scattering.

T = Absolute temperature.

$\Delta = \frac{\text{Angular range of scan } (2\,\delta\Theta)}{\sin 2\Theta}$

$$\overline{K} = \frac{\frac{1}{5}(C_{11}+C_{12})(C_{11}-C_{12}-2C_{44})+C_{44}(2C_{11}+C_{44})}{C_{11}\,C^2_{44}+\frac{1}{105}(C_{11}-C_{12}-2C_{44})^2(C_{11}+2C_{12}+C_{44})+\frac{1}{5}(C_{11}-C_{12}-2C_{44})\,*\,(C_{11}+C_{12})(C_{44})}$$

Weiss (1966)

C_{11}, C_{12}, C_{44} are the elastic constants for lithium fluoride crystal and their values are given by Cottrell (1964). Other symbols have their usual meaning.

The maximum value of correction term α was found to be 0.0048 and hence negligible for (Mo) data set. No absorption corrections were applied to the (Mo) data set, $\mu R(Mo) = 0.071$, R being the radius of lithium fluoride sphere. $\mu R(Cu) = 0.68$ and absorption corrections as applied to the integrated intensities for the (Cu) data set were determined from the transmission factors for each reflection corresponding to a particular value of Θ and μR (International Tables, Volume II, 1962, page 302). The (Cu) data set was used only to deduce the crystal type from a comparison of F_o's and F_{cals}, assuming first the crystal to be of type I and then of type II. Since the absence of absorption corrections to (Cu) data set did not alter the crystal type, the corrections due to thermal diffuse scattering and anomalous dispersion which were relatively smaller, were ignored for (Cu) data set.

4.5 (Mo) Data Set

The data was originally scaled to the molybdenum radiation of Zachariasen (1968) using the high order reflections in the range

$0.7 < \frac{\sin}{\lambda} < 1.3$. The thermal parameters for the lithium and fluorine ions and scale factors were refined by minimizing the function $\sum_{\underline{h}} \omega(\underline{h}) \ |\Delta(\underline{h})|^2$ and is given by

$$\sum_{\underline{h}} \omega(\underline{h}) |\Delta(h)|^2 = \sum_{\underline{h}} \left[\left\{ \frac{\omega(\underline{h}) |F_o(\underline{h})|}{4} - \frac{(-1)^h \ FLI.\exp(-BLI.S^2)}{K} \right\} X \right.$$

$$\left. \exp(BF.S^2) - \frac{FF}{K} \right]^2 .$$

where

$\omega(\underline{h})$ is the weight for an observed structure factor.

FLI, scattering factor for lithium ion.

FF, scattering factor for fluorine ion.

BLI, temperature factor for lithium ion.

BF, temperature factor for fluorine ion.

K, scale factor.

S, $\sin\theta/\lambda$.

$\underline{h}$, reflection index.

$F_o(\underline{h})$, observed structure factor.

A least-squares programme was written for the refinement of thermal parameters and scale factor. The reflections (1,1,1), (2,0,0), (2,2,2), (4,0.0) and (4,2,0) were suspected to be extinguished and therefore omitted from the refinement. The weights $\omega(\underline{h})$ used were

$$\omega(\underline{h}) = \frac{1}{\sigma^2(\underline{h})}$$

but it was found that the final parameters were not significantly different whether these weights or unit weights were employed. From a knowledge of the calculated structure factors for the extinguished reflections, the observed structure factors were corrected

for extinction using the method of Zachariasen (1967) as follows:

The kinematic structure factor $F_K(\underline{h})$ is expressed in terms of the observed structure factor $F_o(\underline{h})$ by

$$F_K(\underline{h}) = F_o(\underline{h}) \; (1 + 2 \; p \; \bar{x}_o)^{\frac{1}{4}} \qquad (3.1)$$

$$\text{where } p = \frac{1 + \cos^4 2\theta}{1 + \cos^2 2\theta}$$

$$\bar{x}_o = \frac{r^* \bar{T} Q_o}{\lambda}$$

$$\text{and } r^* = r\left(1 + \left(\frac{r}{\lambda g}\right)^2\right)^{-\frac{1}{2}}$$

$$Q_o = \lambda^3 \left(\frac{e^2}{mc^2 \, V}\right)^2 F_K^2(\underline{h}) \Big/ \sin 2\theta$$

The symbols have the meaning given in chapter 1.

It is assumed that the observations are made in the equatorial plane containing the incident and diffracted beams and that $r \ll \bar{T}$ and the misalignment of the domains obeys isotropic Gaussian distribution.

$$W(\Delta) = \sqrt{2} \; g \exp\left(-2\pi g^2 \Delta^2\right)$$

Δ is the angular deviation from the mean orientation and half width, $\Delta_{\frac{1}{2}}$, is given by

$$\Delta_{\frac{1}{2}} = g^{-1} (\text{Log}2/2\pi)^{\frac{1}{2}} = \frac{0.332}{g}$$

Using equation (3.1) an estimate of r* was obtained for each extinguished reflection together with an estimated standard deviation of r*. A weighted mean value of r* was calculated and the observed structure factors corrected for extinction.

The weights assigned were calculated as follows

From equation (3.1)

$$\bar{x}_o = \frac{1}{2p}\left[\left(\frac{F_K(\underline{h})}{F_o(\underline{h})}\right)^4 - 1\right] \qquad (3.2)$$

But also $\bar{x}_o = \frac{r^* \bar{T} Q_o}{\lambda}$

$$= \frac{r^* \bar{T}}{\lambda} \cdot \frac{e^4 \lambda^3 \cdot F_K^2(\underline{h})}{m^2 c^4 V^2} \cdot \frac{1}{\sin 2\theta}$$

or $\bar{x}_o = Z.Z'.F_K^2(\underline{h})$

where $Z' = \frac{e^4 \lambda^3}{m^2 c^4 V^2} \cdot \frac{1}{\sin 2\theta}$

and $Z = \frac{r^* \bar{T}}{\lambda}$

$$\therefore Z.Z'.F_K^2(\underline{h}) = \frac{1}{2p}\left[\left(\frac{F_K(\underline{h})}{F_o(\underline{h})}\right)^4 - 1\right]$$

$$\text{or } Z = \frac{1}{2pZ'}\left[\left(\frac{F_K(\underline{h})}{F_o(\underline{h})}\right)^4 - 1\right] \frac{1}{F_K^2(\underline{h})}$$

Now assuming the error to be in $F_o(\underline{h})$ only

$$\sigma(Z) = \frac{1}{2pZ'}\left[\sigma\left(\frac{F_K(\underline{h})}{F_o(\underline{h})}\right)^4\right] \frac{1}{F_K^2(\underline{h})}$$

$$= \frac{2}{pZ'}\left(\frac{F_K(\underline{h})}{F_o(\underline{h})}\right)^3 \cdot \frac{\sigma(F_o(\underline{h}))}{F_o^2(\underline{h})} \cdot \frac{F_K(\underline{h})}{F_K^2(\underline{h})}$$

$$\text{or } \sigma(Z) = \frac{2}{pZ'}\left(\frac{F_K(\underline{h})}{F_o(\underline{h})}\right)^4 \cdot \frac{\sigma(F_o(\underline{h}))}{F_o(\underline{h})} \cdot \frac{1}{F_K^2(\underline{h})}$$

now let $\frac{\sigma(F_o(\underline{h}))}{F_o(\underline{h})} = R$

where R is the fractional error in the observed structure factor.

$$\therefore \sigma(Z) = \frac{2R}{pZ^{r}} \quad \frac{F_K^{2}(\underline{h})}{F_o^{4}(\underline{h})} \qquad (3.3)$$

Assuming $F_K(\underline{h}) = F_c(\underline{h})$ where $F_c(\underline{h})$ is the calculated structure factor, all the quantities on the right hand side of the above equation are known for the extinguished reflections. Therefore $\sigma(Z)$'s for these reflections were obtained and the weights calculated. A weighted mean of r* obtained from the six extinguished reflections was $(1.5 \pm 0.3)10^{-6}$ cm.

All the observed structure factors were corrected for extinction using equation (3.2). The observed structure factors $F_o'(\underline{h})$, the extinction corrected structure factors $F_o(\underline{h})$ and the calculated structure factors $F_c(\underline{h})$ using the thermal parameters (BLI = $0.96A^2$; BF = $0.66A^2$) obtained from the least-squares refinement are given in Table I along with $\sigma(\underline{h})$ for the observed structure factors.

4.6 (Cu) Data Set

There was no direct way of correcting the (Cu) data set for extinction since all the reflections were affected by extinction and hence the data could not be put on the scale of F_{cals}. However, from the weighted mean value of r* obtained for the (Mo) data set, the pairs of extreme values of r* for the (Cu) data set were calculated, assuming the crystal was either of type I or of type II and the (Cu) data set corrected for both cases. The calculated structure factors used for this purpose were the same as those for the (Mo) data set. The data was scaled such that the sum of

calculated structure factors was equal to the sum of the extinction and absorption corrected observed structure factors. Table II shows the absorption corrected observed structure factors with their standard deviations, the structure factors corrected for extinction assuming the crystal to be of both types and the calculated structure factors.

4.7 Results

The agreement between the observed and calculated structure factors was compared using the G-index (Kitaigorodskii, 1957)

$$G = \left[\frac{\sum_{\underline{h}} |\Delta(\underline{h})|^2}{\sum_{\underline{h}} |F_o(\underline{h})|^2} \right]^{\frac{1}{2}}$$

If it is assumed that $\sigma(\underline{h})$ is a measure of the random errors only, then

$$G = \left[\frac{\sum_{\underline{h}} \sigma^2(\underline{h})}{\sum_{\underline{h}} |F_o(\underline{h})|^2} \right]^{\frac{1}{2}}$$

The value of G assuming only random errors $\sigma(\underline{h})$'s, was 0.004 as compared to the G-index of 0.013 obtained on the basis of discrepancies between the observed and calculated structure factors, indicating that some residual systematic errors exist in the data. No refinement was carried out after the extinction corrections were applied to the observed structure factors in view of the systematic errors which these might still contain.

Following Zachariasen for a type I crystal

$$r^*(Cu) = \frac{\lambda(Cu)}{\lambda(Mo)} \cdot r^*(Mo)$$

and for a type II crystal

$$r^*(Mo) = r^*(Cu)$$

The G-index based on $|\Delta F|^2$ was calculated when the (Cu) data set was corrected for both types of extinction using the corresponding r* (Mo) value. The G-index obtained assuming a type I crystal was substantially greater and large discrepancies were found to exist between the final observed and calculated structure factors for the (2,0,0) and the (1,1,1) reflections. These reflections appeared to be very much overcorrected. A much better agreement between the observed and calculated structure factors was obtained assuming a type II crystal, the G index obtained for this type being (0.014) as compared to the G index (0.033) assuming type I crystal.

This procedure of finding r* was repeated by using three more sets of scattering factors (Freeman 1959; Berghuis et al 1955; International Tables for X-ray Crystallography 1962). Table IV shows the values of r* so obtained. It can thus be seen that the r* values do not change significantly for the four refinements and the crystal still approximates closely to type II of the two crystal types. However, as is expected, small changes in least-squares parameters were observed in the four refinements.

The same mode of analysis when applied to Zachariasen's data confirms that his crystal conformed more to type I crystal than a type II crystal, although small changes in the least-squares parameters were obtained (this analysis BLI = $1.02A^2$; $B_F = 0.68A^2$; scale = 0.96) and for Zachariasen's data (BLI = $0.90A^2$; BF = $0.63\ A^2$; scale = 1.00). By the mode of analysis described here it is impossible to obtain r* for a type I crystal.

4.8 Discussion

When observed data are being corrected for extinction, it is usually assumed that the kinematic structure factor may be equated to

the calculated structure factor which is obtained from the positional parameters, thermal parameters and the form factors. Since the various form factors differ up to 10% for $\overline{F}$ ion at low $\sin\theta/\lambda$ values, the calculated structure factors at low $\sin\theta/\lambda$ are subject to considerable systematic error, the magnitude of which is unknown. It is true that the application of extinction corrections will give a better agreement between the observed and calculated structure factors but in view of systematic errors in the form factors this may be an artifact.

By the application of Zachariasen's theory to a small crystal it has been shown that the sample of lithium fluoride used approximates more to a type II crystal than a type I crystal, while Zachariasen (1968) found that his lithium fluoride sample approximates to a type I crystal. The extinction may be dependent upon the sample used and different treatments given to different samples may produce differences in the size and distribution of the mosaic blocks within the crystal, but if the extinction effects were explained on the basis of a reasonably sound theory, this must present the extinction parameters which are physically reasonable.

Johnston and Gilman (1959) have deduced an experimental relationship between the strain, ε, in a lithium fluoride crystal and the density of dislocation n

$$n = 10^9 \varepsilon$$

Density of dislocation being defined as the number of dislocations/cm^2.

Lawrence (1972) has deduced from his experiment on the same batch of material, a mean radius for the mosaic domain in a large thick crystal of lithium fluoride of 2.5×10^{-3} cm, which,

assuming a one to one correspondence between the mosaic domain size and a dislocation (Gay, Hirsch and Kelly 1953) gives a dislocation density of about 10^5 cm^{-2}. The dislocation density of the original sample as quoted by the manufacturer is about 10^6 cm^{-2}. The present analysis of a small fragment of this material ground into a sphere has, applying Zachariasen's theory to a small crystal, given a mean radius for the mosaic domain of 1.5×10^{-6} cm and consequently a dislocation density of 2×10^{11} cm^{-2}; on the basis of the strain equation this is an increase in the internal strain of ($\times 2 \times 10^5$) simply after grinding the crystal. Clearly, this is impossible, as the average strain in the normal crystal lattice is between 10^{-3} and 10^{-4}. It is concluded therefore that even although the strain equation may not hold good for large strains, Zachariasen's theory when applied to small crystals does not successfully account for extinction and gives a value of r* which is physically unreasonable.

In view of the conflicting results obtained for the mean radius of a mosaic domain, it is desirable to perform an experiment in which a single domain can be put into diffracting position. This can be done by using a very narrow, parallel and monochromatic beam of X-rays. Since the sample used by Lawrence (1972) has a large domain size (2.5×10^{-3} cm) and the domains have a very high angular misorientation, it is expected that a slow rotation of the crystal through the diffracting position will give peak maxima, each corresponding to a mosaic domain. This point is made clear in the experiments on NaCl performed by Renninger (1934). However, these experiments were not carried out here due to the non-availability of a special apparatus.

It is concluded that the widely accepted practice of including an extinction parameter in a least-squares analysis, Zachariasen (1968), Larson (1967) and Ibers (1968), has little validity and that no physical deductions can be made from a consideration of the differences between the observed and calculated structure factors, affected by extinction when such a parameter has been included in the analysis. The method of determining extinction corrections without using $F_c(\underline{h})$'s is thus obviously desirable. One such method applied to α-glycine is described in Chapter V.

TABLE I

Experimentally observed, $F_o'(h)$, extinction corrected, $F_o(h)$, and calculated structure factors $F_c(h)$ for the (M0) data set. $\sigma(\underline{h})$ is the standard deviation of the experimentally observed structure factor.

h	k	ℓ	$\sigma(\underline{h})$	$F_o'(h)$	$F_o(\underline{h})$	$F_c(\underline{h})$
2	0	0	0.08	28.47	29.89	29.92
2	2	0	0.03	21.49	21.90	21.73
2	2	2	0.02	16.44	16.60	16.84
4	0	0	0.04	13.60	13.62	13.61
4	2	0	0.04	11.45	11.46	11.34
4	2	2	0.02	9.78	9.78	9.68
4	4	0	0.02	7.51	7.51	7.44
4	4	2	0.02	6.69	6.69	6.64
6	0	0	0.04	6.72	6.72	6.64
6	2	0	0.02	6.04	6.04	5.99
6	2	2	0.03	5.44	5.44	5.45
4	4	4	0.04	4.94	4.94	4.99
6	4	0	0.02	4.57	4.57	4.59
6	4	2	0.02	4.21	4.21	4.23
8	0	0	0.02	3.66	3.66	3.64
8	2	0	0.02	3.42	3.42	3.40
6	4	4	0.01	3.36	3.36	3.40
8	2	2	0.01	3.18	3.18	3.18
6	6	0	0.02	3.17	3.17	3.18
6	6	2	0.01	2.98	2.98	2.97
8	4	0	0.01	2.80	2.80	2.78
8	4	2	0.01	2.62	2.62	2.61
6	6	4	0.02	2.44	2.44	2.45
8	4	4	0.01	2.19	2.19	2.17
10	0	0	0.01	2.06	2.06	2.06
8	6	0	0.01	2.04	2.04	2.06
10	2	0	0.01	1.91	1.91	1.93
8	6	2	0.01	1.91	1.91	1.93
10	2	2	0.01	1.81	1.81	1.82
6	6	6	0.02	1.82	1.82	1.82
1	1	1	0.12	19.82	20.32	19.73
3	1	1	0.02	9.23	9.23	9.47
3	3	1	0.02	6.08	6.08	6.19
3	3	3	0.02	4.64	4.64	4.77
5	1	1	0.02	4.80	4.80	4.77
5	3	1	0.01	4.02	4.02	3.99
5	3	3	0.02	3.48	3.48	3.49
5	5	1	0.02	3.07	3.07	3.12
7	1	1	0.02	3.13	3.13	3.12
7	3	1	0.01	2.82	2.82	2.81
5	5	3	0.01	2.80	2.80	2.81
7	3	3	0.01	2.55	2.55	2.55
7	5	1	0.01	2.31	2.31	2.31
5	5	5	0.01	2.31	2.31	2.31
9	1	1	0.01	2.15	2.15	2.10
7	5	3	0.02	2.11	2.11	2.10
9	3	1	0.01	1.93	1.93	1.91
9	3	3	0.01	1.72	1.72	1.73
7	7	1	0.02	1.73	1.73	1.73
7	5	5	0.02	1.73	1.73	1.73
9	5	1	0.02	1.55	1.56	1.57
7	7	3	0.02	1.58	1.58	1.57

TABLE II

Experimentally observed, $F_o'(\underline{h})$, extinction corrected, $F_o(\underline{h})$, and calculated structure factors $F_c(\underline{h})$ for the (CU) data set assuming type I or type II crystal. $\sigma(\underline{h})$ is the standard deviation of the experimentally observed structure factor.

Type I extinction

h	k	ℓ	$\sigma(\underline{h})$	$F_o'(\underline{h})$	$F_o(\underline{h})$	$F_c(\underline{h})$
2	0	0	0.15	26.45	31.12	29.92
2	2	0	0.02	19.93	21.52	21.73
2	2	2	0.04	15.77	16.63	16.84
4	0	0	0.02	12.93	13.32	13.61
4	2	0	0.02	10.79	11.00	11.34
4	2	2	0.02	9.05	9.22	9.68
1	1	1	0.10	18.66	20.55	19.73
3	1	1	0.02	9.00	9.14	9.47
3	3	1	0.02	5.86	5.89	6.19

Type II extinction

h	k	ℓ	$\sigma(\underline{h})$	$F_o'(\underline{h})$	$F_o(\underline{h})$	$F_c(\underline{h})$
2	0	0	0.15	27.43	29.96	29.92
2	2	0	0.02	20.68	21.48	21.73
2	2	2	0.04	15.02	16.75	16.84
4	0	0	0.02	13.42	13.61	13.61
4	2	0	0.02	11.20	11.30	11.34
4	2	2	0.02	9.39	9.47	9.68
1	1	1	0.10	19.33	20.32	19.73
3	1	1	0.02	9.34	9.41	9.47
3	3	1	0.02	6.08	6.10	6.19

TABLE III

Discrepancies in the scattering factors for $\overline{F}$ ion for selected values of $\frac{\sin\theta}{\lambda}$ for different models.

$\frac{\sin\theta}{\lambda}$	International Tables (I.T.)	Cromer and Waber (C.W.)	A.J. Freeman (A.J.F.)	J. Berghuis et al (J.B.)
0.2	7.13	7.08	6.60	6.92
0.5	2.89	3.02	2.75	2.84
0.8	1.75	1.78	1.72	1.73
1.1	1.40	1.41	1.41	1.40

TABLE IV

The values of r^* obtained for the various sets of atomic form factors

International Tables (I.T.)	Cromer and Waber (C.W.)	A.J. Freeman (A.J.F.)	J. Berghuis et al (J.B.)
$(2.60\pm0.42)\times10^{-6}$ cm	$(1.50\pm0.30)\times10^{-6}$ cm	$(2.50\pm0.45)\times10^{-6}$ cm	$(2.34\pm0.40)\times10^{-6}$ cm

CHAPTER V

ACCURATE KINEMATIC STRUCTURE FACTORS OF α-GLYCINE AFTER EXPERIMENTAL EXTINCTION AND ABSORPTION CORRECTIONS (I.U.Cr. SINGLE CRYSTAL INTENSITY PROJECT, PHASE II)

5.1 Introduction

In most of the previous work (Zachariasen 1967, 68) extinction corrections have been made by the application of Zachariasen's formula for integrated intensities (Zachariasen, 1967) and in general the real crystals have been classified as type I (λ^3 dependent) crystals in which $r \gg \lambda g$, r being the mean radius of the mosaic blocks and g is a measure of the mosaic spread of the crystal. However, as has been already shown in Chapter IV, although the application of Zachariasen's theory to a small crystal gives a good agreement between the observed and calculated structure factors, the value of r* so obtained may be physically unreasonable. It is, therefore, preferable to determine the amount of extinction experimentally than rely on a mathematical equation whose use may be invalid to the problem under consideration.

Both the observed and calculated structure factors have various errors. The observed structure factors are inaccurate due to experimental errors such as instrument setting errors, counting statistics error and errors due to the non-uniformity of response across the scintillation crystal of the detector. The calculated structure factors are inaccurate due to errors in the atomic form factors (Coppens, 1969).

The errors in the calculated structure factors, which arise due to errors in the atomic form factors, are of two types. The first

has a systematic effect on the calculated structure factors due to various approximations in the isolated neutral atoms or ions. The second error which has also a systematic effect on the calculated structure factors arises due to each atom having its electron cloud distorted from the free atom model. This distortion may be highly asymmetric and is due to the bonding of each atom to other atoms. For example, it was shown in Chapter III, for α-rhamnose monohydrate, that this error was of the order of 4%. None of the theoretical atomic form factors (Cromer and Waber 1965, Freeman 1959, Berghuis et al 1955, International Tables for X-ray Crystallography 1962) can be assumed to be a very accurate basis for computing the calculated structure factors. Keeping these points in view, it was considered appropriate to make experimental extinction corrections to the observed structure factors without any reference to the calculated structure factors.

There are various methods which can be employed for making experimental extinction corrections to the integrated intensities. These experiments involve the variation of extinction parameter by a suitable selection of the experimental conditions. For example

(a) In the Chandrasekhar method (Chandrasekhar 1956, Chandrasekhar and Phillips 1961, Chandrasekhar et al 1969) the integrated intensities are measured using parallel and perpendicular components of polarized X-rays. This method has the advantage that the primary and secondary extinction effects are simultaneously eliminated. However, the limitation of this method is that Chandrasekhar's equation for the integrated intensity is ill-conditioned for reflections with θ values approaching 0°, 45° and 90°.

(b) Willis (1962) has measured the integrated intensities by rotating the crystal about the scattering vector, thus varying the path length of the X-ray beam through the crystal and hence the extinction.

(c) The extinction effects are more predominant in bigger crystals than those in the smaller ones. Cochran (1953) has used this property of extinction for obtaining the extinction free integrated intensities by intensity measurements from different sizes of the crystals. However, this method assumes that the various samples of the same material have the same mosaic spread which may not be true in practice.

(d) Since the amount of extinction in a sample is dependent upon the size of the crystal, it is evident that the extinction effects in powder samples are much smaller than those in single crystals. Stewart and Jensen (1969) have exploited this feature of extinction to make experimental extinction corrections by comparing the integrated intensities of single crystals with those of powder samples. By using powders of different grain sizes a stage may be reached where the extinction effects are completely absent in the powder specimen. A comparison of the extinction free integrated intensities obtained in this way with those of the single crystals gives a measure of the extinction effects in single crystals.

(e) Measurements made with two or more than two wavelengths (Demarco and Weiss, 1962) and thus varying the extinction parameter.

In the present experiments, however, due to the non-availability of other techniques, extinction corrections to the observed integrated intensities were applied using four different X-radiations. This method is fully discussed in the experimental part of the extinction corrections for the α-glycine crystal.

The work described here comprises a part of the I.U.Cr. Single Crystal Intensity Project, Phase II, which involved the determination of very accurate kinematic structure factors for α-glycine on an arbitrary scale after experimental extinction and absorption corrections had been made. The reflections were measured up to $\frac{\sin\theta}{\lambda}$ value of 0.5 along with their available symmetry equivalents. No account was taken of the calculated structure factors for the purposes of extinction corrections and the choice of X-radiation was left open to the participant.

5.2 Experimental

A powder sample of α-glycine was easily crystallised by slow evaporation of an aqueous solution at room temperature. The single crystals so obtained were colourless and needle shaped. One crystal parallelopiped of dimensions (0.025 x 0.012 x 0.0025 cm) was chosen and preliminary photographic X-ray diffraction work showed that the crystal was mounted along the c-axis and that it was a single crystal and suitable for intensity data collection. As explained earlier, the crystal was adjusted on the four-circle diffractometer. The diameter of the X-ray exit collimator was such that the crystal was completely bathed in the X-ray beam. The experimental conditions chosen for the measurement of intensities for CuKα and MoKα radiations were the same as those mentioned in the experimental part of the previous chapters but the conditions for CrKα and AgKα radiations were as follows

CrKα radiation ($\overline{\lambda}$ = 2.2909Å)

with vanadium β-filter

Siemens Generator: 30 kV; 14 M.A.

Pulse Height Analysis: Base line = 17 volts in integral position.

Scintillation Counter (NaI window)

E.H.T. applied = 1237.0 volts

Diameter of the collimator at the scintillation counter

= 4 mm

AgKα radiation ($\overline{\lambda}$ = 0.5609Å)

with paladium β-filter

Siemens Generator: 40 kV; 14.0 M.A.

Pulse Height Analysis: Base line = 7 volts in integral position.

Scintillation Counter (NaI window)

E.H.T. applied = 1125.0 volts

Diameter of the collimator at the scintillation counter

= 4 mm

From the setting angles of the three non-coplanar reflections forming a right handed system, the orientation matrix was computed from which the reciprocal and then real cell parameters extracted. The mean values of the cell parameters obtained using four different wavelengths were as follows

$a = 5.100 \pm 0.002$Å

$b = 11.948 \pm 0.003$Å

$c = 5.463 \pm 0.003$Å

$\beta = 111.69° \pm 0.20°$

space group = $P_{2_1/n}$

Molecular formula: $CH_2\ NH_2\ COO\ H$

and those quoted by Marsh (1958) are

$$a = 5.1020 \pm 0.0008\text{Å}$$

$$b = 11.9709 \pm 0.0017\text{Å}$$

$$c = 5.4575 \pm 0.0015\text{Å}$$

$$\beta = 111.70^{\circ} \pm 0.16^{\circ}$$

Before starting the main run for the intensity data collection it was thought desirable to check both the short and long range stability of the X-ray generator and other electronics. For this purpose a set of reference reflections in groups of 4 along with their available symmetry equivalents were measured ten times each using CuKα radiation for a period of 4 hours. A five point measuring cycle was used. Moving crystal moving detector technique was employed with a 2θ scan of $\pm$ 0.80° about the Bragg peak. The counting statistics were kept below 1% of the integrated intensities on most of the reflections. The integrated intensity of each of the reflections measured before starting the main experiment is shown in Table I and is within $2\sigma(I)$, where $\sigma(I)$ is the standard deviation due to the counting statistics for structure factors having the same (h, k, ℓ) indices. To check the long range operation of the diffractometer during the main run, a set of standard reflections (in groups of 4) was measured before every 30 reflections. No significant changes in the integrated intensity were observed over a data collection period of 7 days. A total of 326 pairs of symmetry equivalent reflections were measured within 2θ less than 52°.

In order to make experimental extinction corrections three more sub-sets of data were measured using CrKα, MoKα and AgKα radiations. The experimental procedure for measuring the intensities was the same as that for CuKα radiation, except the angle of scan, which was $\pm$ 0.80° for CrKα, $\pm$ 0.66° for MoKα and $\pm$ 0.60° for AgKα radiations.

During the data collection using AgKα radiation, a special feature was noticed. For low order reflections the half peaks were highly asymmetric and the integrated intensities were higher than the expected ones. This was due to the X-ray tube being operated at an insufficiently high voltage, which resulted in the white radiation hump being very close to the peak for the characteristic radiation of AgK$\bar{\alpha}$ line ($K\bar{\alpha} = 0.5609\text{Å}$) towards low $\sin\theta$. This can be explained from Figure 1, which shows the line profile for the peak of (1, 2, 0) reflection.

From Bragg's law

$$2\, d \sin\theta = n\lambda$$

$$\therefore \frac{d\theta}{d\lambda} = \frac{\tan\theta}{\lambda}$$

Since the resolution $\frac{d\theta}{d\lambda}$ is very poor for the low order reflections the peak P cannot be separated from the white radiation hump C A, resulting in highly asymmetric backgrounds and an apparent increased integrated intensity. In the case of the high order reflections, for which the resolution is better, the hump C A is further away from the peak P, thus making the backgrounds fairly even and no errors were introduced in the integrated intensity. However, for low order reflections line profile analyses were carried out as already explained in Chapter II and an approximate Gaussian curve fitting method employed to obtain the integrated intensities. This effect was not observed for the other radiations used. This error in the integrated intensities can easily be eliminated by using a monochromatic beam of X-rays but due to its non-availability, it was not possible to perform such an experiment.

5.3 Experimental Extinction Corrections

The integrated intensities for the four sets, one for each radiation, were corrected for Lorentz and polarization factors and the appropriate attenuator factors applied. Thus, four sets of relative observed structure factors were derived. The data sets for CrKα and CuKα radiations were corrected for absorption (Appendix A), $\mu(\text{CrK}\alpha) = 39.86\ \text{cm}^{-1}$ and $\mu(\text{CuK}\alpha) = 12.57\ \text{cm}^{-1}$. For MoKα, $\mu(\text{MoK}\alpha) = 1.54\ \text{cm}^{-1}$ and for AgKα, $\mu(\text{AgK}\alpha) = 0.92\ \text{cm}^{-1}$, the transmission factors were not significantly different from unity. The four sets were put on the same scale by using high $\sin\theta$ reflections. After scaling no systematic trend was noticed among the four sets, except for a few reflections having large structure factors indicating extinction in the four data sets.

The extinction corrections were very inadequate when applied using Zachariasen's formula for integrated intensities, (Zachariasen, 1967). More satisfactory corrections were obtained assuming an approximate form of the Zachariasen formula, i.e.,

$$F_o^2(\underline{h}) = F_K^2(\underline{h}) \left[1 - C_1 F_K^2(\underline{h}) \text{ Lp.} \lambda^2 \bar{T} \right]$$

$$\text{or} \quad = F_K^2(\underline{h}) \left[1 - C_2 F_K^2(\underline{h}) \text{ Lp.} \lambda^3 \bar{T} \right]$$

where $F_o(\underline{h})$ is the observed structure factor

$F_K(\underline{h})$ is the kinematic structure factor

$\bar{T}$ is the mean path length through the crystal

$$\text{Lp} = \frac{1 + \cos^4 2\theta}{1 + \cos^2 2\theta} \cdot \frac{1}{\sin 2\theta}$$

C_1 and C_2 are the extinction parameters for the λ^2 and λ^3 extinction-dependent crystals and the other symbols have their usual meaning.

First, assuming the extinction to be λ^3 dependent, graphs were drawn between $F_o^2(\underline{h})$ and $Lp\lambda^3\bar{T}$ for the four radiations and extrapolated to zero path length and hence zero extinction. The intercepts of the graphs gave the value of extinction free $F_K^2(\underline{h})$ from which $F_K(\underline{h})$ were obtained on the scale of the remainder of the data.

Graphs were also drawn assuming the extinction to be λ^2 dependent, i.e., between $F_o^2(\underline{h})$ and $Lp\lambda^2\bar{T}$. The λ^3 graphs gave a better fit rather than λ^2 ones, indicating that the extinction in our particular sample of α-glycine crystal used is λ^3 dependent. This feature of extinction is shown clearly in the graph for (0, 4, 0) reflection, Figure 2, which is most severely affected by extinction. Table II shows the observed structure factors affected by extinction for four radiations all on the same scale and Table III shows the final set of relative kinematic observed structure factors after extinction and absorption corrections.

5.4 Accuracy of the Observed Structure Factors

The experiment was arranged so that the counting statistics were kept below 1% on intensities for most of the structure factors. However, the estimate of the standard deviation of $F_o(\underline{h})$, $\sigma(F_o(\underline{h}))$ was taken to be the average value of $|\Delta|$ between symmetry equivalents in a group of reflections, the groups being shown as below

Number of group	1	2	3	4	5	6	7
Range of structure factors in a group	0.1 to 4.0	4.1 to 8.0	8.1 to 12.0	12.1 to 16.0	16.1 to 20.0	20.1 to 24.0	24.1 to 28.0
Average value of $\|\Delta\|$ in a group	0.10	0.09	0.14	0.18	0.17	0.25	0.30

A graph was drawn between the average value of the structure factor in these groups and the average value of their $|\Delta|$'s. The graph is shown in Figure 3. It is obvious from the graph that the average value of $|\Delta|$ between the symmetry equivalents in a group varies almost linearly with the average value of structure factor in that group.

The standard deviations on extinguished reflections were taken to be the standard deviations of the intercepts of the best least-squares lines and the intercepts gave the values of extinction free structure factors. $\sigma(F)$ on structure factors above 28.0 but not extinguished was assumed to be 0.30, an error which is far greater than the error due to counting statistics. $\sigma(F)$ on reflections from (1, 2, 3) to ($\bar{5}$, 2, 1), Table III, was based upon the counting statistics, as $\sigma(F)$ based upon the average value of $|\Delta|$ is severely underestimated. An estimate of the maximum value of the structure factors for the reflections from ($\bar{1}$, $\bar{2}$, 1) to (3, 4, 1), Table III which have -ve net counts is given by the following expression. This assumes a maximum counting statistics uncertainty of 2 $\sigma(I)$ on the integrated counts (I_{net}).

$$F_o(\underline{h}) = \sqrt{\frac{[I_{net} + 2\sigma(I)] \quad \text{scale}}{Lp}}$$

$$\text{where } Lp = \frac{1 + \cos^2 2\Theta}{2 \sin 2\Theta}$$

and $\sigma(I)$ is the counting statistics on the integrated intensity of a reflection. $\sigma(F)$ is not given for these reflections. According to this analysis, reflections ($\bar{1}$, $\bar{2}$, 1) and ($\bar{1}$, 2, 1) are considered to be accidentally absent.

5.5 Conclusions

An accurate set of relative observed structure factors along with their available symmetry equivalents has been obtained. No account has been taken of the calculated structure factors in applying the extinction corrections. The extinction in a particular sample of the α-glycine crystal used in this experiment has been shown to be λ^3 dependent.

However, the observed structure factors are on a relative scale and the basic difficulty of obtaining the structure factors on an absolute scale poses a problem. In the next chapter a recently developed X-ray method known as the Pendellösung method has been used to obtain accurate kinematic structure factors on an absolute scale for silicon and α-quartz crystals. This method is not suitable for α-glycine because the phenomenon of Pendellösung fringes, essentially, involves the coherent part of the X-ray scattering. In addition, the success of this method requires big samples of perfect or nearly perfect crystals which can be ground into wedges. The α-glycine crystals we had satisfied neither of these conditions.

TABLE I

A set of observed integrated intensities (I) with their standard deviations $\sigma(I)$. P represents the counts at the peak and B is the background.

H	K	L	P	B	I	$\sigma(I)$
0	3	1	30824.	5048.	25775.	189.
1	4	0	34549.	4168.	30380.	196.
-3	1	4	27995.	3877.	24117.	178.
-1	2	2	88256.	6717.	81538.	308.
0	3	1	31120.	5102.	26017.	190.
1	4	0	34017.	4186.	29830.	195.
-3	1	4	27947.	4027.	23919.	178.
-1	2	2	88111.	6649.	81462.	307.
0	3	1	31124.	4982.	26141.	190.
1	4	0	34515.	4186.	30329.	196.
-3	1	4	27961.	3886.	24074.	178.
-1	2	2	88486.	6636.	81850.	308.
0	3	1	31215.	5063.	26151.	190.
1	4	0	34150.	4188.	29961.	195.
-3	1	4	27860.	3737.	24122.	177.
-1	2	2	88059.	6688.	81370.	307.
0	3	1	31384.	5108.	26276.	191.
1	4	0	33953.	4202.	29751.	195.
-3	1	4	27980.	4072.	23907.	179.
-1	2	2	88011.	6847.	81163.	307.
0	3	1	31153.	5104.	26048.	190.
1	4	0	34394.	4292.	30101.	196.
-3	1	4	27982.	3986.	23996.	178.
-1	2	2	87964.	6468.	81495.	307.
0	3	1	31000.	4977.	26023.	189.
1	4	0	34389.	4405.	29983.	196.
-3	1	4	27829.	4072.	23757.	178.
-1	2	2	88626.	7008.	81618.	309.
0	3	1	31129.	5192.	25936.	190.
1	4	0	34123.	4084.	30038.	195.
-3	1	4	27942.	4099.	23843.	179.
-1	2	2	88725.	6705.	82020.	308.
0	3	1	31133.	5230.	25903.	190.
1	4	0	34634.	4392.	30242.	197.
-3	1	4	27970.	3932.	24038.	178.
-1	2	2	88681.	6948.	81732.	309.
0	-3	1	32211.	5398.	26812.	193.
-1	4	0	35532.	4282.	31250.	199.
-3	-1	4	27996.	4104.	23891.	179.
-1	-2	2	89687.	6581.	83105.	310.
0	-3	1	31612.	5090.	26522.	191.
-1	4	0	35256.	4135.	31121.	198.
-3	-1	4	28103.	3981.	24122.	179.
-1	-2	2	90001.	6440.	83561.	310.
0	-3	1	31940.	5343.	26596.	193.
-1	4	0	35276.	4150.	31126.	198.
-3	-1	4	27954.	4052.	23902.	178.
-1	-2	2	89788.	6549.	83239.	310.
0	3	1	30899.	5052.	25846.	189.
1	4	0	33887.	4239.	29647.	195.
-3	1	4	28057.	3943.	24114.	178.
-1	2	2	88480.	6554.	81925.	308.

H	K	L	P	B	I	σ(I)
0	-3	1	31853.	5172.	26680.	192.
-1	4	0	35421.	4335.	31085.	199.
-3	-1	4	28279.	4098.	24180.	179.
-1	-2	2	88431.	6027.	82403.	307.
0	-3	1	32059.	5380.	26679.	193.
-1	4	0	35343.	4255.	31087.	198.
-3	-1	4	28186.	4084.	24102.	179.
-1	-2	2	88455.	6186.	82269.	307.
0	-3	1	31917.	5226.	26690.	192.
-1	4	0	35079.	4231.	30847.	198.
-3	-1	4	27912.	4009.	23902.	178.
-1	-2	2	88089.	6434.	81654.	307.
0	-3	1	31981.	5447.	26533.	193.
-1	4	0	35461.	4255.	31205.	199.
-3	-1	4	28271.	3944.	24326.	179.
-1	-2	2	88881.	6799.	82081.	309.
0	-3	1	32009.	5332.	26676.	193.
-1	4	0	35527.	4297.	31230.	199.
-3	-1	4	28206.	4045.	24161.	179.
-1	-2	2	88974.	6050.	82924.	308.
0	-3	1	31868.	5404.	26463.	193.
-1	4	0	35143.	4184.	30959.	198.
-3	-1	4	28022.	4056.	23966.	179.
-1	-2	2	88612.	6468.	82144.	308.
0	-3	1	31758.	5247.	26511.	192.
-1	4	0	35348.	4196.	31151.	198.
-3	-1	4	27916.	4041.	23874.	178.
-1	-2	2	88135.	6169.	81966.	307.

TABLE 11

α-Glycine

Coordinates for each graph for the reflections suspected to be extinguished

F_o(Ag), F_o(Mo), F_o(Cu), F_o(Cr) are the observed structure factors after scaling and absorption correction

Reflection			F_o^2(Ag) x 10^{-2}	F_o^2(Mo) x 10^{-2}	F_o^2(Cu) x 10^{-2}	F_o^2(Cr) x 10^{-2}	Lp $\lambda^2\overline{T}$ (Cr)	Lp $\lambda^2\overline{T}$ (Cu)	Lp $\lambda^2\overline{T}$ (Mo)	Lp $\lambda^2\overline{T}$ (Ag)	Lp $\lambda^3\overline{T}$ (Ag)	Lp $\lambda^3\overline{T}$ (Mo)	Lp $\lambda^3\overline{T}$ (Cu)	Lp $\lambda^3\overline{T}$ (Cr)
0	4	0	61.84	60.61	52.33	41.86	61.27	53.38	33.36	26.53	14.88	23.71	82.29	140.36
0	1	1	8.63	8.96	8.54	8.23	73.42	48.54	23.04	20.84	11.69	16.37	74.83	168.20
0	$\bar{1}$	1	8.68	9.55	8.17	8.17	73.42	55.48	23.04	20.84	11.69	16.37	85.54	168.20
1	0	1	15.67	15.99	15.62	14.85	35.75	21.01	18.49	8.99	5.04	13.14	32.39	81.90
$\bar{1}$	$\bar{2}$	0	14.64	14.26	14.61	13.50	51.94	37.85	18.21	11.35	6.37	10.21	58.36	118.99
$\bar{1}$	2	0	14.37	14.28	14.33	13.11	59.36	35.15	18.21	11.35	6.37	10.21	54.19	135.99
$\bar{1}$	$\bar{3}$	0	11.99	11.94	12.58	11.76	54.44	34.86	14.88	13.52	7.58	10.58	53.75	124.72
$\bar{1}$	3	0	11.87	11.59	12.28	11.70	54.44	34.86	18.06	13.52	7.58	12.84	53.75	124.72
$\bar{1}$	$\bar{2}$	2	31.85	32.13	27.77	23.39	60.76	47.42	24.51	18.90	10.60	17.42	73.11	139.20
$\bar{1}$	2	2	32.16	32.29	26.84	23.68	64.95	39.24	24.51	18.90	10.60	17.42	60.50	148.79
0	3	1	9.37	9.72	9.32	8.41	80.06	60.75	31.74	24.35	13.66	22.56	93.66	183.41
0	$\bar{3}$	1	9.44	9.92	9.35	8.27	80.06	60.75	31.74	24.35	13.66	22.56	93.66	183.41
0	0	2	20.28	20.86	19.22	19.18	30.80	19.55	15.78	7.68	4.31	11.21	30.14	70.56
$\bar{1}$	$\bar{4}$	0	10.87	9.97	10.30	9.72	50.49	37.21	13.98	11.15	6.25	9.94	57.37	115.67
$\bar{1}$	4	0	10.67	9.85	10.54	9.63	57.07	35.44	13.98	11.15	6.25	9.94	54.64	130.74

TABLE III.

α-GLYCINE

A SET OF OBSERVED KINEMATIC STRUCTURE FACTORS

ON RELATIVE SCALE WITH THEIR STANDARD DEVIATIONS

H	K	L	F_o	$\sigma(F_o)$	H	K	L	F_o	$\sigma(F_o)$
0	0	2	45.31	0.69	1	4	4	4.36	0.09
0	0	4	13.23	0.18	1	5	1	5.74	0.09
0	1	1	29.73	0.29	1	5	2	7.09	0.09
0	1	2	22.79	0.25	1	5	3	14.24	0.18
0	1	3	8.19	0.14	1	6	0	5.41	0.09
0	1	4	9.43	0.14	1	6	1	12.87	0.18
0	2	0	12.30	0.18	1	6	4	14.32	0.18
0	2	1	5.37	0.09	1	7	0	23.05	0.25
0	2	2	13.31	0.18	1	7	1	3.48	0.10
0	2	3	24.23	0.30	1	7	2	4.76	0.09
0	2	4	7.41	0.09	1	7	3	4.31	0.09
0	2	5	1.56	0.10	1	8	0	20.89	0.25
0	3	1	31.17	0.43	1	8	1	10.52	0.14
0	3	2	19.20	0.17	1	8	2	11.56	0.14
0	3	3	7.81	0.09	1	10	0	4.26	0.09
0	4	0	80.30	0.44	1	10	1	8.53	0.14
0	4	1	2.43	0.10	1	10	2	9.62	0.14
0	4	2	16.96	0.17	1	11	0	13.31	0.18
0	4	3	8.35	0.14	1	11	1	4.60	0.09
0	4	4	5.58	0.09	1	12	0	6.14	0.09
0	5	1	11.01	0.14	-2	0	0	19.84	0.17
0	5	2	12.68	0.18	2	0	2	27.30	0.30
0	5	4	12.81	0.18	-2	-1	0	15.32	0.18
0	6	0	13.29	0.18	2	1	1	12.25	0.18
0	6	1	6.98	0.09	-2	-2	0	15.62	0.18
0	6	2	18.02	0.17	2	2	1	11.61	0.14
0	6	3	13.34	0.18	2	2	2	6.54	0.09
0	6	4	12.47	0.18	2	2	3	7.78	0.09
0	7	1	17.18	0.17	-2	-3	0	22.38	0.25
0	7	2	7.55	0.09	2	3	1	16.25	0.17
0	7	3	4.70	0.09	2	3	2	9.54	0.14
0	8	0	20.01	0.25	-2	-4	0	6.07	0.09
0	8	1	2.41	0.10	2	4	1	6.81	0.09
0	8	3	8.53	0.14	2	4	2	15.35	0.18
0	9	2	4.68	0.09	2	5	1	4.72	0.09
0	10	2	7.13	0.09	2	5	2	6.44	0.09
0	11	1	7.89	0.09	2	5	3	2.02	0.10
0	12	2	8.27	0.14	-2	-6	0	18.05	0.17
1	0	1	39.93	0.27	2	6	1	4.16	0.09
-1	-1	0	18.77	0.17	2	6	2	8.97	0.14
1	1	1	9.77	0.14	2	6	3	6.14	0.09
1	1	2	12.65	0.18	-2	-7	0	6.58	0.09
1	1	3	15.15	0.18	2	7	1	9.21	0.14
1	1	4	3.00	0.10	2	7	2	9.35	0.14
-1	-2	0	38.26	0.52	2	8	0	6.38	0.09
1	2	1	7.47	0.09	2	8	1	5.68	0.09
1	2	2	17.05	0.17	2	9	0	7.32	0.09
1	2	4	29.72	0.30	2	10	0	9.15	0.14
-1	-3	0	35.47	0.30	2	11	1	4.86	0.09
1	3	2	9.37	0.14	-3	-1	0	11.99	0.14
1	3	3	8.89	0.14	3	1	2	9.66	0.14
1	4	0	32.44	0.70	3	3	1	2.87	0.10
1	4	1	22.63	0.25	-3	-4	0	11.29	0.14
1	4	2	16.13	0.17	3	4	2	11.72	0.14

H	K	L	F_o	$\sigma(F_o)$
-3	-5	0	12.81	0.18
3	5	2	9.89	0.14
-3	-6	0	5.95	0.09
-3	-7	0	10.47	0.14
3	7	1	4.98	0.09
-3	-8	0	8.51	0.14
3	8	2	10.98	0.14
-3	-9	0	5.41	0.09
-4	0	0	5.86	0.09
-4	-1	0	20.66	0.25
-4	-2	0	3.68	0.10
4	2	1	4.09	0.09
4	2	2	1.76	0.10
-4	-3	0	21.07	0.25
4	3	1	4.25	0.09
-4	-4	0	5.89	0.09
-4	-5	0	9.00	0.14
4	5	1	3.85	0.10
-4	-6	0	5.75	0.09
4	7	1	2.46	0.10
0	0	2	45.50	0.69
0	0	4	13.17	0.18
0	-1	1	30.15	0.90
0	-1	2	22.81	0.25
0	-1	3	7.99	0.09
0	-1	4	9.53	0.14
0	2	0	12.33	0.18
0	-2	1	5.33	0.09
0	-2	2	13.48	0.18
0	-2	3	24.30	0.30
0	-2	4	7.28	0.09
0	-2	5	1.46	0.10
0	-3	1	31.44	0.53
0	-3	2	19.39	0.17
0	-3	3	7.75	0.09
0	4	0	79.79	0.44
0	-4	1	2.29	0.10
0	-4	2	17.04	0.17
0	-4	3	8.41	0.14
0	-4	4	5.47	0.09
0	-4	5	0.62	0.10
0	-5	1	11.11	0.14
0	-5	2	12.89	0.18
0	-5	4	12.83	0.18
0	6	0	13.33	0.18
0	-6	1	6.98	0.09
0	-6	2	18.19	0.17
0	-6	3	13.38	0.18
0	-6	4	12.66	0.18
0	-7	1	17.34	0.17
0	-7	2	7.61	0.09
0	-7	3	4.75	0.09
0	8	0	20.14	0.25
0	-8	1	2.41	0.10
0	-8	3	8.68	0.14
0	9	2	4.68	0.09
0	-10	2	7.13	0.09
0	-11	1	7.83	0.09
0	-12	2	8.49	0.14
1	0	1	40.08	0.27
-1	1	0	18.58	0.17
1	-1	1	9.53	0.14
1	-1	2	12.65	0.18
1	-1	3	15.21	0.18
1	-1	4	2.82	0.10
-1	2	0	38.09	0.36
1	-2	1	7.43	0.09
1	-2	2	16.97	0.17
1	-2	4	29.49	0.30
-1	3	0	35.04	0.30
1	-3	2	9.36	0.14
1	-3	3	8.73	0.14
-1	4	0	32.46	0.30
1	-4	1	22.83	0.25
1	-4	2	16.26	0.17
1	-4	4	4.84	0.09
1	-5	1	6.00	0.09
1	-5	2	7.05	0.09
1	-5	3	14.13	0.18
-1	6	0	5.66	0.09
1	-6	1	12.98	0.18
1	-6	4	14.28	0.18
-1	7	0	23.58	0.25
1	-7	1	3.37	0.10
1	-7	2	4.78	0.09
1	-7	3	4.45	0.09
-1	8	0	21.43	0.25
1	-8	1	10.66	0.14
1	-8	2	11.63	0.14
-1	10	0	4.32	0.09
1	-10	1	8.41	0.14
1	-10	2	9.67	0.14
-1	11	0	13.33	0.18
1	-11	1	4.68	0.09
-1	12	0	6.08	0.09
-2	0	0	19.77	0.17
2	0	2	27.09	0.30
-2	1	0	15.57	0.18
2	-1	1	12.35	0.18
-2	2	0	15.99	0.18
2	-2	1	11.77	0.14
2	-2	2	6.61	0.09
2	-2	3	7.77	0.09
-2	3	0	22.31	0.25
2	-3	1	16.12	0.17
2	-3	2	9.60	0.14
-2	4	0	6.06	0.09
2	-4	1	6.68	0.09
2	-4	2	15.42	0.18
2	-5	1	4.75	0.09
2	-5	2	6.46	0.09
2	-5	3	2.10	0.10
-2	6	0	17.81	0.17
2	-6	1	4.02	0.09
2	-6	2	8.92	0.14
2	-6	3	6.26	0.09

H	K	L	F_o	$\sigma(F_o)$
-2	7	0	6.58	0.09
2	-7	1	9.11	0.14
2	-7	2	9.27	0.14
-2	8	0	6.43	0.09
2	-8	1	5.56	0.09
-2	9	0	7.49	0.09
-2	10	0	9.30	0.14
2	-11	1	4.70	0.09
-3	1	0	12.12	0.18
3	-1	2	9.82	0.14
3	-3	1	2.88	0.10
-3	4	0	11.28	0.14
3	-4	2	11.76	0.14
-3	5	0	13.21	0.18
3	-5	2	10.00	0.14
-3	6	0	6.00	0.09
-3	7	0	10.71	0.14
3	-7	1	4.93	0.09
-3	8	0	8.70	0.14
3	-8	2	11.19	0.14
-3	9	0	5.58	0.09
-4	0	0	5.82	0.09
-4	1	0	20.51	0.25
-4	2	0	3.73	0.10
4	-2	1	3.87	0.10
4	-2	2	1.89	0.10
-4	3	0	21.11	0.25
4	-3	1	4.08	0.09
-4	4	0	5.89	0.09
-4	5	0	8.98	0.14
4	-5	1	3.91	0.10
-4	6	0	5.78	0.09
4	-7	1	2.40	0.10
0	0	2	45.14	0.69
0	0	4	13.31	0.18
0	-1	1	30.05	0.90
0	-1	2	22.81	0.25
0	-1	3	8.09	0.14
0	-1	4	9.66	0.14
0	2	0	12.36	0.18
0	-2	1	5.31	0.09
0	-2	2	13.50	0.18
0	-2	3	24.14	0.30
0	-2	4	7.36	0.09
0	-3	1	31.54	0.53
0	-3	2	19.45	0.17
0	-3	3	7.76	0.09
0	4	0	80.54	0.44
0	-4	2	17.09	0.17
0	-4	3	8.40	0.14
0	-4	4	5.56	0.09
0	-5	1	11.18	0.14
0	-5	2	12.95	0.18
0	-5	4	12.77	0.18
0	6	0	13.29	0.18
0	-6	1	6.96	0.09
0	-6	2	18.22	0.17
0	-6	3	13.38	0.18
0	-6	4	12.59	0.18

H	K	L	F_o	$\sigma(F_o)$
0	-7	1	17.34	0.17
0	-7	2	7.63	0.09
0	-7	3	4.76	0.09
0	8	0	20.24	0.25
0	-8	3	8.66	0.14
0	-9	2	4.81	0.09
0	-10	2	7.25	0.09
0	-11	1	7.76	0.09
-1	0	1	13.83	0.18
-1	0	3	10.63	0.14
-1	-1	0	18.85	0.17
-1	-1	1	2.79	0.10
-1	-1	2	7.10	0.09
-1	-1	3	20.39	0.25
-1	-1	4	9.72	0.14
-1	-1	5	6.24	0.09
-1	-2	0	38.16	0.52
-1	-2	2	57.39	0.34
-1	-2	3	4.77	0.09
-1	-2	4	10.64	0.14
-1	-3	0	35.61	0.30
-1	-3	1	4.64	0.09
-1	-3	2	13.58	0.18
-1	-3	3	12.72	0.18
-1	-3	4	1.84	0.10
-1	-3	5	2.38	0.10
1	4	0	32.24	0.70
-1	-4	1	16.37	0.17
-1	-4	2	15.73	0.18
-1	-4	3	9.21	0.14
-1	-4	4	10.84	0.14
-1	-5	1	5.55	0.09
-1	-5	2	16.12	0.17
-1	-5	3	13.44	0.18
-1	-5	4	8.19	0.14
1	6	0	5.59	0.09
-1	-6	2	17.20	0.17
-1	-6	3	6.11	0.09
1	7	0	22.88	0.25
-1	-7	2	14.08	0.18
-1	-7	3	5.25	0.09
-1	-7	4	5.15	0.09
1	8	0	20.77	0.25
-1	-8	1	7.49	0.09
-1	-8	2	10.07	0.14
-1	-8	3	1.50	0.10
-1	-8	4	9.59	0.14
-1	-9	2	9.29	0.14
-1	-9	3	7.51	0.09
1	10	0	4.32	0.09
1	11	0	13.12	0.18
-1	-11	2	8.09	0.14
-2	0	0	19.85	0.17
-2	0	2	1.07	0.10
-2	-1	0	15.35	0.18
-2	-1	1	7.20	0.09
-2	-1	2	13.97	0.18
-2	-1	3	2.80	0.10
-2	-1	4	3.95	0.10

H	K	L	F_o	$\sigma(F_o)$
-2	-2	0	15.68	0.18
-2	-2	1	10.96	0.14
-2	-2	2	18.87	0.17
-2	-2	3	3.54	0.10
-2	-2	4	6.89	0.09
-2	-2	5	4.83	0.09
-2	-3	0	22.16	0.25
-2	-3	1	14.27	0.18
-2	-3	2	26.89	0.30
-2	-3	3	1.26	0.10
-2	-3	4	14.51	0.18
-2	-3	5	4.72	0.09
-2	-4	0	6.02	0.09
-2	-4	2	1.91	0.10
-2	-4	3	1.65	0.10
-2	-4	4	2.15	0.10
-2	-4	5	6.76	0.09
-2	-5	0	0.98	0.10
-2	-5	2	4.61	0.09
-2	-5	3	6.31	0.09
-2	-5	4	7.36	0.09
-2	-6	0	17.86	0.17
-2	-6	1	6.96	0.09
-2	-6	2	24.47	0.30
-2	-6	4	10.04	0.14
-2	-7	0	6.64	0.09
-2	-7	1	6.45	0.09
-2	-7	2	12.71	0.18
-2	-7	4	10.18	0.14
2	8	0	6.36	0.09
-2	-8	4	6.68	0.09
2	9	0	7.34	0.09
-2	-9	1	4.64	0.09
-2	-9	2	8.64	0.14
-2	-9	3	6.34	0.09
2	10	0	9.05	0.14
-2	-10	1	3.84	0.10
-2	-10	2	15.05	0.18
-3	0	1	19.31	0.17
-3	0	3	12.52	0.18
-3	0	5	13.48	0.18
-3	-1	0	12.02	0.18
-3	-1	1	12.52	0.18
-3	-1	2	26.28	0.30
-3	-1	3	6.55	0.09
-3	-1	4	28.40	0.30
-3	-2	1	6.87	0.09
-3	-2	2	19.79	0.17
-3	-3	0	4.01	0.09
-3	-3	1	7.89	0.09
-3	-3	2	12.15	0.18
-3	-3	3	5.61	0.09
-3	-3	4	18.85	0.17
-3	-4	0	11.18	0.14
-3	-4	1	12.87	0.18
-3	-4	2	6.07	0.09
-3	-4	3	11.11	0.14
-3	-4	4	7.61	0.09
-3	-5	0	12.73	0.18
-3	-5	1	10.70	0.14
-3	-5	2	15.33	0.18
-3	-5	3	4.92	0.09
-3	-5	4	20.36	0.25
-3	-5	5	2.94	0.10
-3	-6	0	5.77	0.09
-3	-6	1	8.54	0.14
-3	-6	2	8.87	0.14
-3	-7	0	10.53	0.14
-3	-7	4	5.91	0.09
-3	-7	5	3.66	0.10
-3	-8	0	8.35	0.14
-3	-8	3	8.00	0.09
-3	-9	0	5.29	0.09
-3	-9	1	7.49	0.09
-4	0	0	5.96	0.09
4	0	2	8.75	0.14
-4	0	4	17.97	0.17
-4	-1	0	20.52	0.25
-4	-1	1	4.51	0.09
-4	-1	3	10.29	0.14
-4	-1	4	11.47	0.14
-4	-2	1	16.86	0.17
-4	-2	3	4.01	0.09
-4	-3	0	21.01	0.25
-4	-3	1	6.40	0.09
-4	-3	2	9.28	0.14
-4	-3	3	13.26	0.18
-4	-3	4	14.80	0.18
-4	-4	0	5.89	0.09
-4	-4	2	3.82	0.10
-4	-4	4	14.53	0.18
-4	-5	0	8.94	0.14
-4	-5	2	10.04	0.14
-4	-6	0	5.69	0.09
-4	-6	1	11.39	0.14
-4	-7	1	5.40	0.09
-4	-7	2	4.31	0.09
-4	-7	4	7.26	0.09
-4	-8	0	4.87	0.09
-4	-9	2	10.48	0.14
-5	0	1	4.06	0.09
-5	0	3	15.27	0.18
-5	-1	1	6.81	0.09
-5	-1	2	14.27	0.18
-5	-2	2	5.17	0.09
-5	-4	3	11.76	0.14
0	0	2	45.29	0.69
0	0	4	13.15	0.18
0	1	1	29.52	0.29
0	1	2	22.90	0.25
0	1	3	8.16	0.14
0	1	4	9.32	0.14
0	2	0	12.28	0.18
0	2	1	5.35	0.09
0	2	2	13.43	0.18
0	2	3	24.08	0.30
0	2	4	7.36	0.09
0	3	1	30.93	0.43

H	K	L	F_o	$\sigma(F_o)$
0	3	2	19.01	0.17
0	3	3	7.79	0.09
0	4	0	79.68	0.44
0	4	2	16.81	0.17
0	4	3	8.31	0.14
0	4	4	5.52	0.09
0	5	1	10.98	0.14
0	5	2	12.64	0.18
0	5	4	12.74	0.18
0	6	0	13.26	0.18
0	6	1	6.95	0.09
0	6	2	18.09	0.17
0	6	3	13.24	0.18
0	6	4	12.41	0.18
0	7	1	17.22	0.17
0	7	2	7.58	0.09
0	7	3	4.68	0.09
0	8	0	20.11	0.25
0	8	3	8.42	0.14
0	9	2	4.62	0.09
0	10	2	7.04	0.09
0	11	1	7.76	0.09
-1	0	1	13.94	0.18
-1	0	3	10.57	0.14
-1	1	0	18.69	0.17
-1	1	1	2.84	0.10
-1	1	2	7.03	0.09
-1	1	3	20.35	0.25
-1	1	4	9.84	0.14
-1	1	5	6.28	0.09
-1	2	0	37.93	0.36
-1	2	3	4.79	0.09
-1	2	2	57.04	1.33
-1	2	4	10.67	0.14
-1	3	0	34.85	0.30
-1	3	1	4.62	0.09
-1	3	2	13.21	0.18
-1	3	3	12.65	0.18
-1	3	4	1.83	0.10
-1	3	5	2.62	0.10
-1	4	0	32.08	0.30
-1	4	1	15.92	0.18
-1	4	2	15.61	0.18
-1	4	3	9.10	0.14
-1	4	4	10.79	0.14
-1	5	1	5.52	0.09
-1	5	2	15.92	0.18
-1	5	3	13.34	0.18
-1	5	4	8.25	0.14
-1	6	0	5.63	0.09
-1	6	2	17.04	0.17
-1	6	3	6.10	0.09
-1	7	0	23.36	0.25
-1	7	2	14.00	0.18
-1	7	3	5.03	0.09
-1	7	4	5.15	0.09
-1	8	0	21.13	0.25
-1	8	1	7.53	0.09
-1	8	2	9.91	0.14
-1	8	3	1.43	0.10
-1	8	4	9.38	0.14
-1	9	2	9.17	0.14
-1	9	3	7.57	0.09
-1	10	0	4.29	0.09
-1	11	0	13.29	0.18
-1	11	2	7.72	0.09
-2	0	0	19.71	0.17
-2	0	6	6.22	0.09
-2	1	0	15.55	0.18
-2	1	1	7.18	0.09
-2	1	2	13.94	0.18
-2	1	3	2.57	0.10
-2	1	4	4.08	0.09
-2	2	0	15.97	0.18
-2	2	1	10.85	0.14
-2	2	2	18.55	0.17
-2	2	3	3.51	0.10
-2	2	4	6.88	0.09
-2	2	5	4.68	0.09
-2	3	0	22.14	0.25
-2	3	1	14.02	0.18
-2	3	2	26.14	0.30
-2	3	3	0.83	0.10
-2	3	4	14.12	0.18
-2	3	5	4.70	0.09
-2	4	0	5.94	0.09
-2	4	2	1.83	0.10
-2	4	3	1.61	0.10
-2	4	4	2.29	0.10
-2	4	5	6.71	0.09
-2	5	0	1.08	0.10
-2	5	2	4.49	0.09
-2	5	3	6.24	0.09
-2	5	4	7.41	0.09
-2	6	0	17.76	0.17
-2	6	1	6.76	0.09
-2	6	2	23.77	0.25
-2	6	4	10.07	0.14
-2	7	0	6.69	0.09
-2	7	1	6.40	0.09
-2	7	2	12.57	0.18
-2	7	4	10.07	0.14
-2	8	0	6.36	0.09
-2	8	4	6.72	0.09
-2	9	0	7.53	0.09
-2	9	1	4.56	0.09
-2	9	2	8.47	0.14
-2	9	3	6.15	0.09
-2	10	0	9.13	0.14
-2	10	1	3.90	0.10
-2	10	2	14.75	0.18
-3	0	1	19.34	0.17
-3	0	3	12.56	0.18
-3	0	5	13.66	0.18
-3	1	0	12.00	0.14
-3	1	1	12.45	0.18
-3	1	2	26.27	0.30
-3	1	3	6.49	0.09

H	K	L	F_o	$\sigma(F_o)$
-3	1	4	28.24	0.30
-3	2	1	6.82	0.09
-3	2	2	19.65	0.17
-3	3	0	4.06	0.09
-3	3	1	7.92	0.09
-3	3	2	11.92	0.14
-3	3	3	5.44	0.09
-3	3	4	18.46	0.17
-3	4	0	11.35	0.14
-3	4	1	12.84	0.18
-3	4	2	5.89	0.09
-3	4	3	10.80	0.14
-3	4	4	7.39	0.09
-3	5	0	13.05	0.18
-3	5	1	10.44	0.14
-3	5	2	14.76	0.18
-3	5	3	4.84	0.09
-3	5	4	19.81	0.17
-3	5	5	2.90	0.10
-3	6	0	5.80	0.09
-3	6	1	8.41	0.14
-3	6	2	8.64	0.14
-3	7	0	10.53	0.14
-3	7	4	5.75	0.09
-3	7	5	3.77	0.10
-3	8	0	8.74	0.14
-3	8	3	7.91	0.09
-3	9	0	5.66	0.09
-3	9	1	7.65	0.09
-4	0	0	5.73	0.09
-4	0	4	18.04	0.17
-4	1	0	20.44	0.25
-4	1	1	4.42	0.09
-4	1	3	10.23	0.14
-4	1	4	11.37	0.14
-4	2	1	16.73	0.17
-4	2	3	4.02	0.09
-4	3	0	20.82	0.25
-4	3	1	6.51	0.09
-4	3	2	9.06	0.14
-4	3	3	13.05	0.18
-4	3	4	14.59	0.18
-4	4	0	5.86	0.09
-4	4	2	3.49	0.10
-4	4	4	14.20	0.18
-4	5	0	8.88	0.14
-4	5	2	9.74	0.14
-4	6	0	5.66	0.09
-4	6	1	11.11	0.14
-4	7	1	5.29	0.09
-4	7	2	4.15	0.09
-4	7	4	7.33	0.09
-4	8	0	4.89	0.09
-4	9	2	10.67	0.14
-5	0	3	15.17	0.18
-5	1	1	6.71	0.09
-5	1	2	14.11	0.18
-5	2	2	5.09	0.09
-5	4	3	11.52	0.14

H	K	L	F_o	$\sigma(F_o)$
1	2	3	0.70	0.21
1	-2	3	1.07	0.14
-1	5	0	0.57	0.20
2	8	3	0.59	0.22
2	10	1	0.94	0.16
2	-10	1	0.67	0.22
3	1	1	0.99	0.14
3	-1	1	0.69	0.21
3	2	2	0.73	0.21
3	-2	2	0.68	0.22
3	-4	1	0.25	0.59
-1	-9	4	1.29	0.11
-1	9	4	1.69	0.10
-2	-4	1	0.54	0.21
-2	4	1	0.40	0.29
-2	-12	2	1.55	0.10
-2	12	2	1.42	0.10
-4	4	3	1.16	0.14
-4	-4	3	0.99	0.16
-4	-4	5	0.58	0.24
-4	4	5	0.62	0.23
-5	-2	1	0.82	0.17
-5	2	1	0.30	0.47
-1	-2	1	0.00	0.00
-1	2	1	0.00	0.00
0	4	5	0.34	0.00
0	12	0	0.43	0.00
1	5	0	0.87	0.00
2	4	3	0.59	0.00
2	-4	3	0.33	0.00
2	-8	3	0.24	0.00
3	4	1	0.50	0.00

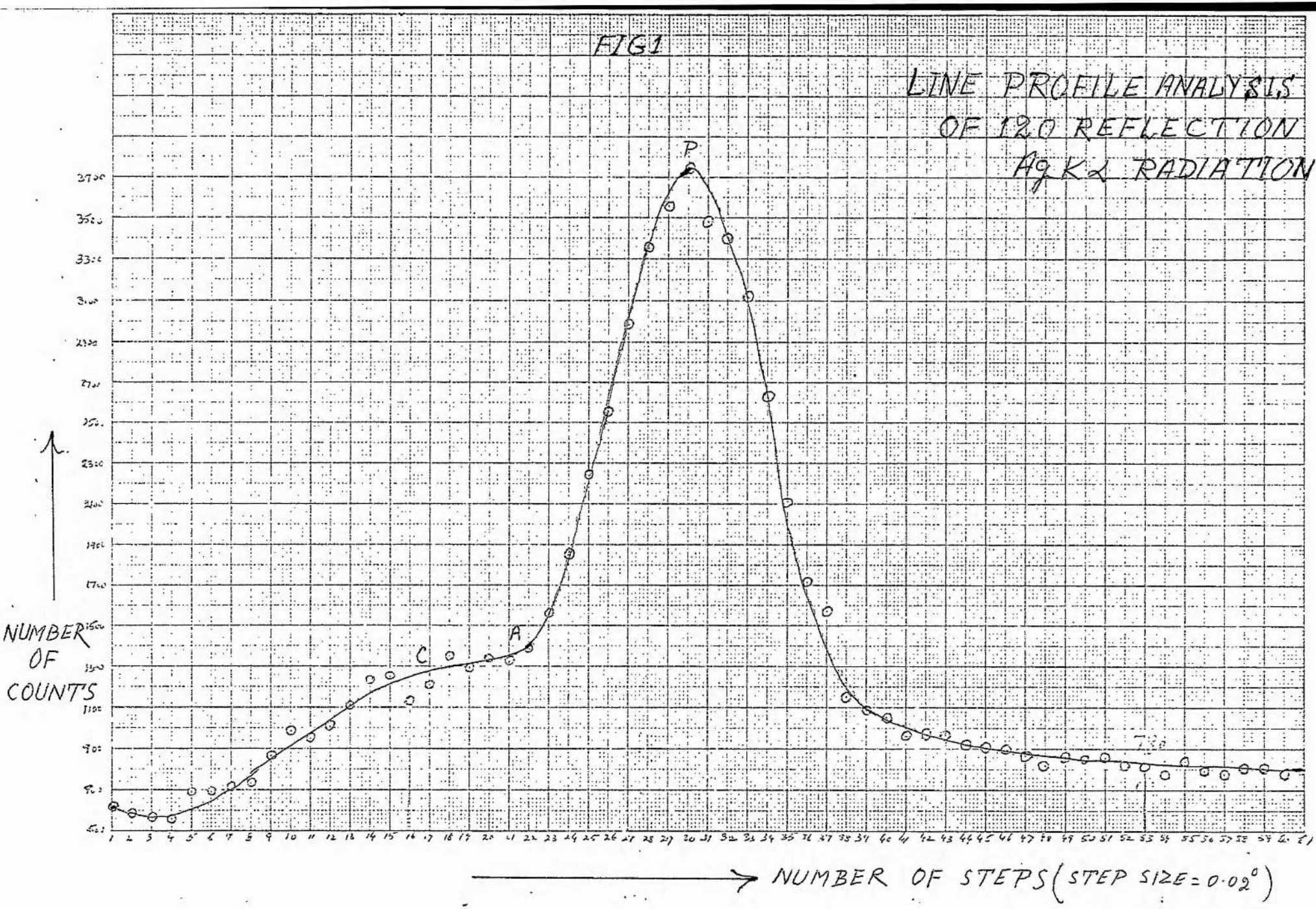
FIG1
LINE PROFILE ANALYSIS OF 120 REFLECTION Ag Kα_1 RADIATION
P
A
C
T.B
NUMBER OF COUNTS
NUMBER OF STEPS (STEP SIZE = 0·02°)

FIG 2

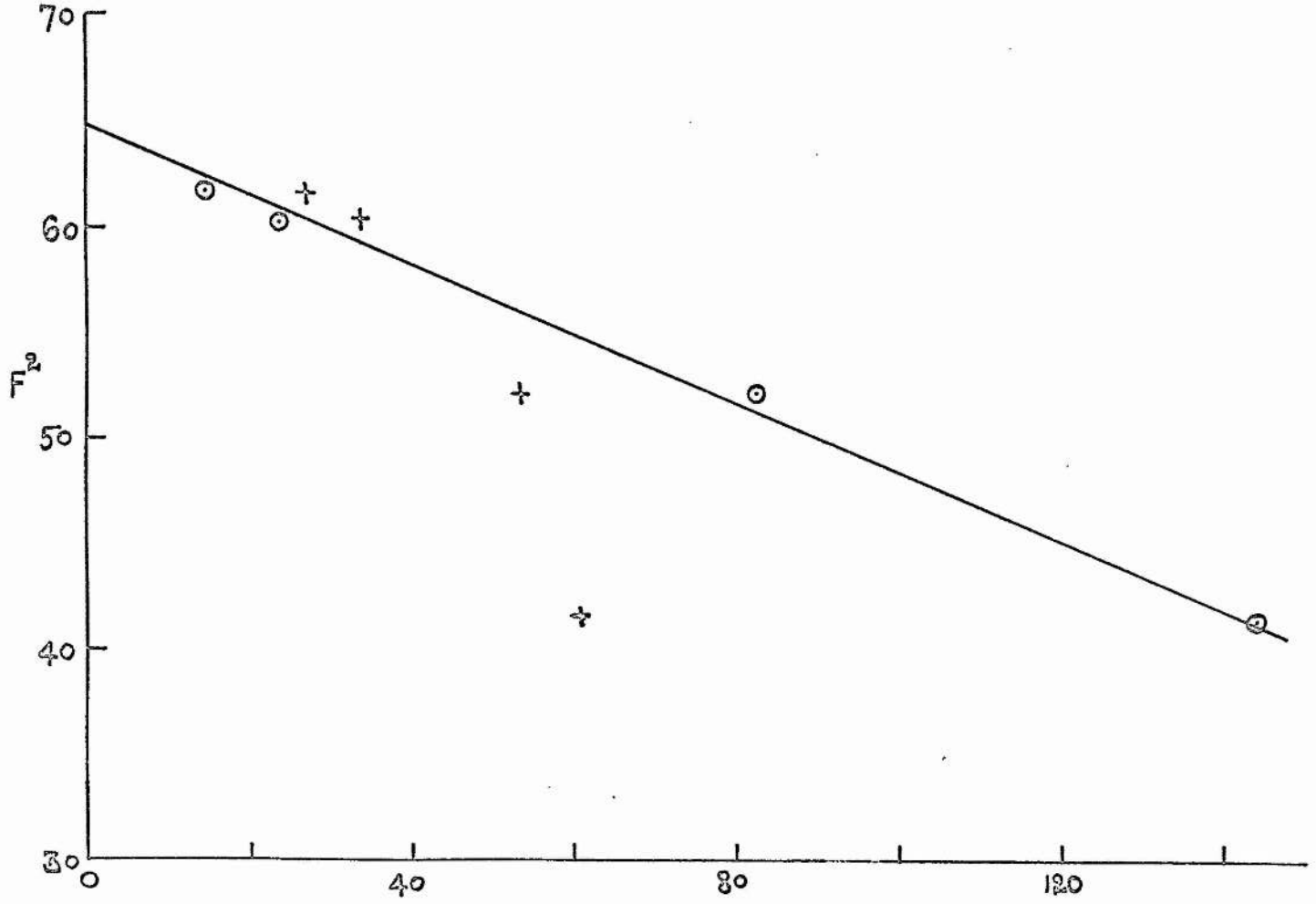

FIG 3

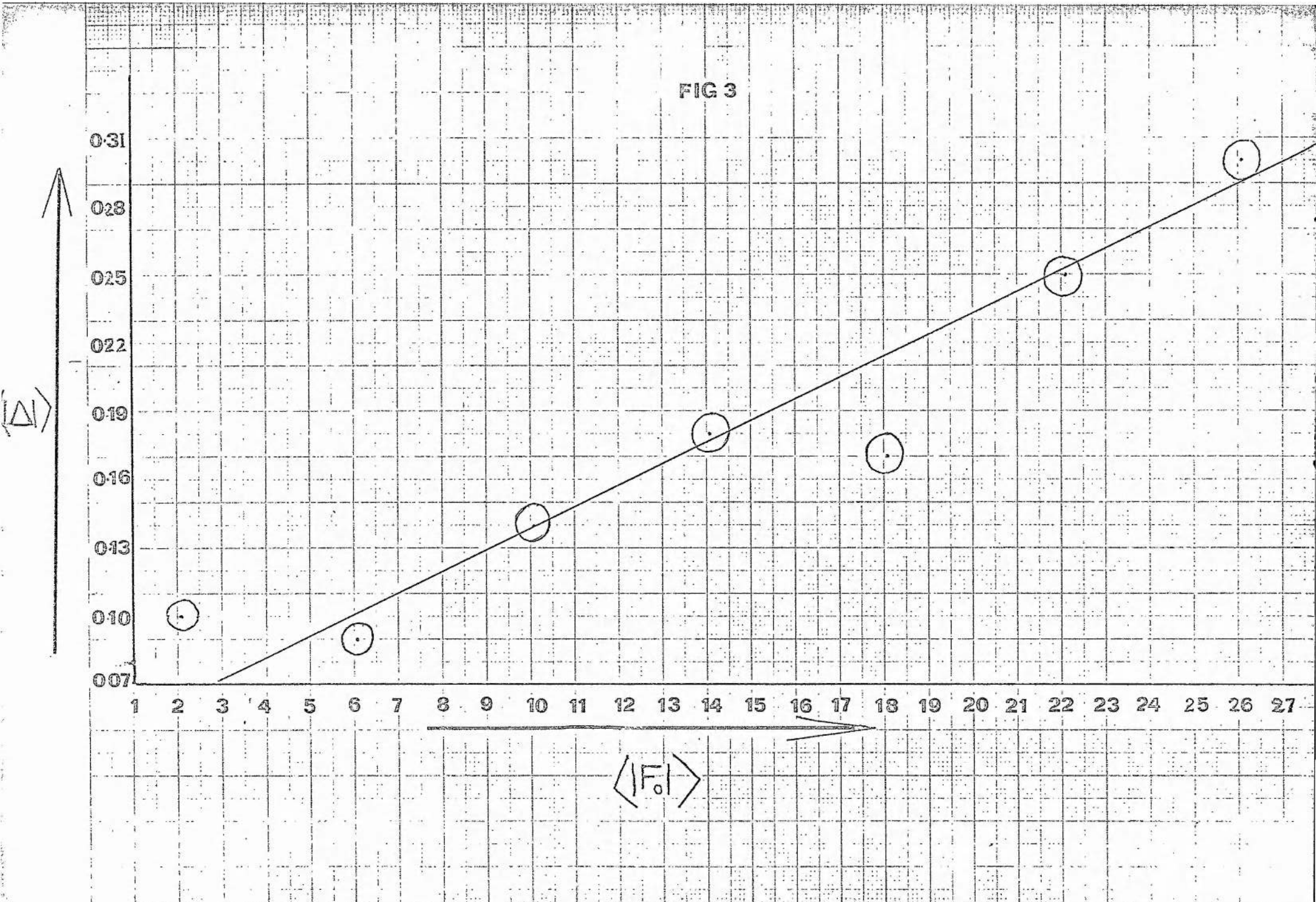
0·31
0·28
0·25
0·22
0·19
0·16
0·13
0·10
0·07
⟨Δ⟩
1 2 3 4 5 6 7 8 9 10 11 12 13 14 15 16 17 18 19 20 21 22 23 24 25 26 27
⟨|F₀|⟩

CHAPTER VI

ABSOLUTE VALUES OF STRUCTURE FACTORS BY PENDELLÖSUNG METHOD

6.1 Introduction

The previous chapters have dealt with obtaining the kinematic structure factors from very accurate X-ray integrated intensity measurements from small crystals, completely immersed in the X-ray beam. However, the measured intensities were on a relative scale and there was no reliable way of putting the structure factors on an absolute scale. In addition, if the extinction effects were large there was no satisfactory means of correcting for extinction. The inadequacy of the extinction corrections generally limits the accuracy of the structure factors and causes an appreciable error in the calculation of the electron density in crystals. To have a satisfactory solution to these problems a new technique known as the Pendellösung method of absolute measurement of the structure factors has been developed. However, this method has also limitations as it can be applied only to perfect or nearly perfect crystals.

The phenomenon of Pendellösung fringes was formulated as early as 1916 by Ewald and the fringes were first observed by Kato and Lang, 1959, in the diffraction topographs of wedge parts of a silicon crystal during the study of dislocations. These fringes are essentially fringes of equal thickness and are due to the intensity variation of the wave fields in the perfect crystals. Owing to the mathematical similarity between the variation of energy flow in the wave fields in the crystal and the energy transfer between coupled pendulums, this phenomenon was called the Pendellösung effect by Ewald.

In the kinematic theory as described in Chapter 1, it was assumed that the X-ray waves travel through the crystal with the velocity of light in free space and that the waves once scattered are not rescattered. The latter assumption that the waves are not rescattered is unrealistic and such scattering must occur within the crystal. Its effect on the observed structure factors may be small for very small crystals but it cannot be ignored for large samples. Consequently, the kinematic theory cannot be applied to X-ray diffraction from large perfect crystals. For such purposes the dynamical theory of X-ray diffraction has been developed.

The dynamical theory of X-ray diffraction was first published by Darwin (1914a), (1914b). He solved the problem of X-ray diffraction from perfect crystals through consideration of multiple reflections from the regularly spaced atomic planes. Ewald (1916a, b),(1917) considered instead the state of dynamical equilibrium between the primary wave and the waves scattered by oscillating dipoles which were assumed to be situated at the lattice points of a hypothetical lattice. Von Laue (1931, 1960) generalised the method of Ewald to the case where there is a continuous periodic distribution of scattering material.

Most of the published work on the dynamical theory of X-ray diffraction has been summarised in books by Zachariasen (1945) and James (1948). In this theory account has been taken of the exchange of energy between the primary and the diffracted waves. In the case of a Laue reflection from a thick, non-absorbing, perfect crystal a stage is reached when a constant phase relation is maintained between the two beams and the amplitude of both the primary and the diffracted beams become equal. The energy oscillates back and forth in the primary and diffracted beams as

a function of depth within the crystal with a definite period. Such an intensity modulation within the crystal is not possible to observe experimentally for a parallel sided thick crystal but can be observed for various thicknesses from a wedge shaped specimen placed in the X-ray beam in the diffracting position. The fringes so obtained are called Pendellösung fringes.

The relationship between the structure factor and the Pendellösung fringe spacing is given by Hart and Milne (1969). They have shown that for an unpolarized X-ray beam, the average polarized value of the Pendellösung fring spacing obtained on a photographic film for a symmetrical Laue reflection, Δ_o is

$$\Delta_o = \frac{\pi . V}{\lambda . \cos\theta \ . \ r_e \ F_o(\underline{h}) \ \mathrm{Tan}\ \alpha} \qquad (6.0)$$

where θ is the Bragg angle

r_e is the classical radius of an electron

$F_o(\underline{h})$ is the observed structure factor

α is the angle of the crystal wedge

V is the volume of the unit cell

Therefore the observed structure factor $F_o(\underline{h})$ may be obtained on an absolute scale from measurements of the angle of wedge and the fringe spacing.

In Chapter IV, an attempt was made to obtain accurate structure factors for lithium fluoride. One obstacle to the determination of these was the difficulty to obtain the absolute scale of the data. It was hoped that the samples of lithium fluoride which were being used were sufficiently perfect that they may exhibit Pendellösung fringes, Kato and Lang (1959). However, before undertaking such an experiment it was desired to investigate the phenomena of Pendellösung fringes using more perfect materials such as silicon and α-quartz.

6.2 Experimental

A perspective view of the apparatus known as Lang Camera is shown in Figure 1 and its optics in Figure 2. The base of the camera consists of a circular plate marked in degrees and is supported by three levelling screws. The goniometer carrying the specimen unit and the detector arm are mounted concentrically on the circular plate. The detector arm is fitted with a Geiger tube to detect the peak maxima of the diffracted beam. The crystal orientation is arranged so that the diffracted beam is always received in the horizontal plane. The X-ray source used was a fine focus tube (focal spot dimensions at anode 0.8 mm x 0.3 mm) and the X-ray beam was collimated by a long collimator 3 cm in diameter, followed by a smaller and narrow collimator having a slit width of 0.1 mm at its end. The total length of the collimator was 80 cm. The specimen crystal A was mounted on the Nonius goniometer in a known orientation in front of the exit collimator slit, 1 cm in height. The wedge edge lies in the horizontal direction and the wedge is mounted parallel to the longer dimension of the collimator slit which lies in the vertical direction. B is a 3 mm thick tantalum slit just behind the crystal and can be adjusted so that only diffracted beam passes through it and the direct beam is stopped from reaching the photographic plate which is placed at right angles to the diffracted beam behind the slit system. The photographic plates used were G5 for all the experiments, having nuclear emulsion thickness of 5 μm.

Since the width of the ribbon of X-rays is 0.1 mm, only a very narrow portion of the crystal wedge diffracts the X-rays. To scan the whole area of the wedge specimen, the specimen and

film are moved back and forth across the X-ray beam while the tantalum slit stays stationary. Such a motion is achieved by pushing forward the platform P carrying the goniometer by a micrometer screw head driven by a a.c. or d.c. motor against the restoring force of a light spring. The range of linear scan can be adjusted by the limit switches which reverse the motion of the platform at the end of each traverse. As the micrometer head moves back, the platform is pulled in the backward direction by the restoring force of the spring. Thus the crystal scans across the X-ray beam many times and a diffraction topograph from a large volume of the crystal is obtained. The exposure time for a topograph was 72 hours. This type of experiment is called a 'traverse experiment' and the pattern so obtained a traverse pattern, Kato and Lang (1959). If the crystal and film are kept stationary then another kind of fringe pattern called 'section pattern' is obtained. An example of such a pattern is shown in Figure 3. Pendellösung fringes may be described as the locus of the apex points of the hyperbolic fringes obtained in the section pattern for the various parts of a wedge shape crystal, Hattori et al (1965).

The Lang camera is widely used to detect dislocations and other defects in crystalline materials. At the places of dislocations the crystal diffracts kinematically, which gives rise to sharp contrast of the dislocation image on the diffraction topograph. This camera is thus a very simple device for demonstrating the kinematic effects during dynamic diffraction from large perfect crystals with a relatively low number of dislocations ($\approx 10^6/cm^2$).

In the present experiments of Pendellösung fringes, to simplify the geometrical factors which govern the accuracy of the final results, only symmetrical Laue reflections are considered (Hart and Milne, 1969).

6.3 Geometrical Resolution

Depending upon the experimental arrangement used, the resolution of an X-ray topographic image can vary between 2 and 50 μm. In the present experiments, since the photographic plates used have emulsion thickness of 5 μm, it is desirable to maintain the resolution of this order of magnitude by a suitable selection of the experimental conditions. The geometrical resolution can be discussed under the following two headings:

(a) Horizontal Direction: The resolutions in the horizontal and vertical direction of a topograph using the Lang camera are in general different. In the horizontal direction it is governed by diffraction experiments and is given by the horizontal divergence ψ_H of the X-ray beam.

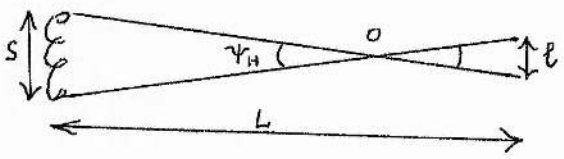

$$\psi_H = \frac{(S + \ell)}{L} \qquad (6.1)$$

where S - width of the X-ray source

L - source to crystal distance

ℓ - width of the exit collimator slit

The resolution in the horizontal direction is determined by the separation $\Delta\lambda$ of the $K\alpha_1$ and $K\alpha_2$ lines of the X-radiation. If the divergence of the incident beam is more than the angular separation of $K\alpha_1$ - $K\alpha_2$ doublet, it gives rise to two topographic images each corresponding to $K\alpha_1$ and $K\alpha_2$ lines respectively and overlapping of the two images results in poor definition of the image. To obtain a well resolved topograph, therefore, $K\alpha_2$ component must be suppressed. This is achieved by controlling the angular divergence of the incident beam.

From Bragg's law

$$2\,d\sin\theta_B = n\lambda$$

$$\therefore \quad \Delta\theta_{1-2} = \frac{n.\,\Delta\lambda}{2\,d\cos\theta_B} \tag{6.2}$$

Using this expression, $\Delta\theta_{1-2}$ for (2, 2, 0) reflection for silicon crystal for $MoK\alpha_{1-2}$ radiation is $\approx 4'$. Therefore to avoid double image due to $K\alpha_1$ - $K\alpha_2$ doublet, the horizontal divergence of the incident beam should be less than $4'$. This condition was achieved by choosing the following experimental conditions

$$S = 0.3 \text{ mm}$$

$$\ell = 0.1 \text{ mm}$$

$$L = 800 \text{ mm}$$

$$\therefore \quad \psi_H = \frac{0.4}{800} \text{ radians} \approx 2'$$

The intrinsic width of (2, 2, 0) reflection peak is approximately 20", Parratt (1933, 1944). Hence in the present experiments the horizontal divergence of the incident beam was enough to take a topographic record of integrated reflection of the Bragg peaks under consideration and yet so small as to diffract only $K\alpha_1$ radiation. For very low order reflections where $\Delta\theta_{1-2}$ is

very small, decreasing of ℓ or using a very low take-off angle with a view to improve resolution will result in extremely long exposure times and this is avoided in the present experiments.

(b) Vertical Direction: This is the direction parallel to the longer dimensions of the slit. The geometrical resolution in this direction is obtained by the projection of the focal size in that direction.

If H is the height of the X-ray source as viewed at a given take-off angle, S_1 the distance from the crystal specimen to the photographic plate and L the length of the collimator, then the resolution R_S in the vertical direction is given by

$$R_S = \frac{S_1 H}{L} \qquad (6.3)$$

Now the specimen to slit distance S_1 cannot be less than 10 mm in practice, as for smaller distances the direct and diffracted beams cannot be separated. In the present experiments

$$R_S = \frac{10 \times 0.3}{800} \approx 4 \ \mu m.$$

6.4 Topographic Distortion due to Vertical Divergence

Even the well-collimated X-rays are slightly divergent and therefore the fringe separation as recorded on the photographic plate is more than the true value by a factor $\frac{(S_1 + L)}{L}$. To obtain the true average fringe spacing, the observed fring spacing is divided by the above factor. The vertical divergence varies from point to point in the topograph unless the emulsion surface is held parallel to the mean plane of the specimen crystal. In the present experiments this correction factor is 1.013.

6.5 Preparation of Specimens

Ultra pure single crystals of silicon in special orientation were kindly supplied by Dr. Milne of the University of Edinburgh. These crystals were grown free of strains and X-ray topographic experiments showed that these were free of any dislocations. Four samples were ground into wedges and one known face of each of the four specimens was left unground. Since the silicon crystals are very hard and brittle the depth of the damage caused to the surface due to mechanical griding is of the order of 40 μm.

Figure 4 shows the diffraction topograph of a silicon wedge after mechanical grinding. The damaged surface shows the scratches and fine pits caused by grinding. The same crystal after etching with a CP_4 solution (a mixture of 5 parts 48% HF + 1 part conc. HNO_3) for about 3 minutes has given Pendellösung fringes. The maximum and minimum thickness of the four silicon wedge samples varied from 0.1 mm to 2.5 mm and the height of these wedges was about 1 cm in each case. The α-quartz wedges were prepared in a similar way and the damaged layers removed by etching with 48% hydrofluoric acid. Table I lists the special orientation of the four silicon wedges and two natural α-quartz wedges. A direct check on the uniform slope of the specimen wedges was made by recording the transmitted X-ray beam. No detectable spurious intensity peaks were noticed on the photographs and the wedges were good enough for the purposes of the present experiments.

6.6 Determination of the Angle of Wedge and Fringe Spacing

After obtaining the Pendellösung fringe patterns there are two basic quantities to be determined for finding the absolute values of the structure factors using equation (6.0). The first

one is the angle of wedge and the second, the fringe spacing.

Two independent methods were employed to determine the angles of various wedges used in the present experimental work. In the first method the length and thickness of the wedges were measured by a travelling microscope and the wedge angle α determined.

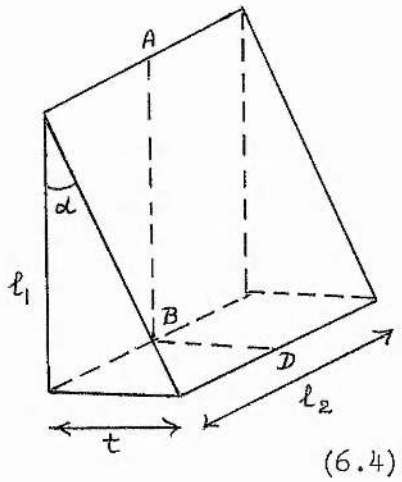

$$\tan \alpha = \frac{t}{\ell_1} \qquad (6.4)$$

The maximum variation of the wedge thickness t as measured across the length ℓ_2 was 1.6%. However, the fringe spacing was measured along the line AB which is the middle line of the wedge and the wedge thickness at the position BD was measured with an accuracy of 0.3%. Thus the maximum % error in the calculation of the wedge angle by this method is 0.6%.

To make an internal check on the values of wedge angles obtained by microscopic measurements a second method was employed. In this method a very narrow laser beam was used. The laser beam was made to shine on the two faces of the silicon wedge and the reflected images so obtained were received on a screen about a meter away from the wedge. By measuring the separation of the two reflected images from the central position of the direct image and from the distance between the crystal wedge and the screen, the angle α was determined. The wedge angles determined by this method have the maximum error of 0.8% as compared to 0.6% in the microscopic method. The wedge angles determined by both of these methods have been listed in Table I. It can be seen from this

Table that there is no detectable systematic trend in the results obtained by the two methods. However, the wedge angles determined by microscopic measurements are considered to be more reliable than those determined by the laser beam due to the ambiguity of finding the central position of the reflected spots due to their natural spread on the screen. This method was not very accurate for the α-quartz wedges where the spread of the spots was enormous and therefore the wedge angles of α-quartz wedges were not determined using a laser beam.

The fringe spacing was measured using "The Rapid Photometer G II", (Carl Zeiss, Jena). Each measurement was repeated ten times and the standard deviation of the mean fringe spacing was 0.4%. Thus the total error introduced in the structure factor due to errors in the measurement of the wedge angle and the fringe spacing may be 1%. The structure factors of silicon, (1, 1, 1), (2, 2, 0), (4, 4, 0) and α-quartz crystals $(1, 0, \bar{1})$ reflection were determined using equation (6.0).

Figures 6, 7, 8, 9, 10, 11 and 12 show the various fringe patterns for silicon and α-quartz wedges. A few fringes near the edges of the wedges were not considered for the fringe spacing measurements due to the rounding of the wedge edges during the etching process, which results in decreasing the fringe spacing, Hattori et al (1965).

Figures 6 and 7 show the effect of the two planes of polarization on the fringe visibility for a $(\bar{2}, 2, 0)$ reflection. The fringes disappear after a certain number. The phenomenon of disappearing of the fringes is called 'fading' and the regions where the fringes disappear are called the 'fading regions'. Fading of the fringes at regular intervals is due to the superposition of

the two types of fringes with different spacing corresponding to each plane of polarization. Figure 14 shows a photometric trace of the Pendellösung fringes of Figure 6 within the first fade. It shows the oscillatory character of the intensity variation of the fringes, which, in turn, represents the oscillatory characteristic of the wave field inside the crystal wedge.

Many attempts were made to obtain the Pendellösung fringes of lithium fluoride. The wedges were ground as described earlier and the damaged surface etched using 46% HF acid. A typical topograph of a lithium fluoride wedge is shown in Figure 13, which shows a large number of crystal defects and surface scratches. No Pendellösung fringes were obtained from any of the samples used.

6.7 Conclusions

Absolute values of the scattering factors for the (1, 1, 1), (2, 2, 0), (4, 4, 0) reflections for silicon crystals and the structure factor for $(1, 0, \bar{1})$ reflection for α-quartz have been presented (Table II). The experiments for silicon wedges using $MoK\alpha_1$ radiation have been repeated using $AgK\alpha_1$ radiation and the results are found to be in good agreement with each other within the experimental errors. In the case of α-quartz, the Pendellösung experiments have been performed with two α-quartz wedges using $MoK\alpha$ radiation. As can be seen from Figures 11 and 12, there are many discontinuities in the fringe pattern for α-quartz wedges and hence there are liable to be systematic errors in the measurement of fringe spacing arising due to the crystal imperfection, Hart (1966). The results obtained from Pendellösung measurements for silicon wedges are comparable to very accurate intensity measurements and are compared with the results of other authors, Table II. No corrections were made for

anomalous dispersion since these are not reliably determined. The results of other authors used for comparison were also not corrected for anomalous dispersion. The present results are in good agreement with the values obtained by these authors and are within our 4 standard deviations. However, the values obtained for the (1, 1, 1), (2, 2, 0) reflections of silicon in this experiment are systematically higher than those obtained by Tanemura and Kato (1972) but agree well with the values reported by Hattori et al (1965). The possible reason for the systematically higher values obtained in the present experiments is that the samples used had strain resulting in the decrease of the fringe spacing, Hart and Milne (1969).

In the present experiments, although the crystal samples originally supplied were free of any strain it is possible that mechanical griding induced strain in the crystals giving rise to systematic errors in the structure factors, the magnitudes of which are unknown. Also the determination of the structure factors assumes the average polarized value of fringe spacing which is not strictly true. The fringe spacings are different for two planes of polarization and a gradual fringe shift does occur with higher fringe orders, although care was taken to use those fringes for structure factor calculation for which the fringe shift was minimum. However, the possibility is that there is still some systematic error in the structure factors.

The great merit of Pendellösung method over other methods is that the structure factors are directly obtained on an absolute scale. However, this method has limitations, as it can be applied only to perfect or very nearly perfect crystals. The future success of this method to other crystalline materials depends upon

the technique of growing big samples of perfect crystals. In spite of this limitation, this technique still remains a very powerful tool for the detection of dislocations and other defects in large samples of crystals where electron microscope techniques cannot, successfully, be applied.

TABLE I

Wedge material	Unground entrance surface	Wedge edge direction	Diffracting planes	Angle of wedge	
				Microscopic method	Laser beam method
Silicon wedge 1	$\bar{2}\ 2\ 0$	$1\ 1\ \bar{2}$	$1\ 1\ 1$	9°-36'	9°-29'
Silicon wedge 2	$2\ 2\ 0$	$1\ \bar{1}\ 2$	$\bar{1}\ 1\ 1$	9°-33'	9°-26'
Silicon wedge 3	$1\ 1\ 1$	$1\ 1\ \bar{2}$	$\bar{2}\ 2\ 0$	9°-40'	9°-49'
Silicon wedge 4	$1\ 1\ 1$	$1\ 1\ \bar{2}$	$\bar{2}\ 2\ 0$	6°-4'	6°-7'
α-quartz wedge 1	$1\ 1\ 1$	-	$1\ 0\ \bar{1}$	10°-51'	-
α-quartz wedge 2	$1\ 1\ 1$	-	$1\ 0\ \bar{1}$	4°-24'	-

TABLE II

Scattering factors of silicon at room temperature

Reflection	Scattering factors. (present results)	Scattering factors. (Results of other authors)		
		Kato 1972	Hattori et al 1965	Hart and Milne 1969
1 1 1	10.75 ± 0.08	10.664 ± 0.005	10.98 ± 0.16	-
2 2 0	8.64 ± 0.08	8.463 ± 0.004	8.58 ± 0.09	8.478 ± 0.008
4 4 0	5.41 ± 0.10	5.408 ± 0.003	5.41 ± 0.14	-

Structure factors of α-quartz at room temperature

Reflection	Present work	Zachariasen's value F_{cal}
1 0 $\bar{1}$	39.56 ± 0.33	39.31

FIG1

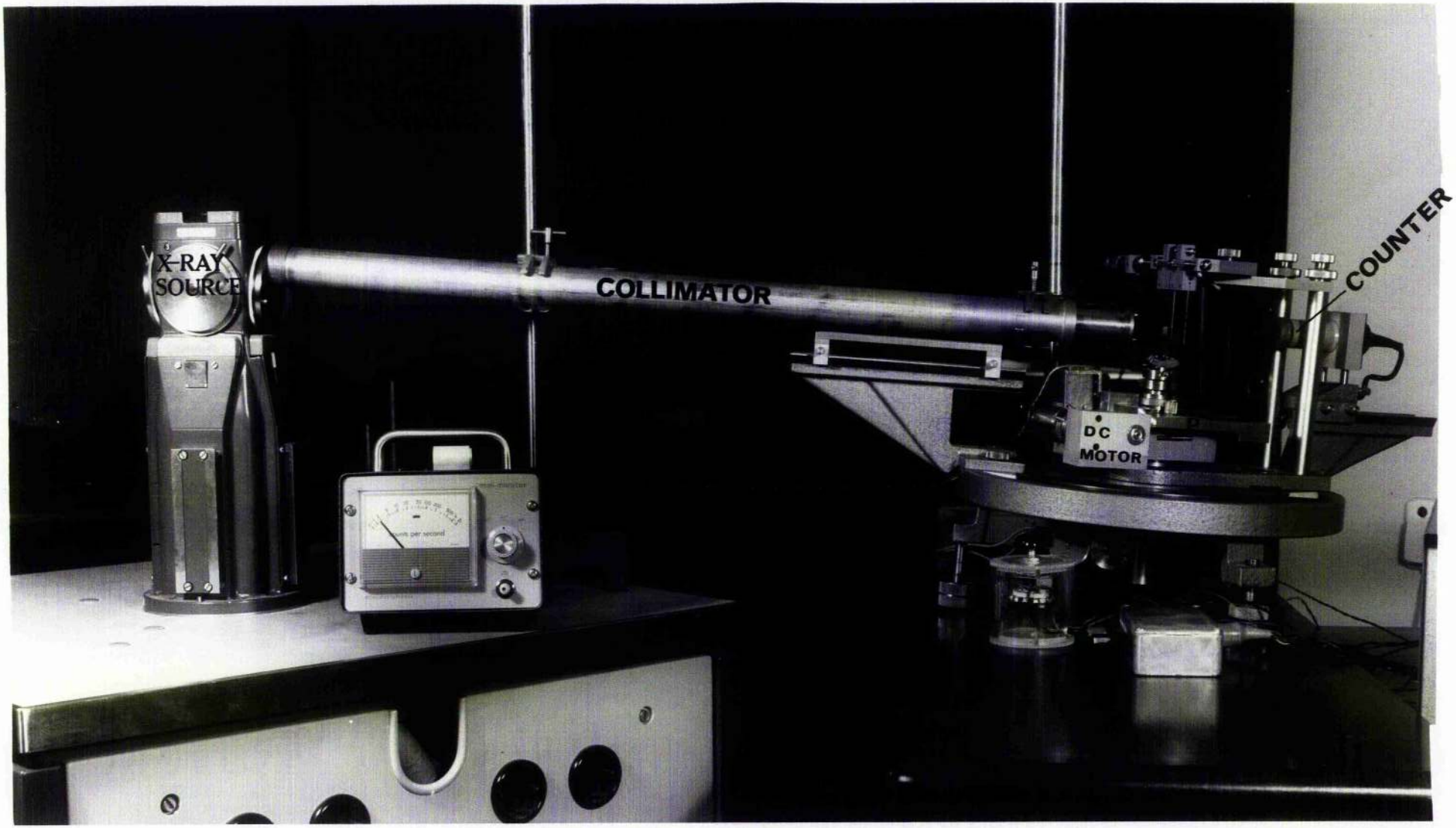

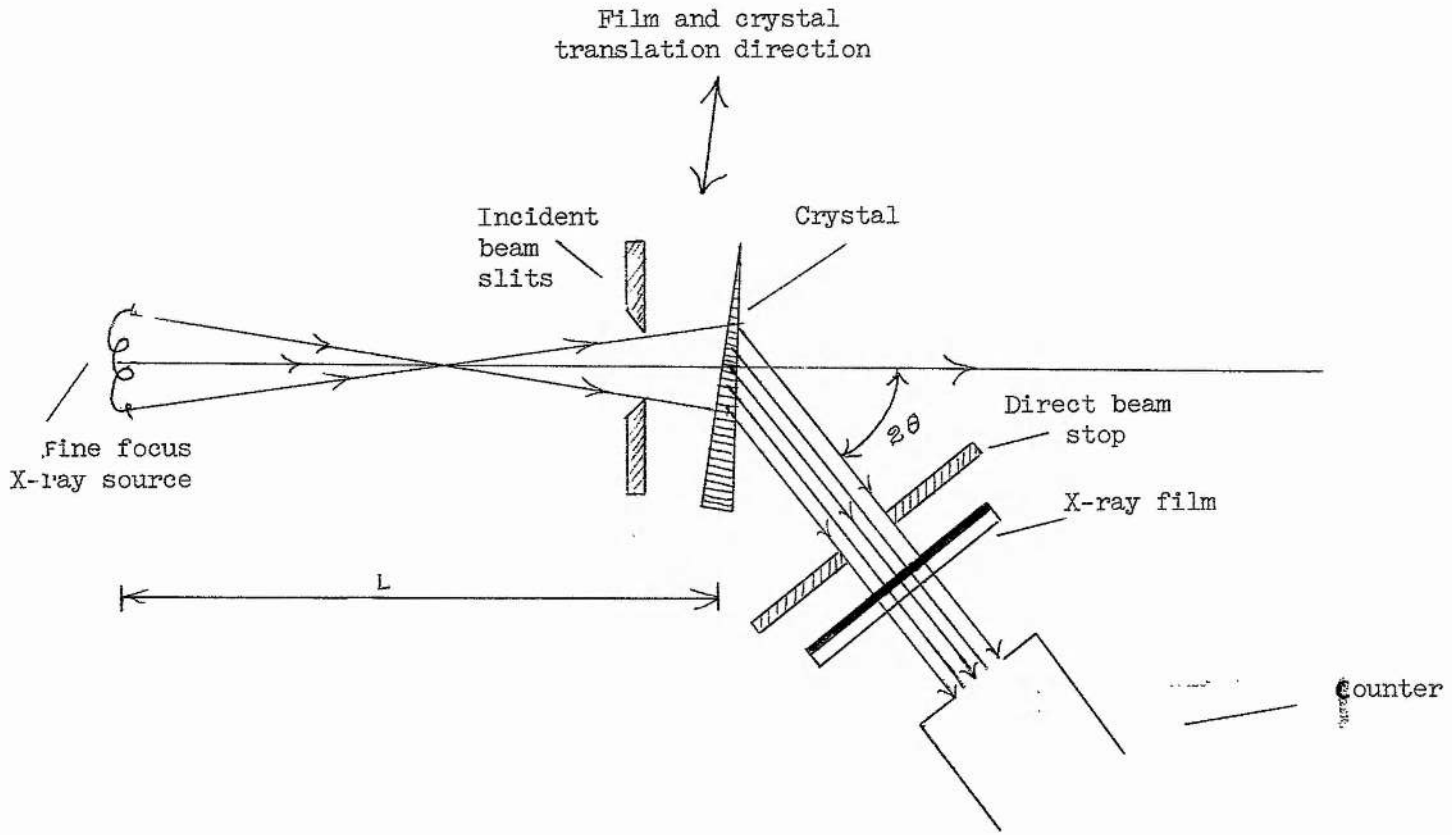
Film and crystal
translation direction
Incident
beam
slits
Crystal
Fine focus
X-ray source
2θ
Direct beam
stop
X-ray film
L
Counter

FIG. 2.

X160

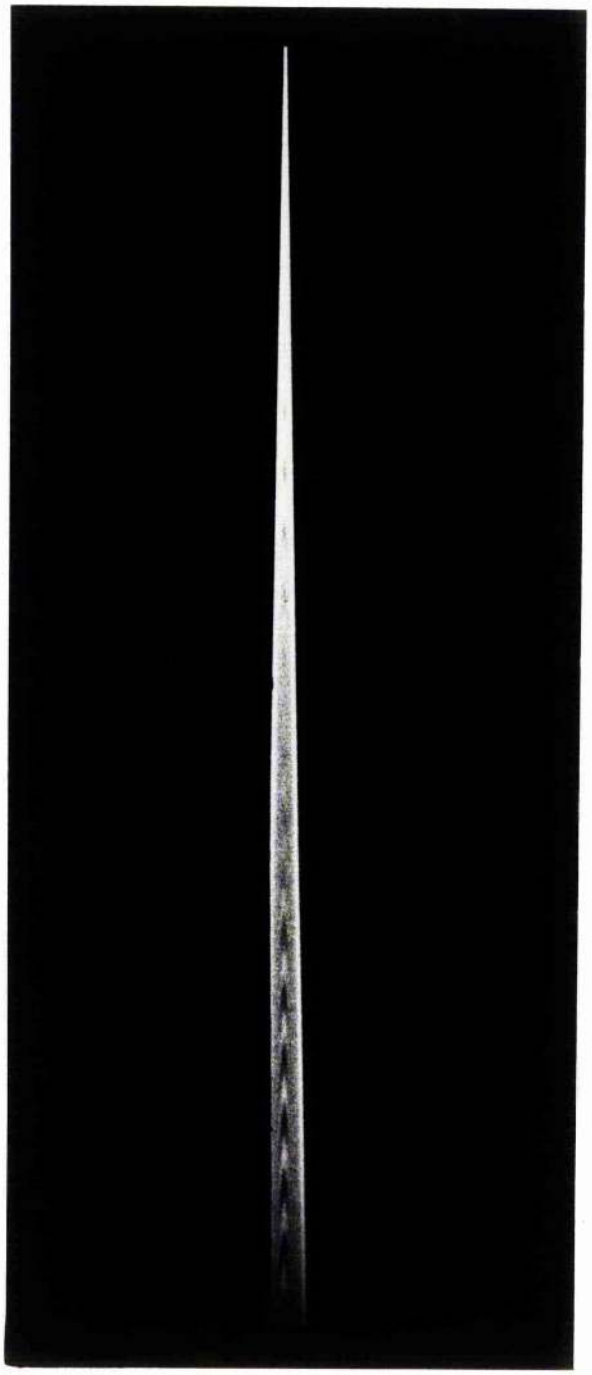

FIG. 3. Section topograph of a wedge-shaped crystal of silicon for $(\bar{2}, 2, 0)$ reflection.
(MoKα radiation)

X160

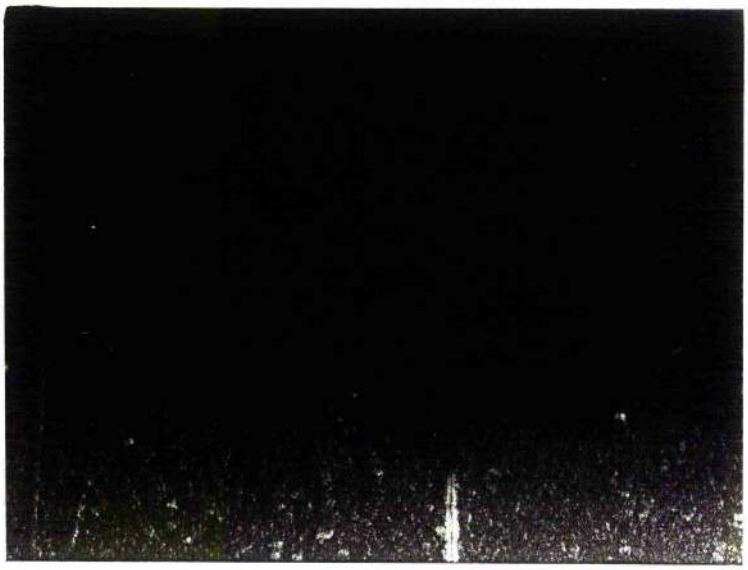

FIG. 4. Diffraction topograph of a wedge-shaped crystal of silicon after mechanical grinding, (2, 2, 0 reflection). ($MoK\alpha_1$ radiation)

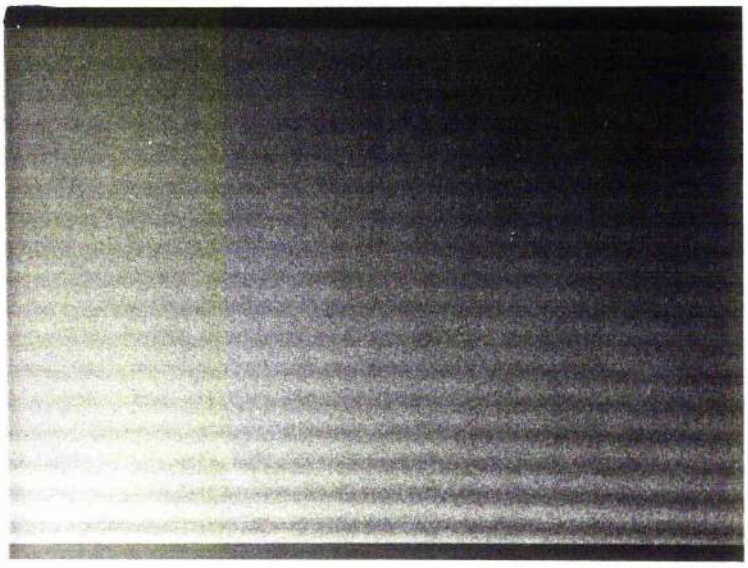

FIG. 5. Diffraction topograph of the above crystal after etching with CP4 solution.

×150

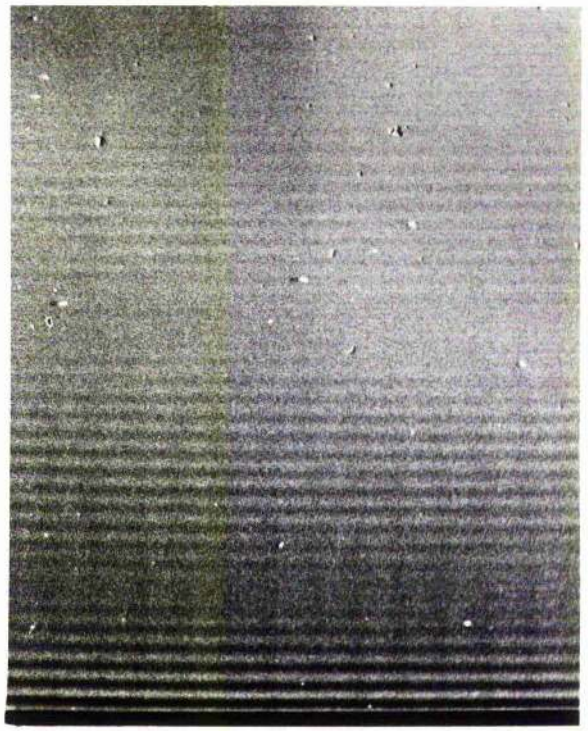

FIG. 6. Effect of unpolarized X-rays. $(\bar{2}, 2, 0)$ reflection. $MoK\alpha_1$ radiation. Si wedge.

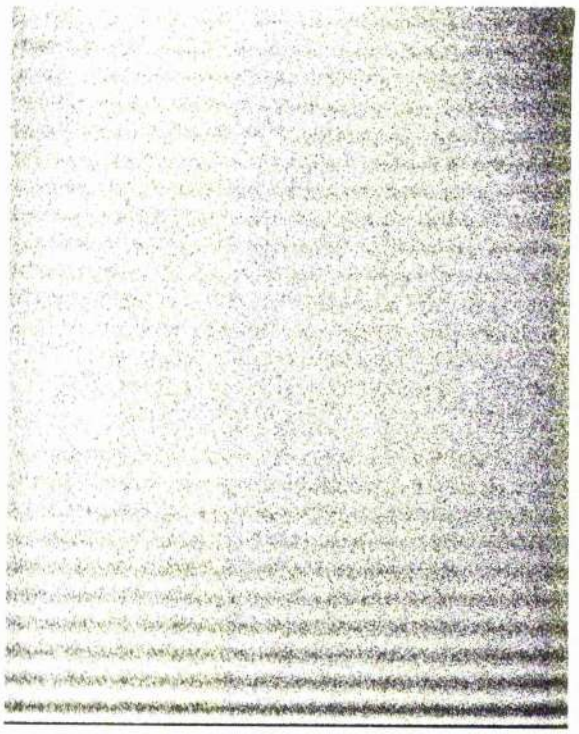

FIG. 7. The diffraction topograph of the above wedge using $AgK\alpha$ radiation.

X160

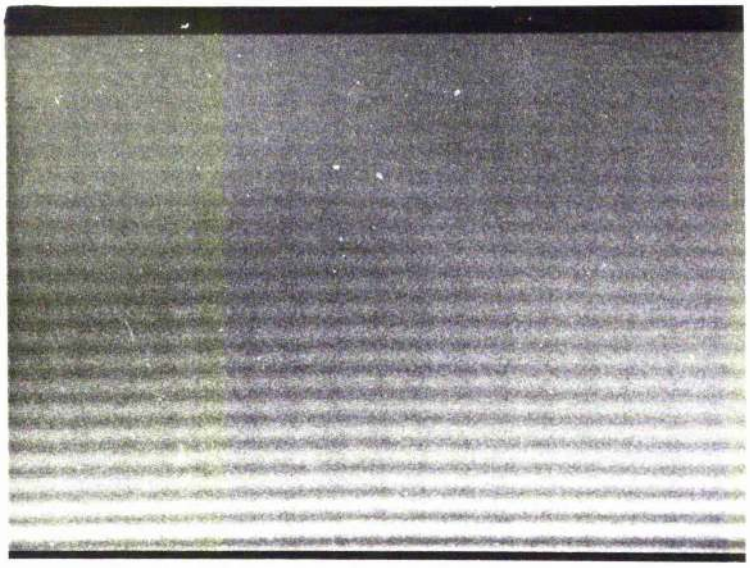

FIG. 8 Pendellösung fringes.
(1, 1, 1) reflection)
Silicon wedge.
MoKα radiation.

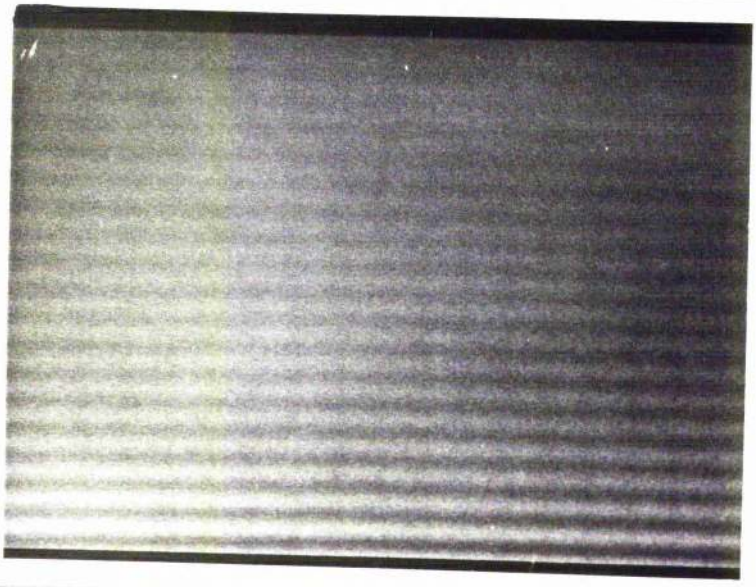

FIG. 9 Pendellösung fringes.
(1, 1, 1) reflection.
Silicon wedge.
AgKα radiation.

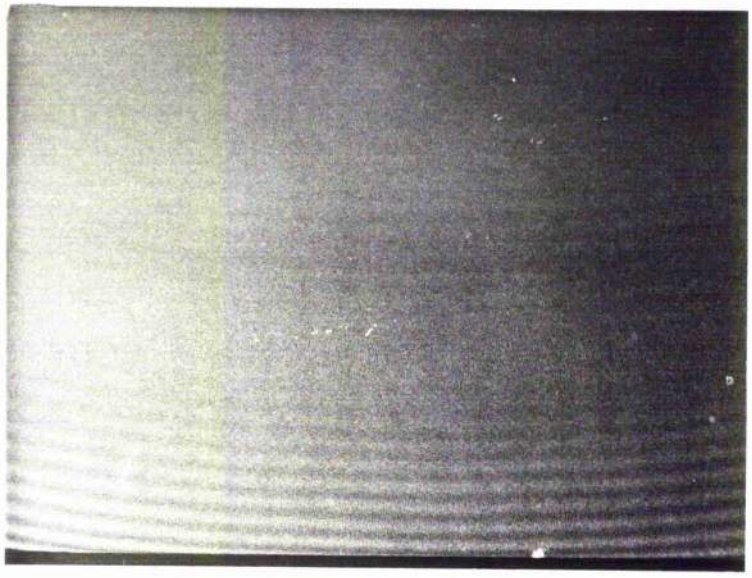

FIG. 10. Effect of rounding of the wedge edges of Pendellösung fringes due to excessive etching. Silicon wedge, $(\bar{2}, 2, 0)$ reflection, MoKα_1 radiation.

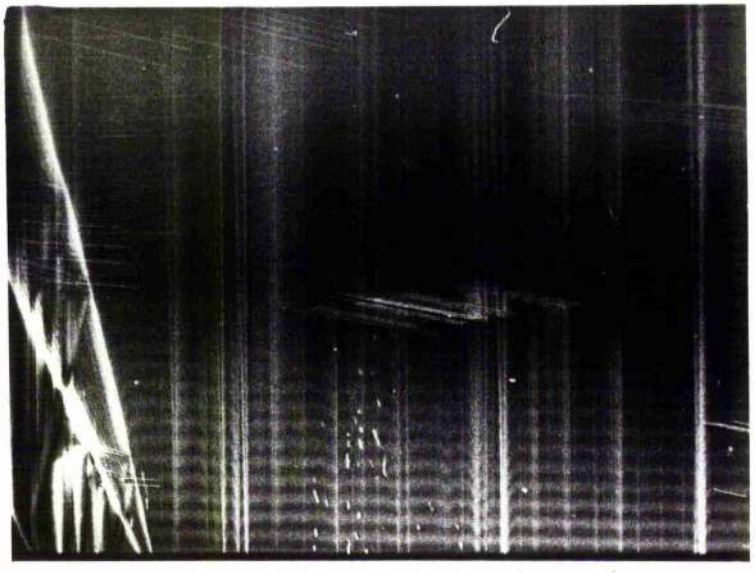

FIG. 11. Pendellösung fringes $(1, 0, \bar{1})$ reflection. α-quartz wedge MoKα radiation.

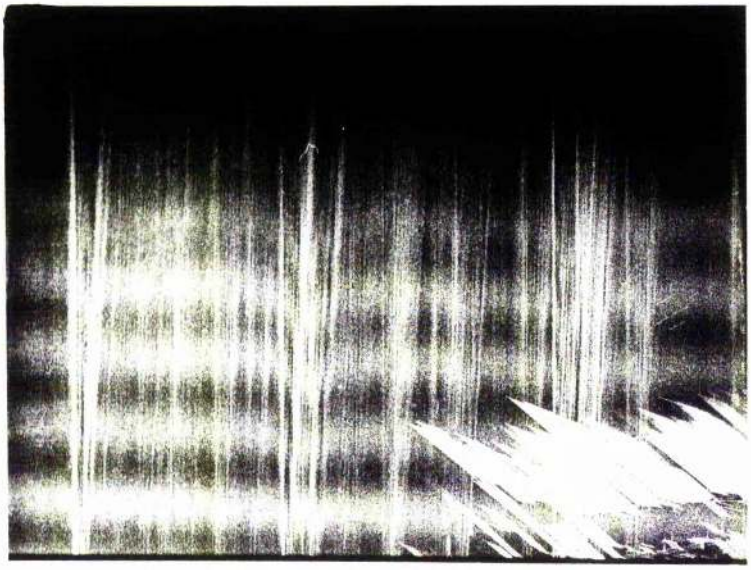

FIG. 12. Pendellösung fringes.
(1, 0, $\bar{1}$) reflection.
α-quartz wedge.
MoKα radiation.

FIG. 13. X-ray diffraction topograph of a lithium fluoride wedge-shaped crystal. (2, 0, 0) reflection.
MoKα radiation.

FIG. 14

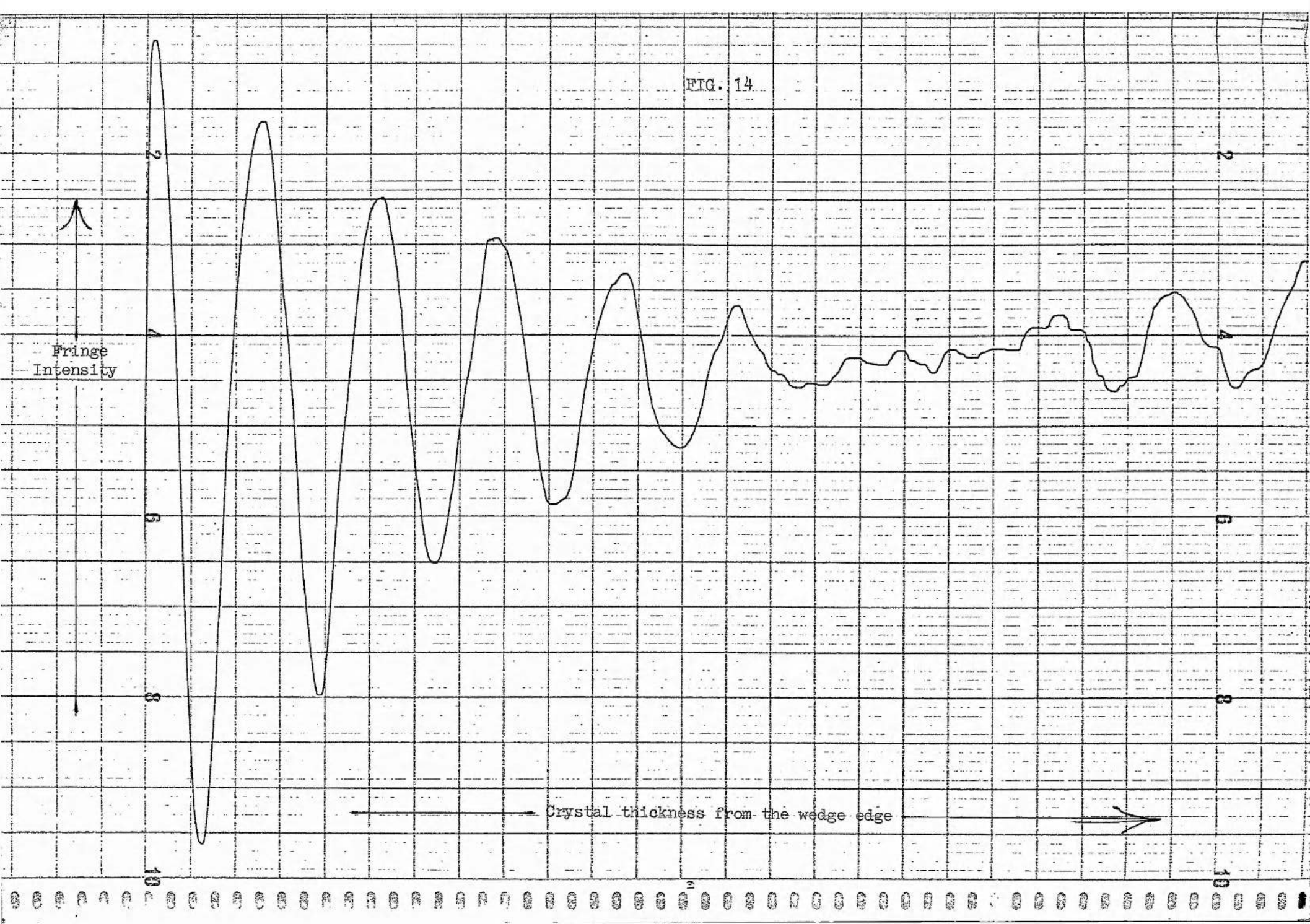

APPENDIX A

The Absorption Programme

The absorption programme was written for applying absorption corrections to a regular parallelopiped of α-glycine crystal. For this purpose three sets of axial systems were considered. The reciprocal crystal axial system a* b* c*, and a right handed orthogonal axial system X', Y', Z' in the crystal such that X'-axis is along the a* direction, Y' axis along the b* direction and Z' axis at right angle to the plane containing these two axes and pointing toward the c-axis (as shown in figure 1). The third axial system was a right handed ϕ-axial system of the diffractometer.

The application of the absorption programme consisted of the following steps

(I) Transformation of the direction cosines of the crystal faces with respect to the crystal system, to the orthogonal axial system X', Y', Z':

If h, k, ℓ is a vector with respect to the crystal system then h' k' ℓ', the corresponding vector in the orthogonal system is given by

$$\begin{pmatrix} h' \\ k' \\ \ell' \end{pmatrix} = \lambda \underset{\sim}{T} \begin{pmatrix} h \\ k \\ \ell \end{pmatrix} = \lambda \begin{pmatrix} a^* & o & c^* \cos \beta^* \\ o & b^* & o \\ o & o & c^* \sin \beta^* \end{pmatrix} \begin{pmatrix} h \\ k \\ \ell \end{pmatrix}$$

where $\underset{\sim}{T}$ is the orthogonal matrix,

(Rollet, 1965) for a monoclinic system.

Since the crystal has the natural faces (100), (010), (001), the new direction cosines are given by

$$\begin{pmatrix} h' \\ k' \\ \ell' \end{pmatrix}_{100} = \lambda \begin{pmatrix} a^* & o & c^* \cos\beta^* \\ o & b^* & o \\ o & o & c^* \sin\beta^* \end{pmatrix} \begin{pmatrix} 1 \\ o \\ o \end{pmatrix} = \begin{pmatrix} \lambda a^* \\ o \\ o \end{pmatrix}$$

also $$\begin{pmatrix} h' \\ k' \\ \ell' \end{pmatrix}_{010} = \lambda \begin{pmatrix} a^* & o & c^* \cos\beta^* \\ o & b^* & o \\ o & o & c^* \sin\beta^* \end{pmatrix} \begin{pmatrix} o \\ 1 \\ o \end{pmatrix} = \begin{pmatrix} o \\ \lambda b^* \\ o \end{pmatrix}$$

and $$\begin{pmatrix} h' \\ k' \\ \ell' \end{pmatrix}_{001} = \lambda \begin{pmatrix} a^* & o & c^* \cos\beta^* \\ o & b^* & o \\ o & o & c^* \sin\beta^* \end{pmatrix} \begin{pmatrix} o \\ o \\ 1 \end{pmatrix} = \begin{pmatrix} \lambda c^* \cos\beta^* \\ o \\ \lambda c^* \sin\beta^* \end{pmatrix}$$

(II) Determination of the equations of crystal faces with respect to orthogonal system:

If d_1, d_2, d_3 are the perpendicular distances from the origin o of the orthogonal axes taken to be the point of intersection of the diagonals of the parallelopiped to the crystal faces (100), (010) and (001) respectively, then the normalized equations of the faces are

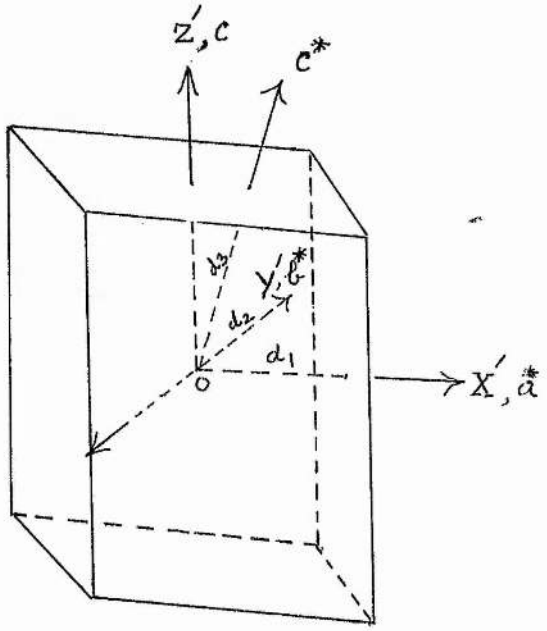

Figure 1

$$X' = d_1$$

and $X' = -d_1$

$$Y' = d_2$$

and $Y' = -d_2$

$$X' \cos \beta^* + Z' \sin \beta^* = d_3$$

and $X' \cos \beta^* + Z' \sin \beta^* = -d_3$

where $d_1 = 0.0056$ cm; $d_2 = 0.00125$ cm and $d_3 = 0.0116$ cm.

(III) Transformation of the equations of crystal faces from the orthogonal set in the crystal system to the orthogonal set of ϕ axial system:

In the adjoining figure two sets of axes have been shown. The crystal orthogonal axial system X', Y', Z' and the ϕ-axial system X, Y, Z. The X-axis is chosen along the direction corresponding to $\phi = 0$ when $\chi = 0$ and Y axis at $\phi = 90°$ when $\chi = 0$ and the Z-axis is pointing along the ϕ-axis of the ϕ-circle at $\chi = 0$.

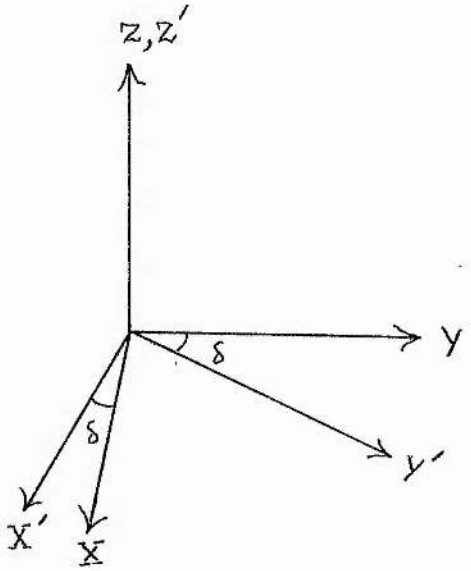

The coordinates of any point X', Y', Z' in the crystal parallelopiped, referred to the crystal orthogonal system can be transformed into the ϕ-axial system using the transformation given by Rollet (1965)

$$\begin{pmatrix} X \\ Y \\ Z \end{pmatrix} = \begin{pmatrix} X' \\ Y' \\ Z' \end{pmatrix} \begin{pmatrix} \cos\delta & -\sin\delta & 0 \\ \sin\delta & \cos\delta & 0 \\ 0 & 0 & 1 \end{pmatrix}$$

The angle δ was determined from the orientation matrix and it represents the initial setting of the crystal with respect to the right handed ϕ-axial system.

(IV) Determination of the direction cosines of the primary and diffracted beams with respect to the ϕ-axial system:

If ϕ, χ and θ are the setting angles for a reflection in the diffraction position then the direction cosines of the reverse primary and diffracted beams with respect to the ϕ-axial system are given by (Busing and Levy, 1967).

$$-p_\phi = \begin{pmatrix} \sin\theta & \cos\chi & \cos\phi + & \cos\theta & \sin\phi \\ \sin\theta & \cos\chi & \sin\phi - & \cos\theta & \cos\phi \\ \sin\theta & \sin\chi & & & \end{pmatrix} = \begin{pmatrix} \ell_p \\ m_p \\ n_p \end{pmatrix}$$

and

$$d_\phi = \begin{pmatrix} \sin\theta & \cos\chi & \cos\phi - & \cos\theta & \sin\phi \\ \sin\theta & \cos\chi & \sin\phi + & \cos\theta & \cos\phi \\ \sin\theta & \sin\chi & & & \end{pmatrix} = \begin{pmatrix} \ell_d \\ m_d \\ n_d \end{pmatrix}$$

where ℓ_p, m_p, n_p and ℓ_d, m_d, n_d are the direction cosines of the primary and diffracted beams respectively.

(V) Determination of path lengths of the primary and the diffracted beams and the calculation of transmission factors:

Now assuming the equations of the crystal faces to be $a_n X + b_n Y + c_n Z + d_n = 0$ with respect to the ϕ -axial system, the perpendicular distance of a point X_i, Y_i, Z_i from a crystal face is given by

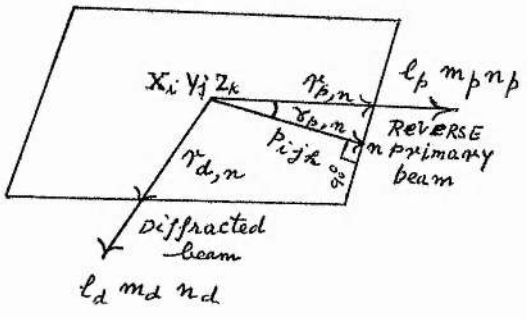

$$p_{ijk} = \frac{-a_n X_i - b_n Y_j - C_n Z_k - d_n}{(a_n^2 + b_n^2 + c_n^2)^{\frac{1}{2}}}$$

$$\text{now } p_{ijk} = r_{p,n} \cos \gamma_{p,n}$$

$$\therefore r_{p,n} = \frac{-a_n X_i - b_n Y_j - C_n Z_k - d_n}{a_n . \ell_p + b_n . m_p + C_n . n_p}$$

The intersection of the primary beam with face (n) lies towards the X-ray source if, and only if, $\gamma_{p,n} < 90°$ and this will be so if the denominator of the $r_{p,n}$ expression is -ve. If the denominator is ≥ 0 then the numerator and $r_{p,n}$ for that face was not calculated. The required r_p value is thus the smallest +ve $r_{p,n}$ value.

Similarly

$$r_{d,n} = \frac{-a_n X_i - b_n Y_i - C_n Z_i - d_n}{a_n . \ell_d + b_n . m_d + C_n . n_d}$$

and the required r_d is the smallest +ve $r_{d,n}$ value. After having computed the r_p and r_d values for each of the N grid points set inside the crystal parallelopiped, the transmission factor for a reflection (h, k, ℓ) was determined from the following summation

$$\text{Transmission factor} = \frac{\sum_{a=1}^{a=N} e^{-\mu (r_p + r_d)_a}}{N}$$

The optimum choice of the total number of grid points set in the crystal parallelopiped was based upon the computation of transmission factors by increasing this number until the transmission factor stayed constant. The minimum number at this point gave the number of grid points set inside the crystal and this number was 3,200. The shape of the grid was the same as that of the crystal parallelopiped. The transmission factors were calculated for all the reflections and absorption corrections applied to the integrated intensities.

APPENDIX B

Calculation of Orientation Matrix and Extraction of Reciprocal and Real Cell Parameters

A three or four-circle diffractometer is a device that will allow a reciprocal space vector h to be turned with respect to the incident beam so that diffraction can occur, i.e., the scatterirg vector bisects the angle between the incident and diffracted beams.

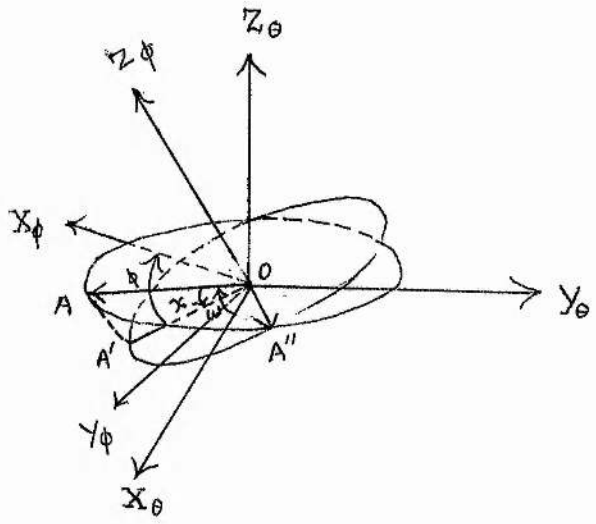

The Θ-axial system and ϕ-axial systems are shown in the adjoining figure. In Θ-axial system X_θ is in the direction of the diffraction vector, Y_θ bisects the angle 2Θ and Z_θ is parallel to the Θ-axis of the diffractometer. In the ϕ-axial system, the axis X_ϕ is chosen along the direction at $\phi = 0$, Z along the ϕ axis of the diffractometer and Y_ϕ at right angles to these two axes forming a right handed system. If ω, ϕ, χ are the three setting angles to transform a unit vector in the direction X_Θ to the ϕ-axial system of the instrument then the transformation matrix (Busing and Levy, 1967) is

$$\begin{pmatrix} \cos\omega \cos\chi \cos\phi & - \sin\omega \sin\phi \\ \cos\omega \cos\chi \sin\phi & + \sin\omega \cos\phi \\ \cos\omega \sin\chi & \end{pmatrix} \qquad (1)$$

Thus a vector having magnitude $\frac{2 \sin \theta}{\lambda}$, in diffraction position would have the transformation

$$\begin{pmatrix} X_\phi \\ Y_\phi \\ Z_\phi \end{pmatrix} = \frac{2 \sin \theta}{\lambda} \begin{pmatrix} \cos\omega & \cos\chi & \cos\phi - \sin\omega & \sin\phi \\ \cos\omega & \cos\chi & \cos\phi + \sin\omega & \cos\phi \\ \cos\omega & \sin\chi & & \end{pmatrix} \qquad (2)$$

Any vector $\underline{h}$ in the crystal axis system may be transformed into orthogonal axial system X_c, Y_c, Z_c set inside the crystal by the transformation

$$\begin{pmatrix} X_c \\ Y_c \\ Z_c \end{pmatrix} = \underset{\sim}{T} \begin{pmatrix} h \\ k \\ \ell \end{pmatrix} \qquad (3)$$

where $\underset{\sim}{T}$ is the orthogonality matrix (Rollet, 1965) and is given by

$$\begin{pmatrix} a^* & b^* \cos \gamma^* & c^* \cos \beta^* \\ o & b^* \sin \gamma^* & -c^* \sin \beta^* \cos \alpha \\ o & o & 1/c \end{pmatrix} \qquad (4)$$

X_c lies along a*, Y_c in the a*b* plane and Z_c at right angles to that plane.

Now in order that the vector $\underline{h}$ may be in the diffracting position there must exist a rotation matrix R which will rotate the above orthogonal system to coincide with the ϕ-axial system.

$$\therefore \quad \begin{pmatrix} X_\phi \\ Y_\phi \\ Z_\phi \end{pmatrix} = \underset{\sim}{R} \begin{pmatrix} X_c \\ Y_c \\ Z_c \end{pmatrix} = \underset{\sim}{R}.\underset{\sim}{T} \begin{pmatrix} h \\ k \\ \ell \end{pmatrix} \qquad (5)$$

Equating (2) and (5), since both are under diffraction position

$$\underset{\sim}{R}.\underset{\sim}{T}\begin{pmatrix} h \\ k \\ \ell \end{pmatrix} = \frac{2\sin\theta}{\lambda}\begin{pmatrix} \cos\omega\ \cos\chi\ \cos\phi - \sin\omega\ \sin\phi \\ \cos\omega\ \cos\chi\ \sin\phi + \sin\omega\ \cos\phi \\ \cos\omega\ \sin\chi \end{pmatrix} \quad (6)$$

For a three circle geometry in bisecting position ($\omega = 0$)

$$\therefore \underset{\sim}{R}.\underset{\sim}{T}\begin{pmatrix} h \\ k \\ \ell \end{pmatrix} = \frac{2\sin\theta}{\lambda}\begin{pmatrix} \cos\chi\ \cos\phi \\ \cos\chi\ \sin\phi \\ \sin\chi \end{pmatrix} \quad (7)$$

Now $\underset{\sim}{R}.\underset{\sim}{T}$ is a 3 x 3 matrix having components R_{ij}, thus:-

$$\begin{pmatrix} R_{11} & R_{12} & R_{13} \\ R_{21} & R_{22} & R_{23} \\ R_{31} & R_{32} & R_{33} \end{pmatrix}\begin{pmatrix} h \\ k \\ \ell \end{pmatrix} = \frac{2\sin\theta}{\lambda}\begin{pmatrix} \cos\chi\ \cos\phi \\ \cos\chi\ \sin\phi \\ \sin\chi \end{pmatrix} \quad (8)$$

To find the nine elements of the above matrix it is necessary to choose at least three non-coplanar reflections of known indices and known setting angles. By solving the nine equations so obtained, the nine elements of the matrix can be determined.

To find the reciprocal and real cell parameters a matrix Tensor G^{-1} is formed in terms of the rotation matrix and is given by

$$G^{-1} = \widetilde{\underset{\sim}{RT}}.\underset{\sim}{RT} \quad (9)$$

$$\text{or } G^{-1} = \begin{pmatrix} R_{11} & R_{21} & R_{31} \\ R_{12} & R_{22} & R_{32} \\ R_{13} & R_{23} & R_{33} \end{pmatrix}\begin{pmatrix} R_{11} & R_{12} & R_{13} \\ R_{21} & R_{22} & R_{23} \\ R_{31} & R_{32} & R_{33} \end{pmatrix} \quad (10)$$

Metric Tensor G^{-1} can also be written as

$$G^{-1} = (\widetilde{RT}) \cdot \underset{\sim}{RT} = \widetilde{\underset{\sim}{T}}\,\widetilde{\underset{\sim}{R}} \cdot \underset{\sim}{RT} = \widetilde{\underset{\sim}{T}}\,\underset{\sim}{T} \tag{11}$$

Now substituting for $\widetilde{T}$ and T from equation (4) into equation (9)

$$G^{-1} = \widetilde{\underset{\sim}{T}}\,\underset{\sim}{T}$$

$$= \begin{pmatrix} a^* & 0 & 0 \\ b^* \cos\gamma^* & b^* \sin\gamma^* & 0 \\ c^* \cos\beta^* & -c^* \sin\beta^* \cos\alpha & 1/c \end{pmatrix} \begin{pmatrix} a^* & b^* \cos\gamma^* & c^* \cos\beta^* \\ 0 & b^* \sin\gamma^* & -c^* \sin\beta^* \cos\alpha \\ 0 & 0 & 1/c \end{pmatrix} \tag{12}$$

which after a little simplification becomes

$$G^{-1} = \begin{pmatrix} a^{*2} & a^* b^* \cos\gamma^* & a^* c^* \cos\beta^* \\ a^* b^* \cos\gamma^* & b^{*2} & b^* c^* \cos\alpha^* \\ a^* c^* \cos\beta^* & b^* c^* \cos\alpha^* & c^{*2} \end{pmatrix} \tag{13}$$

Now matrices (10) and (13) are the same. Therefore equating (10) and (13) element by element we get

$$a^{*2} = R_{11}^{\,2} + R_{21}^{\,2} + R_{31}^{\,2} \tag{14}$$

$$b^{*2} = R_{12}^{\,2} + R_{22}^{\,2} + R_{32}^{\,2} \tag{15}$$

$$c^{*2} = R_{13}^{\,2} + R_{23}^{\,2} + R_{33}^{\,2} \tag{16}$$

$$\cos\alpha^* = \frac{R_{12} R_{13} + R_{22} R_{33} + R_{32} R_{33}}{b^* c^*} \tag{17}$$

$$\cos\beta^* = \frac{R_{11} R_{13} + R_{21} R_{23} + R_{31} R_{33}}{c^* a^*} \tag{18}$$

$$\cos\gamma^* = \frac{R_{11} R_{12} + R_{21} R_{22} + R_{31} R_{32}}{a^* b^*} \tag{19}$$

Thus the reciprocal cell parameters and, therefore, the real cell parameters can be determined.

APPENDIX C

Siemens AED/IBM1130 Four-circle Diffractometer system

Control Program, DIFF6

Written by D. F. Grant

I. Introduction

DIFF6 is a Core Image program for controlling the diffractometer for routine data collection. The X-circle is always in the bisecting ($\omega = 0$) position and if a particular reflection is outside the range of the quarter X-circle then the Friedel equivalent reflection is measured. A 5-point measurement routine is used. The data is stored on the named file, DFDAT, and the standard reflection data on the file DFSTA.

II. Functions of DIFF6

1. From the orientation matrix, from information about the segments of reciprocal space to be measured, from the minimum and maximum value of 2θ required, from the order in which the indices are to be taken and from the specification of systematic absences, reciprocal space can be explored in a systematic manner.

   Each h, k, ℓ is tested against the expression

   $$Ah + Bk + C\ell = Dm + E$$

   to determine whether the particular combination of indices is acceptable and, if so, the ϕ, X and θ values for the four-circle diffractometer in the bisecting ($\omega = 0$) are calculated.

2. The ϕ, X and θ circles are driven simultaneously to the angles calculated and the fractional part of the angular setting checked. The program adjusts the setting if it is within $\pm 0.25^\circ$ of the correct value. If the program fails to correct the setting all circles are returned to zero and the setting begun again.

3. By counting for 0.5s at the peak of the reflection with attenuator 6 in use, the correct attenuator setting is made to ensure that the maximum count rate is not exceeded during measurement. If, using the largest attenuator (No. 6) the maximum count rate would still be exceeded then attenuator 6 will be used, but 7 output as the attenuator number.

4. A sample (or trial) time per step q and a maximum time T_m are specified in the input data. A prestated counting statistics percentage accuracy p required and a percentage accuracy p_c for the weak reflection criterion are also specified. All reflections are measured for a time per step q and a time per step T calculated to ensure the required accuracy p. If $T < T_m$ the reflection is then measured using this time. If $T > T_m$ a predicted accuracy p' for the reflection is calculated if it were to be measured for T_m. If $p' < p_c$ the reflection is measured; if $p' > p_c$ it is not further measured and is considered to be accidentally absent.

5. A five-point measurement routine (θ - 2θ scan) is performed about the calculated θ position. The range of scan is $\pm \Delta\theta = P + Q \tan\theta$ where P and Q are specified in the input data. The scan is in steps of 0.01°, counting at each step for the time given in paragraph 4 above. The background on each side is counted for the same time as the counting time in the scan from peak to background and thus varies automatically with the scan angle ($\Delta\theta$) and the time per scan step. The net peak intensity is thus always given by $(I_1 + I_3 + I_5) - 2(I_2 + I_4)$ and must be scaled for attenuator setting or counting time per step.

6. At the beginning of each segment of reciprocal space measured, all the circles are returned to zero and a specified number (m) of standard reflections are measured. This routine is also repeated after every n reflections measured. Long term variations in the quality of the crystal and in the performance of the x-ray generator and counting chain can thus be checked.

7. If the data collection is interrupted at any time, the measurements can be resumed at any specified reflection.

III. Input

The input is all from punched cards.

Card 1. Title Card

c.c. 1-70, up to 70 alphanumeric characters of information about the particular data collection.

Card 2. Wavelength Card (Format F8.5)

c.c. 1-8 xx.xxxxx Wavelength of x-radiation.

Card 3. Number of Standard Reflections Card (Format 3 (I3,1X))

c.c. 1-4 xxxb Number (N) of standard reflection cards following. $1 \leqslant N \leqslant 4$

5-8 xxxb Number (m) of standards to be measured every n reflections. $1 \leqslant m \leqslant N$

9-12 xxxb Number (n) of reflections between measurement of standards $1 \leqslant n < 1000$

Card 4.→ Card(3+N) Standard Reflection Cards (Format 3 (I3,1X),3(F8.4,1X))

c.c. 1-4 xxxb h

5-8 xxxb k

9-12 xxxb ℓ

13-21 xxx.xxxxb ϕ

22-30 xxx.xxxxb χ values for h k ℓ reflection

31-39 xxx.xxxxb θ

If the three reflections used to define the orientation matrix are also used as standards then the reflection cards ouput with the orientation matrix cards from DSET2 can be used.

Card (4+N)→ Card(6+N) Orientation Matrix Cards

Three cards output from DSET2; for details see the specification to DSET2.

Card (7+N) Limits Card (Format I3,1X,2F6.2,2F6.4,2(1X,I4),2F6.3)

c.c. 1-4 xxxb Number of reciprocal space segments (NMSEG)

5-10 xxx.xx Minimum value of 2θ

11-16 xxx.xx Maximum value of 2θ

17-22 x.xxxx P

23-28 x.xxxx Q

$\Delta\theta = P + Q \tan \theta$

29 b

30-33 xxxx Sample time per step (q)

34 b

35-38 xxxx Maximum time per step (T_m)

39-44 xx.xxx Percentage accuracy required (p)

45-50 xx.xxx Accuracy criterion for weak reflections (p_c)

Both q and T_m are expressed as integers where each integer represents 5 ms. $1 \leqslant q \leqslant T_m \leqslant 2000$. If $q = T_m$ then all significant reflections are measured for the same time per step.
If Q = 0.0, all reflections are measured with the same θ-scan.
The total time for a five-point measurement is $3\Delta\theta T$ s.

Example The following limits card

2 0.0 90.0 1.2 0.2 5 100 2.0 10.0

indicates (i) that two segments of reciprocal space are to be measured,

(ii) that $2\theta_{min} = 0.0$ and that $2\theta_{max} = 90.0$,

(iii) that $\theta = 1.20 + 0.20 \tan\theta$; $\Delta\theta$ varies from 1.20 at $\theta = 0$ to 1.40 at $\theta = 45°$,

(iv) that the sample counting time per step is $5 \times 5 \times 10^{-3} = .025$s,

(v) that the maximum counting time per step for measurement is $100 \times 5 \times 10^{-3} = 0.5$s,

(vi) that the total measurement time per reflection could vary from 18s for a strong reflection at $\theta = 0$ to 420s for a weak reflection at $\theta = 45°$,

(vii) that any reflection measured with a counting time less than T_m will have at least 2.0% accuracy.

(viii) that those weak reflections measured at T_m will have at least 10.0% accuracy,

(ix) that those very weak reflections for which a measurement at T_m would not have at least 10.0% accuracy, the total measurement time will be the time to take the sample, i.e., 18 - 21s.

Card (8+N) Number of Reflection Conditions Card (Format I3)

c.c. 1-3 xxx Number of reflection conditions (NCOND)

Card (9+N)→ Reflection Conditions Cards (Format 6 (I3,2X))
Card(8+N+NCOND)

There are NCOND cards, one for each reflection conditions

c.c. 1-3 xxx Type of reflection (see below)

4-8 bbxxx A)

9-13 bbxxx B)

14-18 bbxxx C) used in $Ah + Bk + C\ell = Dm + E$

19-23 bbxxx D) see II.1.

24-28 bbxxx E)

1	00ℓ	reflections only
2	0k0	" "
3	h00	" "
4	0kℓ	" "
5	h0ℓ	" "
6	hk0	" "
7	hkℓ	" "

e.g. 2 0 1 0 2 0 means for 0k0 reflections
k = 2n only would be present.

7 1 1 1 2 0 means for hkℓ reflections
h + k + ℓ = 2n only would be present.

Card (9+N+NCOND) Reflection and Standard Numbers Card (Format 2I4)

c.c. 1-4 xxxx Number (NREF) of the starting reflection ($h_s k_s \ell_s$) on the data file DFDAT.

5-8 xxxx Number (NSTD) of the next standard reflection on the data file DFSTA.

This card ensures that when a data collection is restarted the data and standards already on the disk files are not overwritten.

Card (10+N+NCOND)→ Segment Cards (Format 15 (I3,1X)
Card (9+N+NCOND+NMSEG)

i.e. NMSEG cards, each card dealing with the indexing of one segment of reciprocal space.

c.c. 1-4	xxxb	h_o)	
5-8	xxxb	k_o)	origin defining reflection
9-12	xxxb	ℓ_o)	
13-16	xxxb	h_{11})	
17-20	xxxb	h_{21})	increment steps in hkℓ for layers
21-24	xxxb	h_{31})	
25-28	xxxb	h_{12})	
29-32	xxxb	h_{22})	increment steps in hkℓ for lines
33-36	xxxb	h_{32})	
37-40	xxxb	h_{13})	
41-44	xxxb	h_{23})	increment steps in hkℓ for points
45-48	xxxb	h_{33})	
49-52	xxxb	h_s)	
53-56	xxxb	k_s)	starting reflection
57-60	xxxb	ℓ_s)	

Example (1) Suppose all the unique reflections in a monoclinic system are to be measured then the number of segments is 2. If h and k are taken to be positive only and ℓ positive or negative, then for the first segment

h_o, k_o, ℓ_o	= 0, 0, 0	
h_{11}, k_{21}, h_{31}	= 0, 1, 0	increment layers by k = 1
h_{12}, h_{22}, h_{32}	= 1, 0, 0	increment lines by h = 1
h_{13}, h_{23}, h_{33}	= 0, 0, 1	increment points by ℓ = +1
h_s, k_s, ℓ_s	= 0, 0, 0	

and for the second segment

$h_o,\ k_o\ \ell_o = 1,\ 0,\ -1$		This origin avoids repeating reflections with h = 0 and ℓ = 0
$h_{11},\ h_{21},\ h_{31} = 0,\ 1,\ 0$		
$h_{12},\ h_{22},\ h_{32} = 0,\ 1,\ 0$		
$h_{13},\ h_{23},\ h_{33} = 0,\ 0,\ -1$		increment points by ℓ = -1
$h_s,\ k_s,\ \ell_s = 1,\ 0,\ -1$		

Example (2) A segment for a monoclinic crystal with h negative, k changing fastest, h next and ℓ least, and with -3, 2, 4 as the starting reflection

$h_o\ \ k_o\ \ell_o = -1,\ 0,\ 1$	
$h_{11},\ h_{21},\ h_{31} = 0,\ 0,\ 1$	
$h_{12},\ h_{22},\ h_{32} = -1,\ 0,\ 0$	
$h_{13},\ h_{23},\ h_{33} = 0,\ 1,\ 0$	
$h_s,\ k_s,\ \ell_s = -3,\ 2,\ 4$	

IV. Program operation

1. Program called with // XEQ DIFF6.

2. Initially the program returns all circles to zero.

3. If SWITCH 1 is ON, then the measurement of the m standard reflections is omitted. The circles are however returned to zero at the beginning of each segment and after every n reflections.

4. If SWITCH 2 is ON, then the output on the typewriter of the data is suppressed.

5. If SWITCH 3 is ON, then the output in the typewriter of the standards is suppressed.

6. If, during the checking and correction of the angular setting, the angle is still incorrect, the program returns all circles to zero and begins again by measuring the m standard reflections before starting again at the reflection it failed at and then proceeding. (Unless SWITCH 1 is ON and then it will at once remeasure the reflection it failed at.)

7. If, at any time, an end-contact is sensed then as in 6 above the circles are returned to zero and the measurement resumed.

8. If, during the measurement routine, the capacity of the intensity counter in the interface is exceeded, the program stops and the overflow value displayed in the accumulator extension. Pressing PROGRAM START continues the program.

V. Output

Typewriter

1. Line of alphanumeric information given in Card 1.

2. Maximum values of h, k, ℓ.

3. "h k ℓ is NEXT REFLECTION NUMBER r AND STANDARD s" where r = NREF and s = NSTD

4. The heading H K L PHI CHI THETA LP-1 is printed.

5. h, k, ℓ, ϕ, X, θ, five intensity values, attenuator number, time per step are printed for the m standard reflections as they are measured. This is suppressed if SWITCH 1 is ON, or if SWITCH 3 is ON.

6. h, k, ℓ, ϕ, X, θ, Lp^{-1}, five intensity values, attenuator number, time per step are printed for each of the next n reflections as they are measured. The time per step in output as zero for the very weak reflections for which is is not possible to satisfy the accuracy criterion p_c. This output is suppressed if SWITCH 2 is ON. 4, 5 and 6 are repeated until the first segment is finished, and then 4, 5 and 6 are repeated until all segments have been completed.

Disk

h, k, ℓ, five intensity values, attenuator number, Lp^{-1}, time per step are stored on disk in the named file DFDAT for the reflections measured. Up to 2000 reflections can be stored at any one time and users are advised not to leave the results of more than a few days work on the disk.

h, k, ℓ, five intensity values, attenuator number, Lp^{-1}, time per step and the next reflection number (NREF) are stored on disk for the standard reflections in the named file DFSTA. Up to 200 standards can be stored at any one time.

References

Arndt, U.W. and Willis, B.T.M. (1966), Single Crystal Diffractometry, Cambridge University Press.

Berghuis, J., Haanappel, IJ.M., Potters, M., Loopstra, B.O., MacGillavry, C.H. and Veenendaal, A.L. (1955), Acta. Cryst. 8, 478.

Bond, W.L. (1951), Rev. Sci. Instr., 22, 344.

Bragg, W.L., James, R.W. and Bosanquet, C.H., (1921a), Phil. Mag. 41, 309.

Bragg, W.L., James, R.W. and Bosanquet, C.H., (1921b), Phil. Mag. 42, 1.

Brown, G.M. and Levy, H.A. (1965), Science 147, 1038.

Busing, W.R. and Levy, H.A. (1967), Acta. Cryst. 22, 457.

Buerger, M.J. (1942), X-Ray Crystallography, John Wiley, New York, London.

Buerger, M.J. (1960), Crystal Structure Analysis, John Wiley, New York, London.

Chandrasekhar, S. (1956), Acta. Cryst. 9, 954.

Chandrasekhar, S. and Phillips, D.C. (1961), Nature, London, 190, 1164.

Chandrasekhar, S., Ramaseshan, S. and Singh, A.K. (1969), Acta. Cryst., A25, 140.

Chu, S.C. and Jeffrey, G.A. (1968), Acta. Cryst. B24, 830.

Coppens, P. (1969), Acta. Cryst. A25, 180.

Cochran, W. (1953), Acta. Cryst. 6, 260.

Cooper, M.H. and Rouse, K.D. (1968), Acta. Cryst. A24, 405.

Cottrell, A.H. (1964), The Mechanical Properties of Matter, New York, London.

Cromer, D.T. and Waber, J.T. (1965), Acta. Cryst. 18, 104.

Cruickshank, D.W.J. (1956), Acta. Cryst. 9, 747.

Darwin, C.G. (1914a), Phil. Mag., 27, 315.

Darwin, C.G. (1914b), Phil. Mag., 27, 675.

Darwin, C.G. (1922), Phil. Mag., 43, 800.

DeMarco, J.J. and Weiss, R.J. (1962), Acta Cryst. 15, 1125.

Ewald, P.P. (1916a), Ann. d. Physik., 49, 1.

Ewald, P.P. (1916b), Ann. d. Physik., 49, 117.

Ewald, P.P. (1917), Ann. d. Physik., 54, 519.

Fisher, R.A. and Yates, F. (1953), Statistical Tables, 4th ed., Edinburgh, Oliver and Boyd.

Freeman, A.J. (1959), Acta. Cryst. 12, 261.

Gay, P., Hirsch, P.B. and Kelly, A. (1953), Acta. Met. 1, 315.

Hart, M. (1966), Z. Phys. 189, 269.

Hart, M. and Milne, A.D. (1969), Acta. Cryst., A25, 134.

Hattori, H., Kuriyama, H., Katagawa, T. and Kato, N. (1965), J. Phys. Soc, Japan, 20, 988.

Ibers, J.A. (1968), Private Communication.

International Tables for X-Ray Crystallography (1962), Volume I, II and III.

Johnston, W.G. and Gilman, J.J. (1959), J. Appl. Phys. 30, 129.

James, R.W. (1948), The Optical Principles of the Diffraction of X-Rays, G. Bell and Sons Ltd., London.

Kato, N. and Lang, A.R. (1959), Acta. Cryst. 12, 787.

Killean, R.C.G. and Lawrence, J.L. (1969), Acta. Cryst., B25, 1750.

Kitaigorodskii, A.I. (1957), Theory of Crystal Structure Analysis, Translation 1961, New York, Heywood.

Larson, A.C. (1967), Acta. Cryst. 23, 664.

Laue, M.v. (1931), Ergeb. der exact. Naturwiss, 10, 133.

Laue, M.v. (1960), Röntgenstrahlinterferenzen, Frankfurt A/M, Akad. Verlag.

Lawrence, J.L. (1972), Acta. Cryst., In Press.

Lipson, H. and Taylor, C.A. (1958), Fourier Transforms and X-Ray Diffraction, G. Bell and Sons Ltd., London.

Lipson, H. and Cochran, W. (1966), The Determination of Crystal Structures, G. Bell and Sons Ltd., London.

Marsh, R.E. (1958), Acta. Cryst., 11, 654.

McGeachin, H.M. and Beevers, C.A. (1957), Acta. Cryst. 10, 227.

Parratt, L.G. (1933), Phys. Rev. 44, 695.

Parratt, L.G. (1934), Phys. Rev. 46, 749.

Renninger, M. (1934), Z. Krist., 89, 344.

Roggers, D. and Hough, E. (1968), Private Communication.

Rollet, J.S. (1965), Computing Methods in Crystallography, Pergammon Press.

Snyder, R.L., Rosenstein, R.D., Kim, H.S., and Jeffrey, G.A. (1970), Carbohydrate Research, 12, 153.

Stewart, R.F. and Jensen, L.H. (1969), Z. Krist., 128, 133.

Tanemura, S. and Kato, N. (1972), Acta. Cryst., A28, 69.

Thewlis, J. (1955), Acta Cryst. 8, 36.

Vand, V. (1955), J. Appl. Phys. 26, 1191.

Weiss, R.J., (1952), Proc. Phys. Soc. London, B65, 553.

Weiss, R.J. (1966), X-Ray Determination of Electron Distributions, John Wiley and Sons, Inc., New York.

Werner, S.A. (1969), Acta. Cryst. A25, 639.

Werner, S.A. (1972), Acta. Cryst. A28, 143.

Willis, B.T.M. (1962), Pile Neutron Research in Physics, P. 455, (Vienna, I.A.E.A.).

Zachariasen, W.H. (1963), Acta. Cryst. 16, 1139.

Zachariasen, W.H. (1967), Acta. Cryst. 23, 558.

Zachariasen, W.H. (1968), Acta. Cryst. A24, 324.

Zachariasen, W.H. (1945), Theory of X-Ray Diffraction in Crystals, John Wiley and Sons, New York, London.